

**Transport of metal oxide nanoparticles
across the human air-blood barrier - in-
teractions with physiologically relevant
media and proteins**

Dissertation

zur Erlangung des Grades

Doktor der Naturwissenschaften

der Naturwissenschaftlich-Technischen Fakultät III

Chemie, Pharmazie, Bio- und Werkstoffwissenschaften

der Universität des Saarlandes

von

Christine Schulze

Saarbrücken

2010

Tag des Colloquiums: 17.12.2010

Dekan: Prof. Dr. Stefan Diebels

Mitglieder des Prüfungsausschusses:

Vorsitzender: Prof. Dr. Gerhard Wenz

1. Gutachter: Prof. Dr. Claus-Michael Lehr

2. Gutachter: Prof. Dr. Ingolf Bernhardt

Akademischer Mitarbeiter: Dr. Ulrich F. Schaefer

Meinem Mann Sascha

Table of Contents

<i>Zusammenfassung</i>	<i>III</i>
<i>Abstract</i>	<i>V</i>
1 Background and aim of this thesis	1
1.1 Nanoparticles	1
1.2 Project NanoCare.....	2
1.3 The human lung	3
1.4 My contribution to the NanoCare Project and the subject of this work	4
2 Not ready to use – overcoming pitfalls when dispersing nanoparticles in physiological media	7
2.1 Abstract	8
2.2 Introduction.....	9
2.3 Materials & Methods.....	9
2.4 Results & Discussion	15
2.5 Conclusion	28
3 Intrinsic physico-chemical properties of CeO₂ nanoparticles do not mirror their biorelevant protein adsorption	31
3.1 Abstract	32
3.2 Introduction.....	33
3.3 Materials & Methods.....	34
3.4 Results & Discussion	41
3.5 Conclusion	55
4 Interaction of metal oxide nanoparticles with lung surfactant protein A	57
4.1 Abstract	58
4.2 Introduction.....	59

4.3	Materials & Methods	60
4.4	Results & Discussion	66
4.5	Conclusion	74
5	<i>Transport of metal oxide nanoparticles across an in vitro air-blood barrier model: adaptations and results</i>	75
5.1	Abstract	76
5.2	Introduction	77
5.3	Materials & Methods	78
5.4	Results & Discussion	85
5.5	Conclusion	92
	<i>Summary and outlook</i>	95
	<i>Zusammenfassung und Ausblick</i>	99
	<i>Abbreviations</i>	105
	<i>References</i>	107
	<i>Publication List</i>	121
	Publications	121
	Oral Presentations	121
	Poster Presentations	121
	<i>Danke</i>	123
	<i>Curriculum Vitae</i>	125

Zusammenfassung

Noch immer ist die Schere zwischen der Produktion und großtechnischer Nutzung von Nanopartikeln einerseits und deren toxikologischen Potentials andererseits recht groß. *In vitro*-Versuche sind ein oft genutztes Mittel zur Bestimmung der Toxizität von Substanzen, für Nanopartikel jedoch müssen in diesem Zusammenhang bestimmte Fallen erkannt und umgangen werden, um so generierte Ergebnisse richtig zu interpretieren. Eine Besonderheit von Nanopartikeln ist deren Interaktion mit Proteinen in Zellkulturmedien, aber auch mit physiologisch relevanten Proteinen. Einerseits können solche Interaktionen einen Einfluss auf den Agglomerationsgrad der Partikel, andererseits auf die Reaktion der Zelle auf einen solchen, mit Proteinen überzogenen Partikel haben. Somit kann sich das toxikologische Potential von Nanopartikeln in beide Richtungen verschieben.

Bei Untersuchungen mit dem Modellprotein BSA bzw. FCS konnten Unterschiede in der Adsorption an drei Nanopartikel gleichen Materials als auch sehr ähnlichen physikalisch-chemischen Eigenschaften aufgezeigt werden. Dabei zeigte sich, dass BSA wahrscheinlich in unterschiedlichen Konformationen an die Partikel bindet. Außerdem muss, um Proteinadsorption richtig einschätzen zu können, der Agglomerationsgrad der Partikel mit einbezogen werden.

Protein-Adsorption konnte nicht nur für Modellproteine, sondern auch für das physiologisch relevante Surfactant Protein A an acht verschiedene Partikel, teilweise aus gleichem Material, nachgewiesen werden. Im Gegensatz zu BSA hat die Dispersion in Sp-A-haltigem Medium keinen positiven Einfluss auf das Deagglomerationsverhalten der Partikel.

Inhalierte Partikel können möglicherweise die Blut-Luft-Schranke passieren und so in den Blutkreislauf gelangen. Um den Partikelübertritt zu untersuchen, wurde ein *in vitro* Zellkultur-Modell an die Besonderheiten von Transportversuchen mit Nanopartikeln angepasst. Die Zellkultur-Bedingungen wurden angepasst und anschließend die Transporteigen-

schaften der Zellen mit diesen veränderten Gegebenheiten bestätigt. Mit Ausnahme der beiden getesteten CeO₂-Partikel konnte im Rahmen der Versuchsdurchführung bei keinem Nanopartikel ein Transport festgestellt werden.

Schlagwörter:

Metalloxid-Nanopartikel, Nanotoxikologie, Proteinadsorption, Partikeltransport

Abstract

There is still a big gap between nanoparticle production and industrial use on one hand and the knowledge of their toxicological potential on the other. *In vitro* assays are a common tool to investigate toxicity of substances, but for nanoparticles, some especially dispersion related pitfalls must be recognized and bypassed prior to correct interpretation of results. One special feature of nanoparticles is the possible interaction with proteins in cell culture media and with physiological proteins as well. On one hand, those interactions can have an influence on the agglomeration state, on the other hand cell reactions and hence the toxicological potential can be altered.

Investigations with the model protein BSA or FCS, respectively, revealed differences for the adsorption onto nanoparticles, although the particles tested had very similar physico-chemical properties. BSA seemed to adsorb to the particles in different conformations, and the state of agglomeration must be taken into account to draw conclusions about protein adsorption.

Protein adsorption was also confirmed for physiologically relevant Surfactant protein A to eight different nanoparticles of partially the same bulk material. Also here, differences in protein adsorption could be detected. In contrast to BSA, Sp-A does not have much impact on the agglomeration state of the particles.

Inhaled particles might cross the air-blood barrier and enter the blood stream. Hence, an *in vitro* air-blood barrier model was adapted to transport experiments with nanoparticles. The cell culture conditions were adapted and the transport characteristics of the cells confirmed. Except two different CeO₂ particles, no metal oxide nanoparticle transport could be detected.

Keywords:

metal oxide nanoparticle, nanotoxicology, protein adsorption, particle transport

1 Background and aim of this thesis

1.1 Nanoparticles

Nanotechnology is a key technology of the 21st century. Nanoparticles are used in many industrial sectors, as micro-electronics, materials, paper, textile, energy, and cosmetics [1, 2]. The industrial relevance is expressed in an estimated annual turnover of nanoparticle-based products in the range of 1.1 - 2.5 trillion us dollars by the year 2015 [3]. The advantages of nanotechnology are the production of light and durable materials, cleaner energy, inexpensive clean water production, as well as several beneficial pharmaceutical and medical applications [1, 4]. Nanoparticles are defined as particles with at least one dimension smaller than 100 nm [5], the dimensions are compared in Figure 1.1. The very high surface to mass ratio gives them their unique properties, which are summarized in Table 1.1. This surface to mass ratio is not changed significantly by agglomeration or aggregation. Thereby, aggregates and agglomerates also count as nanoparticles even if their size is much bigger, but only if the size of the primary particles does not exceed 100 nm. Hence, an additional definition based on the particle surface is discussed and a lower limit of 60 m²/g suggested (corresponding to the specific surface area of spherical particles of 100 nm in diameter and unit density) [5].

Table 1.1. Unique features of nanomaterials (adopted from [6])

Size:
➤ 20-50 nm enters CNS
➤ 70 nm, able to escape defense system in vivo
High surface to mass ratio
High strength, conductivity, solubility, durability and reactivity
Catalytic promotion of reactions
Ability to adsorb and carry other compounds
Ability to escape defense system in vivo
Ability to cross cellular and sub-cellular membranes
Surface coating (e.g. lecitin, albumin)
➤ Enhance uptake by type I/II pneumocytes
➤ Transcytosis across capillary
Charged particle (higher inhaled deposition)

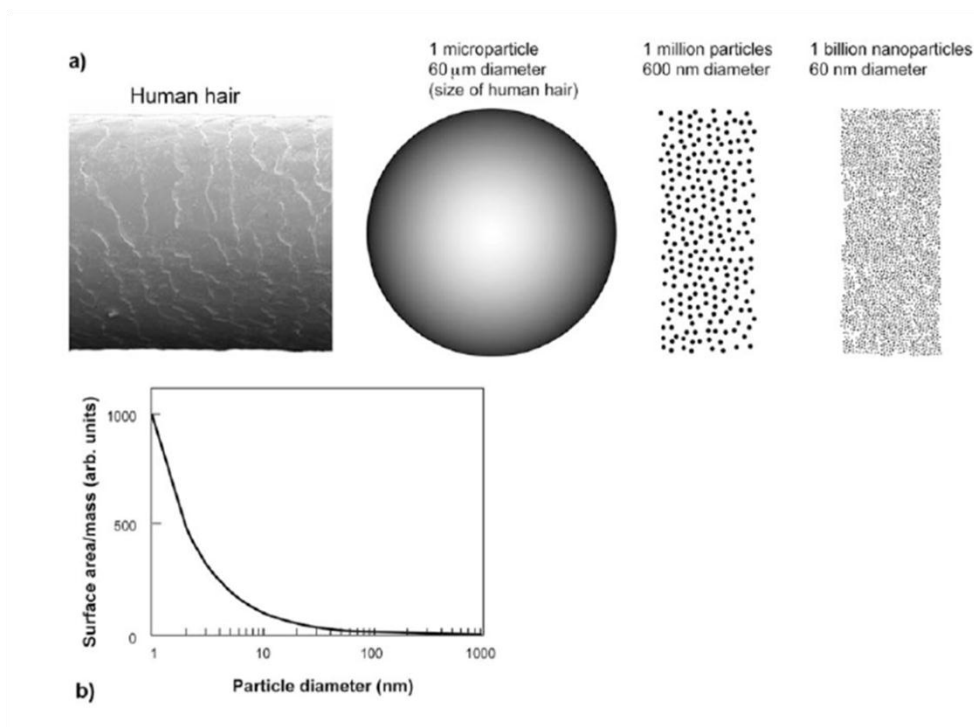


Figure 1.1. a) Comparison of a microparticle of 60 μm diameter (about the size of a human hair) with particles of 600 nm and 60 nm, respectively. When all particles have the same mass, a reduction of the diameter of 1 decade increases the number of particles one thousand fold. b) Surface area normalized to mass versus particle diameter, i.e. decreasing particle diameter is leading to exponentially growing particle surface area (Illustration adopted and modified from [7])

1.2 Project NanoCare

The benefits of nanoparticles are opposed to unknown health risks, as the development of new nanoparticles exceeds their toxicological risk assessment by far. In the late 1990's, a perception of possible health risks came up and first guidelines were developed [8]. Kuhlbusch and co-workers and Bower and co-workers published the first studies related to exposure of engineered nanoparticles [9-11], the first publications related to nanotoxicology date back to 1992, e.g. Oberdörster and co-workers [12]. As the gap between nanoparticle production and nanoparticle safety research was still very big, the German Federal Ministry of Education and Research (Bundesministerium für Bildung und Forschung, BMBF)

initiated a trilogy of projects: INOS, TRACER and NanoCare. The aim of TRACER was the evaluation of biocompatibility, especially cytotoxicity of Carbonanotubes (CNTs), along the value creation chain of CNTs. INOS contributed to the risk assessment of ceramic and metal nanoparticles, based on *in vitro* methods. The NanoCare project was a cooperation of 13 partners from university, industry and research institutes that developed a research plan concerning the risk assessment of nanomaterials and started in March 2006. NanoCare aimed to sustain nanoparticle development, combining the identification of possible exposure and hazard of new industrially relevant nanoparticles with the innovation in material science. As a possible human or ecological hazard significantly influences the public perception of nanoparticles negatively, nanotechnology might not be accepted and lead to nanotechnology crisis. Hence, NanoCare turned to three major routes: The first was knowledge generation, i.e. research of nanoparticle exposure and toxicity in *in vivo* and *in vitro* test systems. The second was knowledge management, based on literature studies and the research work within the project. A combination of these data was fed into a partially public data base, so an exchange between the partners was possible at any time. Finally, knowledge transfer and communication was supposed to facilitate the exchange between scientists and the public by explaining generated results in a generally understandable manner at workshops, dialogues and a website (www.nanopartikel.info).

1.3 The human lung

The human lungs can be divided into two functional regions. The conducting airways, i.e. nose cavity, trachea, bronchi and several generations of bronchioles, direct the air to and from the respiratory zone. Consisting of respiratory bronchioles and the alveoli, the respiratory zone is up to 140 m² big [13] and is the site of gas exchange [14]. The columnar epithelium of the airways is gradually thinning, from 3-5 mm of the bronchial epithelium to 0.5-1 mm thickness of the bronchiolar epitheli-

um [14, 15]. The tracheobronchiolar region is protected by a mucus layer, and landing foreign matter is transported towards the larynx via mucociliary clearance [16]. However, the alveoli consist of type I and type II pneumocytes, whereas 93 % of the alveolar epithelial area is covered by type I cells [17]. The epithelial air-blood barrier here is only about 400 nm thick [18]. Type II cells produce the Alveolar Lining Fluid (ALF), by which the alveolar region is covered. Pulmonary surfactant, a major component of ALF, is required for normal respiration, as it increases the surface tension forces at the air-ALF interface. This avoids the collapse of alveoli during exhalation and also reduces the force needed to ventilate them [19]. This lung surfactant contains of approximately 85-90 % phospholipids (by weight), predominantly Phosphatidylcholine. Also, pulmonary surfactant contains about 10 % proteins, the so called surfactant proteins A, B, C and D (Sp-A, Sp-B, etc., collective name Sp-X) [20]. The lipophilic Sp-B and Sp-C function as stabilizers for the surfactant film, whereas the hydrophilic Sp-A and Sp-D play a role in host defense. Sp-A is the most prominent of the four Surfactant proteins and is opsonizing bacteria by binding to carbohydrate groups with its lectin binding site [21]. Also, it is involved in the recycling of surfactant, i.e. the reuptake into type II pneumocytes [22]. This pulmonary surfactant represents the first barrier inhaled substances interact with, prior to contacting the alveolar epithelium.

1.4 My contribution to the NanoCare Project and the subject of this work

Generally, there are three possibilities for particles to enter the body: penetration through the skin, adsorption in the gastrointestinal tract or by inhalation. The most prominent exposure route for nanoparticles is the lung, as particle deposition in the airways is size-dependent (Figure 1.2). The maximum of particle deposition in the alveoli with its immense size of up to 140 m² lies with 10 to 100 nm exactly in the nanoparticle

range. Hence, the exposition as well as the inhalation toxicity of nanoparticles plays a key role in nanoparticle risk assessment.

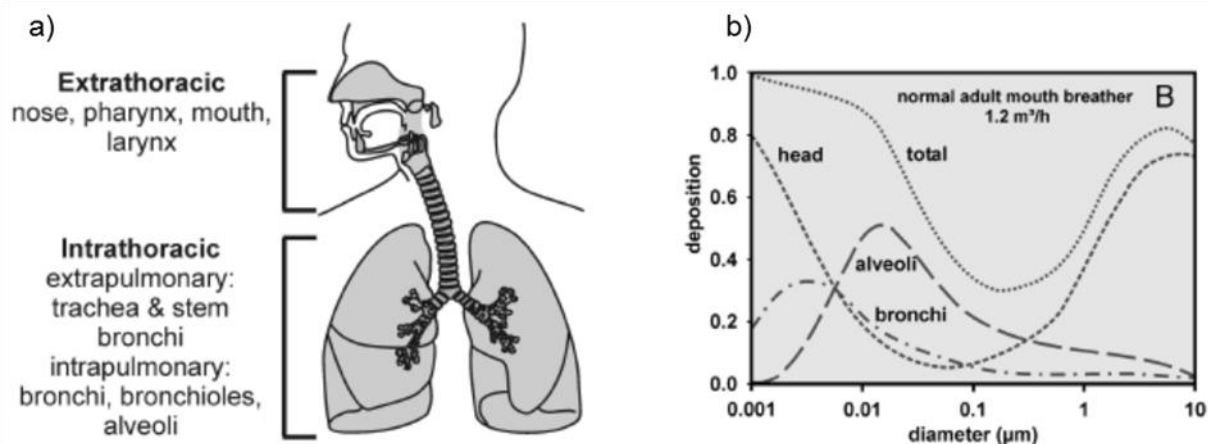


Figure 1.2. a) The respiratory tract and b) the particle deposition as a function of size in a normal breathing male human at rest. The data of bronchi are the sum of deposition in bronchi and bronchioles (adopted from [23]).

Inhalation is the most significant exposure route for airborne nanoparticles [24, 25]. The distance between alveolar lumen and blood flow is with 400 nm very small and combined with the large surface area of the alveoli those characteristics make this region less protected against inhaled substances compared to the conducting airways [26]. Hence, the particle interaction with lung barrier systems was investigated in *in vitro* models. This work as a part of the NanoCare project was the investigation of particle interaction with ALF as first barrier and permeation of nanoparticles through the lung into the blood stream. For this purpose, we used a well-established *in vitro* model of the air-blood-barrier, i.e. Calu-3 cells grown on filter supports (Figure 1.3). Not every lung cell line is convenient for use in this model: the cells must display special epithelial barrier characteristics, i.e. development of tight junctions, which parts the system in an apical and a basolateral compartment with a polarized epithelial mono-

layer, denying passive diffusion processes, but allowing specific transport of substances.

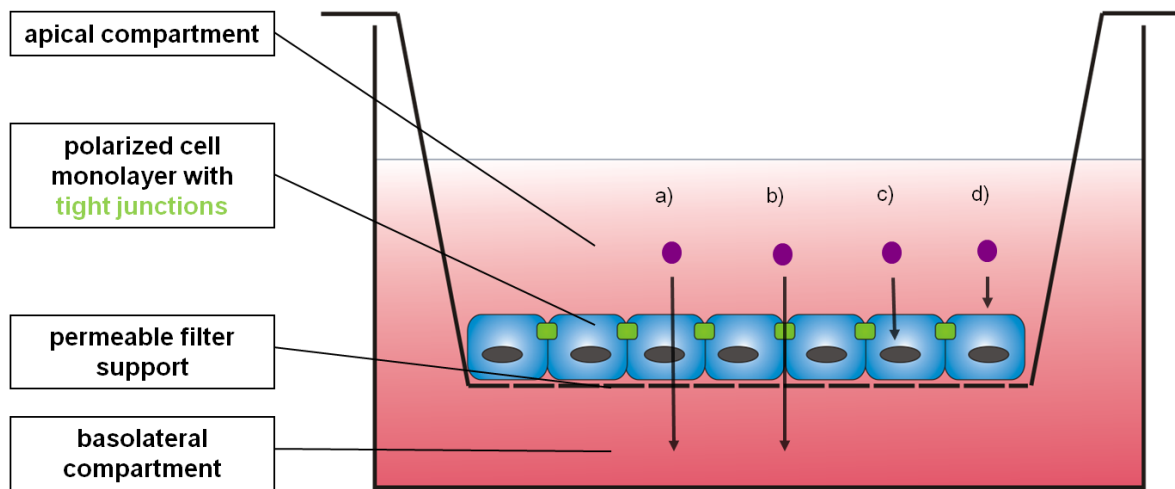


Figure 1.3. The Transwell system, containing of a filter insert and a permeable filter support, on which cells with characteristic epithelial traits are cultivated. With this model, nanoparticle transport through the cells (a), paracellular transport via opening of the tight junctions (b), uptake into the cell (c) as well as adsorption onto the cell surface (d) can be investigated.

Prior to transport experiments, the particles must be characterized in the physiological medium used for testing, as those engineered mostly metal oxide nanoparticles used in the NanoCare project are not adapted to cell culture testing.

2 Not ready to use – overcoming pitfalls when dispersing nanoparticles in physiological media

The data presented in this chapter have been published in parts as a research article in the journal Nanotoxicology:

Christine Schulze, Alexandra Kroll, Claus-Michael Lehr, Ulrich F. Schaefer, Karsten Becker, Jürgen Schnekenburger, Christian Schulze Isfort, Robert Landsiedel, Wendel Wohlleben: Not ready to use - Overcoming pitfalls when dispersing nanoparticles in physiological media. Nanotoxicology 2008, 2:51-61.

DOI: 10.1080/17435390802018378

Web-Link:

<http://informahealthcare.com/doi/abs/10.1080/17435390802018378>

Contributions:

I characterized the model polystyrene nanoparticle in the different media and contributed to the characterization of the metal oxide particles. Furthermore, I prepared the manuscript.

Alexandra Kroll, Karsten Becker and Jürgen Schnekenburger from Westfälische Wilhelms-Universität Münster, Gastroenterologische Molekulare Zellbiologie, Medizinische Klinik und Poliklinik B and Institut für Medizinische Mikrobiologie, performed the Endotoxine study and sterility testing of the nanoparticles.

Christian Schulze-Isfort (Evonic-Degussa GmbH, R & D Aerosil, Hanau, Germany) and Robert Landsiedel (BASF Aktiengesellschaft, Experimental Toxicology, Ludwigshafen, Germany) helped to interpret the results and partially characterized the TiO₂ B particle.

Wendel Wohlleben from BASF Aktiengesellschaft, Polymer Physics Research, Ludwigshafen, Germany, performed the Analytical Ultracentrifugations and helped characterize the metal oxide particles.

Ulrich F. Schaefer and Claus-Michael Lehr helped to discuss and interpret the results.

2.1 Abstract

Industrial nanoparticles are not developed to be compatible with in vitro cell culture assays which are carried out in isotonic solutions at physiological pH and often in the presence of proteins. The tendency of nanoparticles to deagglomerate or agglomerate is strongly sensitive to these parameters. The state of agglomeration and the protein corona bear an important influence on the level of toxic effects *via* the change of transport mechanisms and surface coating. Here we rigorously characterized the interaction of nanoparticles with physiological media for in-vitro nanotoxicology experiments. Beyond adsorption of proteins on metal oxide and polymeric nanoparticles, we quantified nanoparticle deagglomeration due to adsorbing proteins acting as protection colloids. We report on previously neglected, but indispensable testing of sterility and measures to ensure it. Our findings result in a checklist of pre-requirements for dispersion of nanoparticles in physiological media and for reliable attribution of potential toxic effects.

2.2 Introduction

Industrial NPs are not developed to be compatible with *in vitro* cell culture assays, as nano-suspensions use non-physiological pH values or cytotoxic stabilizing agents. Their tendency to deagglomerate or agglomerate is strongly sensitive to pH and ionic strength. For the use of NPs in *in vitro* assays, the dispersions must be isotonic, adapted to a pH of 7.4 and applicable in the presence of divalent ions and protein mixtures. The interaction of the NPs with the wealth of other components in the physiological media is one pitfall of nanotoxicology. Many individual aspects of NP dispersion and protein adsorption have been investigated recently [27-32], including the binding enthalpy of proteins on polymer particles [33] and the change of ζ -potential [30]. Due to the enormous colloidal polydispersity, size characterization constitutes in itself another major pitfall [34]. Ultrafine particles and agglomerates have to be quantified in an excess of proteins with 5 nm diameter (BSA monomer). Qualitatively, aqueous NP suspensions have been stabilized to prevent agglomeration by addition of BSA and FCS [31] and much enhanced dispersion has been observed for carbon nanotubes with a range of proteins [27, 29]. Here, the interaction of nanoparticles with physiological media for *in vitro* nanotoxicological experiments were rigorously characterized and the adsorption and drastic dispersing action of serum proteins with appropriate fractionating methods quantified. Also, the need of particle sterilization and methods to achieve this are presented.

2.3 Materials & Methods

Materials. The ingredients for phosphate buffer (PB; 50 mM; pH 7.4, 16 mM NaH_2PO_4 , 33 mM Na_2HPO_4), isotonic phosphate buffer (50 mM; pH 7.4, 10 mM NaH_2PO_4 , 39 mM Na_2HPO_4 , 2.4 mM NaCl) and Krebs-Ringer-Buffer (KRB, 114.2 mM NaCl , 3 mM KCl , 1.5 mM $\text{K}_2\text{HPO}_4 \times 3 \text{H}_2\text{O}$, 10 mM HEPES, 3.996 mM D-Glucose, 1.405 mM CaCl_2 , 2.562 mM MgCl_2) as well as bovine serum albumin (BSA), Penicillin, Streptomycin, Amphotericin B and sodiumazide were purchased from Sigma-Aldrich Chemie GmbH, Munich, Germany. Dulbecco's Modified Eagle's Medium

(DMEM without Phenolred, with L-Glutamine), Fetal Calf Serum Gold (FCS Gold) and DMEM were purchased from PAA Laboratories GmbH, Cölbe, Germany. The Kinetic-QCL® Kinetic Chromogenic Assay was bought from Lonza AG, Cologne, Germany.

Nanoparticles. The carboxylated 50 nm Polystyrene nanoparticles were from Polysciences Europe GmbH, Eppelheim, Germany. The CeO₂ C and TiO₂ B were synthesized in pyrogenic processes; ZrO₂ was synthesized and modified with an organic acid in solution. The nanoparticles were used as received without purification. The most relevant intrinsic properties are summarized in Table 2.1. The particle morphology and primary particle size are characterized without physiological media by monolayer TEM (Figure 2.1). Particle surface chemistry was determined by photoelectron spectroscopy (XPS) and crystallinity by X-Ray diffraction (XRD). The experimental details for those methodologies can be found in chapter 3.3. We find atomic concentrations of oxygen and metal in the ratio 2.2 (TiO₂ B), 2.6 (ZrO₂) and 2.0 (CeO₂ C). The solubility was determined by dispersing 10 mg/ml of the particles in water under stirring for 24h, removing the particles by centrifugation at 40,000 rpm, and finally determining the ion content in the supernatant by inductively coupled plasma optical emission spectroscopy (ICP-OES).

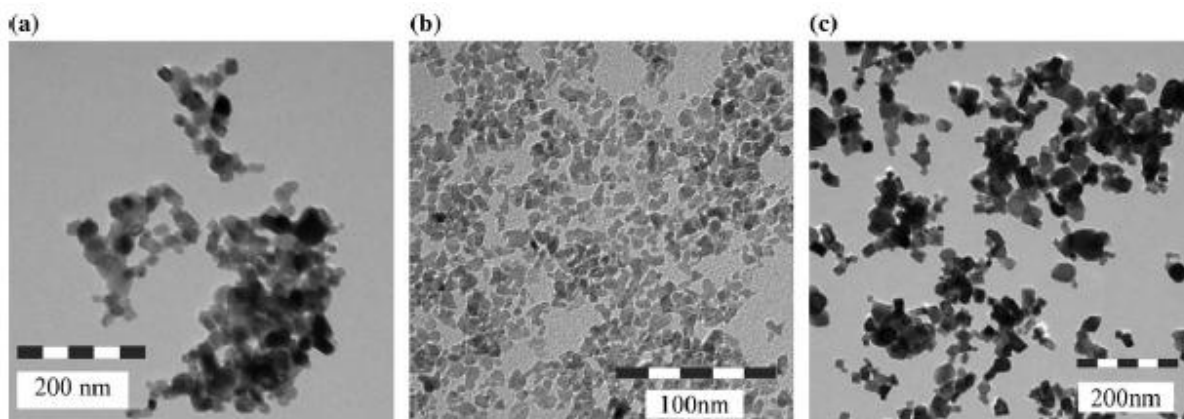


Figure 2.1. Monolayer TEM images of the nanoparticles, showing primary particles sizes of a) TiO₂ B 21nm; b) ZrO₂ 14nm; c) CeO₂ C 30nm.

Table 2.1. Physico-chemical properties of the used nanoparticles (values adopted from [35]).

Sample	Chemical composition; crystallinity	Mean primary particle size; morphology	Surface chemistry	Organic modification	Water solubility
TiO ₂ B	> 99.5 % TiO ₂ rutile and anatase, tetragonal	27 nm irregular but globular	O 58 % Ti 26 % C 14 % N 0.5 % Cl 1%	none	1 ppm
ZrO ₂	ZrO ₂ monoclinic Baddeleyite, tetragonal	14 nm irregular but globular	O 55 % Zr 21 % C 24 % Cl 0.6 %	organic acid	190 ppm
CeO ₂ C	> 99 % CeO ₂ Cerianite, cubic	70 nm irregular but globular	O 53 % Ce 26 % C 20 % Cl 0.6 %	none	<1 ppm

Dispersing nanoparticles in different media. Stock solutions contained a mass concentration of 1-10 g/L. For this purpose, the nanoparticles were weighed into snap-on lid glasses (diameter 20 mm, height 40 mm) and covered with 5-6 ml of dispersion medium. A small magnetic stirrer (length: 12 mm) was added and the glass covered with a lid. Stock solutions had to be stirred at 900 rpm for 1 hour. Then, aliquots could be taken and added to the already stirring dispersion medium to get the fi-

nal dilution. This dispersion was stirring for 24 h at room temperature and 900 rpm before use. If the particles were dispersed in rich media, the particles and all other devices had to be sterilized and contamination during the dilution step be avoided. Buffers and Media were used as follows: Millipore® water, phosphate buffer, isotonic phosphate buffer, Krebs-Ringer-Buffer, Dulbecco`s Modified Eagle`s Medium (DMEM without Phenolred, with L-Glutamine), Fetal Calf Serum Gold (FCS Gold) with varying concentrations of FCS.

Size and ζ -Potential measurements via Dynamic light scattering. For normal size and ζ -potential measurements, the nanoparticle dispersion (concentration 2.5 %) was diluted 1:100 in the dispersion medium and then measured with the Zetasizer Nano ZS (Malvern Instruments, Herrenberg, Germany). Size measurements were performed at 25 °C with an equilibration time of 1 min in disposable sizing cuvettes at automatic mode. Every measurement was performed 3 times with the automatic attenuator set and the data processed in general purpose mode. For ζ -potential determination, the model of Smoluchowski was used and the automatic measurements (10-100 runs) performed 3 times at a temperature of 25 °C and an equilibration time of 1 min. The attenuator and voltage were selected automatically and the data processed with monomodal mode.

Analytical Ultracentrifugation (AUC). The particle size distribution was determined by analytical ultracentrifugation (AUC) of ~500 μ L of a test substance preparation with 0.1 mg/ml of NPs. At the acceleration of up to 300,000 g used in AUC, solutes and nanoparticles sedimented into fractions that were separated according to their size in the range 0.5–100.000 nm. Simultaneous detection by synchronized optics quantified the amount and the diameter of each fraction independently [36]. When there was a low concentration of nanoparticles in a high-concentration protein medium, nanoparticles were easily discerned from sedimenting proteins because of their much higher density and resultant faster sedimentation of many orders of magnitude, and because of their higher re-

fractive index and high turbidity. We used a Beckman model XL ultracentrifuge (Beckman Coulter GmbH, Krefeld, Germany) that we modified for the online recording of sedimentation with turbidity, interference, and Schlieren or ultraviolet (UV) detection [37]. This modification allows the use of interference and turbidity optics with a ramped rpm-profile to quantify the amounts of ultrafine fraction (diameter <100 nm), fine fraction (100 – 1000 nm), and larger-scale material (>1 μm).

The evaluation of the AUC raw data incorporated the fractal morphology of nanoparticle aggregates and applied the fractional dimension of 2.1 together with the sedimentation relation as specified in Eq. (6) of the reference [38]. This value of the fractional dimension has been shown to be universal for all reaction-limited colloid aggregates [38, 39]. If in the specific test substance application preparation the fractional dimension of the aggregates were higher (lower), corresponding to a more compact (loose) structure of the aggregates, the retrieved particles sizes would shift to lower (higher) values.

The adsorption of BSA onto polymeric particles was quantified in density gradient experiments in a Schlieren-optics AUC [37]. Nycodenz was used as gradient medium, and the sample was added in 0.5 mg/ml concentration. It accumulated at the isopycnic point, where its buoyant mass corresponded to the local density determined by the local Nycodenz concentration. The Schlieren optics measures the derivative of radial concentration $dc/dr(r)$, the meniscus is left, the outer boundary of the cell is right, the column height is 1cm. A gaussian distribution of density fractions gives a positive-negative modulation of the positive-slope signal from the rising concentration of Nycodenz.

Sterilisation of glasses and nanoparticle dispersion for microbiological analyses. 10 ml glasses, lids and magnetic stir bars were washed twice with autoclaved, sterile filtered (Millipore GmbH, Schwalbach, Germany) bi-distilled water and once with 70 % ethanol diluted from 100 % ethanol with autoclaved, sterile filtered (Millipore®) bi-distilled water. The glasses and the magnetic stir bars (5x12mm) were then autoclaved for 20 min at 134°C and 2.5 bar/vacuum in a Varioklav 135S (H + P Labor-

technik GmbH, Oberschleißheim, Germany) whereas the lids were stored in 70 % ethanol in autoclaved 100 ml Schott bottles. Before use, the lids were dried in a laminar air flow and irradiated with UV light for 15'. A stir bar was placed into each glass which was then covered with a dried and irradiated lid before determination of the net weight. A small amount of TiO₂ B or CeO₂ C powder (~20 mg) was transferred into a glass under laminar air flow and the mass of the powder was determined. An appropriate amount of DMEM (10 % FCS) was added to the powder to yield a concentration of 3.2 mg/ml. To generate a 3.2 mg/ml dispersion of ZrO₂ (stabilized with an organic acid, 46 % w/v), the original dispersion was stirred on a magnetic stirrer for 1 h at 900 rpm and room temperature and 417 µl of the original dispersion were then added to 5.683ml of DMEM (10 % FCS) in a glass prepared as described above. The dispersions were stirred for 1 h at 900 rpm and then diluted 1:10 in DMEM (10 % FCS). The dilutions were stirred for another 24 h at 900 rpm and room temperature.

Sterilisation of nanoparticles for microbiological analyses. To test the suitability of standard cell culture antibiotics and wet antiseptics, particle dispersions were generated using DMEM containing Penicillin, Streptomycin, and Amphotericin B or 200 mM sodiumazide. Heat sterilization was performed in an H+P Varioklav 135S for 20 min at 134 °C and 2.5 bar/vacuum. A Biobeam 8000 (STS Steuerungstechnik und Strahlenschutz GmbH, Braunschweig, Germany) with a 137 Cs γ-ray source was used for γ irradiation.

Microbiological analyses. Microbiological analyses were performed at the Institute for medical microbiology at the Münster university hospital. Dispersions of ZrO₂, TiO₂ B, and CeO₂ C (320 µg/ml) were tested aerobically and anaerobically for sterility according standard procedures applying fluid and solid media under long-term cultivation [40].

Determination of endotoxin concentration. The Kinetic-QCL[®] Kinetic Chromogenic Assay (sensitivity range 0.005 EU/ml – 50.0 EU/ml) was used to determine endotoxin concentrations. The test was performed ac-

according to the manufacturer's instructions. The absorption was monitored using the microplate reader NOVOstar (BMG Labtech, Offenburg, Germany). Apart from testing pure dispersions of ZrO₂, TiO₂ B and CeO₂ C (320 µg/ml), nanoparticle dispersions were mixed with a standard endotoxin solution (0.25 or 0.5 EU/ml) in order to investigate the influence of the particles on the enzymatic reaction. The surface modifier of ZrO₂ was tested likewise. Four endotoxin standards (5-0.05 EU/ml) were used to generate a standard curve to calculate endotoxin concentrations. Therefore, Trend2k (Thomas Risi Softwaredevelopment, Vilsheim, Gemrany) was applied to calculate fifth degree polynomials describing the development of absorption of the standards. The y-values (in seconds) of the polynomials at x = 0.2 were calculated and used to generate a logarithmic equation describing the relationship between the standard endotoxin concentrations and the time after which the absorption had increased by 0.2 units. This equation was used to calculate the endotoxin concentrations of the nanoparticle dispersions. Values < 0.005 EU/ml were equated with 0 as they lie below the detection limit of the assay.

2.4 Results & Discussion

Polystyrene nanoparticles. Before studying the specific pitfalls with metal oxide NPs, the test systems were established by characterization of model NPs (polystyrene NPs from Fluoresbrite, carboxylated, Ø 50 nm; c50) in size and ζ-potential via Dynamic Light-Scattering in different dispersion media with increasing complexity (Table 2.2). In Millipore® water, the hydrodynamic diameters of the particle were 49.5 ± 1.7 nm and had a ζ-potential of -64.4 ± 4.2 mV. In phosphate buffer (0.05 M; ionic strength 0.116 M), and isotonic phosphate buffer (0.05 M; ionic strength 0.154 M) the c50 particle showed a slightly higher size of 67 ± 3.5 nm or 57.5 ± 1.7 nm, respectively. The ζ-potentials increased to -58.6 ± 0.8 mV and to -51.2 ± 3.9 mV when isotonized. When dispersed in Krebs-Ringer-Buffer (KRB), the c50 agglomerated and showed a size of more than 3000 nm. Also, the ζ-potential increased nonlinear to -29 ± 1.4 mV (Figure 2.2).

Since the presence of Ca^{2+} ions is a significant difference between phosphate buffers and KRB, CaCl_2 -titrations in water and both phosphate buffers were performed and the sizes of the particles at concentrations of 0-5 mM Ca^{2+} determined. The experiments revealed the Ca^{2+} as main factor in the agglomeration of c50 in KRB. At CaCl_2 concentrations from 0.5 to 2.5 mM Ca^{2+} (CaCl_2 concentration in KRB: 1.4 mM), particles agglomerated in all buffers tested (Figure 2.3).

Addition of bovine serum albumin (1 %) lead to complete deagglomeration (hydrodynamic diameter decreased to 70.2 ± 1 nm) and a further ζ -potential increase up to -10.4 ± 2.7 mV (for comparison: 1 % of BSA in KRB without particles had a ζ -potential of -5.6 ± 2.7 mV). The slight increase in diameter compared to the values in water and the similar ζ -potential in relation to the ζ -potential of BSA in KRB without particles suggested a protein coating of the particles.

Table 2.2: Increasing complexity of the dispersion media used to find the reason for agglomeration of the c50 model polystyrene particle in KRB

	H ₂ O	PB (pH 7.4)	PB, isotonic (pH 7.4)	KRB	KRB + 1 % albumin
pH	-	+	+	+	+
isotony	-	-	+	+	+
[Ca ²⁺]	-	-	-	+	+
presence of protein	-	-	-	-	+

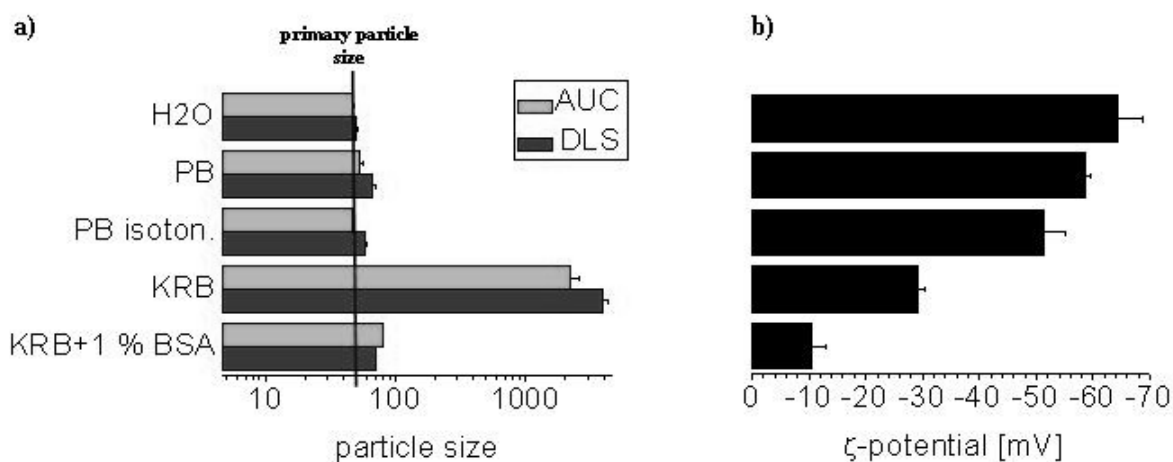


Figure 2.2. Sizes and ζ -potentials of c50 NPs in different dispersion media. a) hydrodynamic diameters of the c50 NPs, measured via Dynamic Light Scattering (DLS) and Analytical Ultracentrifugation (AUC); the black line corresponds to the primary particle size. In Milipore water and both phosphate buffers, the sizes ranged around 50-70 nm. In KRB, large agglomerates occurred, which were not present when dispersing the particles with KRB containing 1 % of BSA. b) ζ -potentials of the particles in the same buffers.

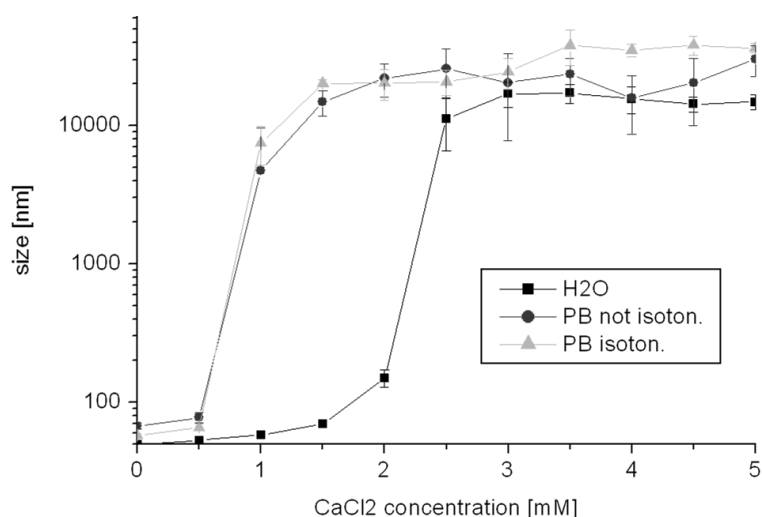


Figure 2.3. Ca²⁺-depending size of a carboxylized 50 nm polystyrene particle in different dispersion media.

To prove this hypothesis, a density gradient ultracentrifugation [36] was performed. The density gradient fractionated the sample according to the buoyant density and hence was direct evidence of the chemical composition, but insensitive to diameters. In repeated experiments, no signal at the density of pure polystyrene (1.57 g/cm^3) was detected, but a strong signal at $1.26 \pm 0.06 \text{ g/cm}^3$, corresponding to composite particles of $\sim 40/60$ BSA/PS (Figure 2.4). The width of the distribution indicated a distribution of densities; hence the adsorption was not uniform. The non-uniform adsorption was reflected also by the significant increase and broadening of the particle sedimentation velocities upon mixing with BSA (data not shown). From the velocity increase, an adsorption of 20–60 wt% BSA on the PS core was deduced, in good agreement with the density gradient approach. Finally, the binding of protein onto the carboxylated particle surface was monitored by a loss of freely dispersed BSA monomer and dimer as quantified by their characteristic sedimentation coeffi-

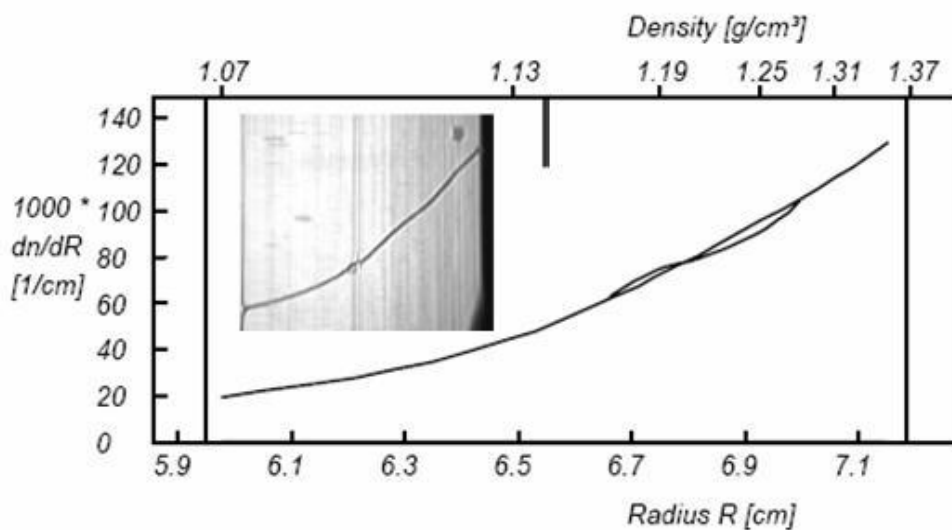


Figure 2.4. Density gradient measurement of the density of polystyrene NP c50, dispersed in KRB + 1 % BSA. The left margin corresponds to the meniscus at a density of 1.07 g/cm^3 , the right to the boundary of the cell at 1.36 g/cm^3 , i.e. the force is directed to the right. The particles accumulate at their isopycnic point, where their density corresponds to the density of the gradient medium, in this experiment around 1.20 g/cm^3 . Unprocessed CCD image in the inset: The Schlieren-AUC measures $dc/dr(r)$ and a gaussian distribution of density fractions induces a positive-to-negative modulation (original) superimposed with the positive-slope signal from the rising concentration of the gradient medium. (see materials and methods)

cients (data not shown).

Taken together, these data were the first direct and quantitative in-solution evidence of adsorption of proteins on (polymeric) NPs (Figure 2.4) with ensuing dispersing action, as seen by DLS and AUC in excellent agreement. (Figure 2.2a).

It is known that electrostatically stabilized NP dispersions with a ζ -potential converging to zero become unstable [34, 39]. That is exactly what happens when dispersing the c50 in KRB containing 1.4 mM CaCl_2 : the electrostatic stabilization is not sufficient to avoid agglomeration anymore. Presumably, the deprotonated, negatively charged carboxyl groups at the particle surface interact directly with the positively charged Ca^{2+} -ions. The increase in size of c50 when dispersed in KRB containing 1 % of BSA was due to covering the particles with albumin. The coating of particles with BSA was shown with colloidal gold [41], polymer colloids [33, 42] and aluminum hydroxide [43] particles already. The originally electrostatically stabilized particles can be dispersed in media containing Ca^{2+} via a switch to a steric stabilization by addition of albumine [39].

Metal oxide nanoparticles. The results found for model particles were then transferred to much less defined metal oxide NPs. In cell culture the addition of serum to the culture medium, mostly fetal calf serum (FCS), is mandatory for many cell lines to guarantee an ideal cell growth [44]. Therefore, FCS replaced BSA as the protein component in the test systems. Dry CeO_2 C and TiO_2 B particles (both used as manufactured without any modifications; this condition will be referred to as 'naked') and predispersed ZrO_2 (organically modified and stabilized with an organic acid with a molecular weight of 180 g/mol) were dispersed in different physiological media and Millipore[®] water to test which medium suits best for *in vitro* assays. The NPs were weighed into a snap-on lid glass, covered with the dispersion medium and stirred for 24 h without any ultrasound treatment. Particles sedimented immediately in media free of proteins. However, dispersions were stable in protein-containing media for the ζ -potential measurement period. The ζ -potentials of all particles in protein-containing buffered media were very similar to the ζ -potentials of parti-

cles in pure buffered media. Particles in ion free water showed completely different ζ -potentials (Figure 2.5).

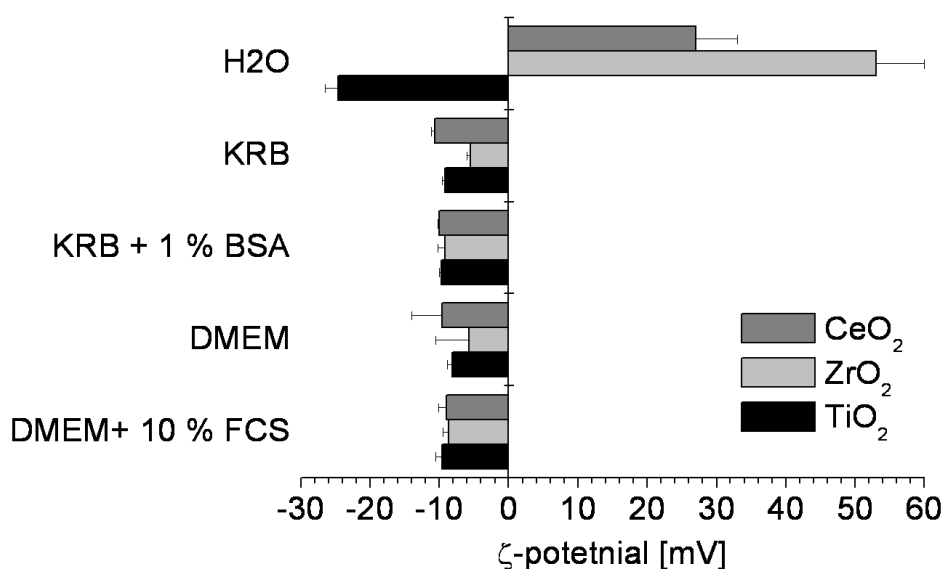


Figure 2.5. ζ -potential of CeO₂ C, TiO₂ B and ZrO₂ in different dispersion media. Except in water, the ζ -potentials of the particles are more or less the same. No difference can be seen between KRB and DMEM with or without addition of proteins, i.e. from this measurement no adsorption of the proteins onto the particle surface can be concluded.

The ζ -potential measurements gave no direct evidence for a protein coating of the inorganic industrial particles tested. However, the stabilization of particle dispersions by added proteins indicated a coating. The switch of the originally positive ζ -potentials of CeO₂ C and ZrO₂ in Milipore water to negative values in media containing 10 % FCS was in good correlation to the findings of Limbach et al., but they postulated that this switch leads to agglomeration of CeO₂ C and also other metal oxide NPs because of a loss of electrostatical stabilization [28]. Contrary to these results a correlation of particle size and protein concentration in the dispersions was seen in this work (see Figure 2.6).

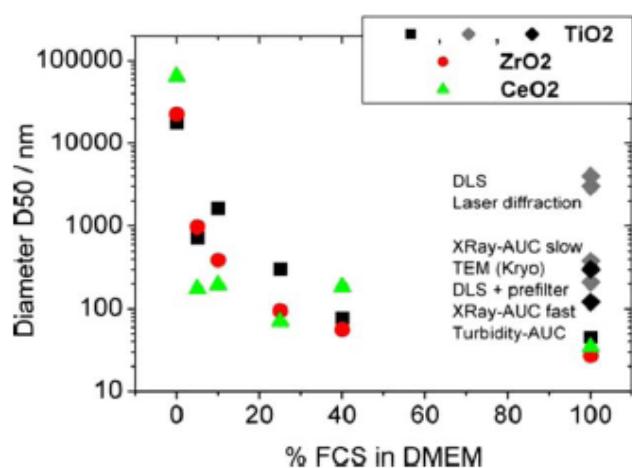


Figure 2.6. Diameters of CeO₂ C (green triangles), TiO₂ B (black squares) and ZrO₂ (red dots) in DMEM with different concentrations of FCS from turbidity-AUC. d₅₀ values represent the weight-average agglomerate size. In complete reproductions of preparation and measurement the values scatter by $\pm 30\%$. In all cases, the particle size decreases with increasing concentration of FCS, which shows its disagglomerating properties, leading to significant fractions of ultrafine particles in the dispersions (lines are guides to the eye). Grey diamonds come from inappropriate methods, black diamonds show differing results from several valid approaches, all on TiO₂ B in 100% FCS.

Size characterization constitutes a major pitfall due to the enormous colloidal polydispersity [34]. Ultrafine particles (NPs < 100 nm in diameter) [45] and agglomerates have to be quantified in a hundredfold excess of proteins with 5 nm diameter (BSA monomer) plus salts. The most widespread methods of characterization on the example of TiO₂ B in pure FCS were cross-checked (Figure 2.6, diamonds). The nominal working range of DLS does cover all components, but even after prefiltering (450 nm pore size) DLS fails to detect the proteins that constitute 99% of the sample. The same is true for laser diffraction, whose lower working limit is exceeded. TEM images the NPs and agglomerates, but with comparably low statistics. Even without particles, we found that drying and/or cryo-preparation of FCS induces artefacts [34]. Optical AUC [36, 38] is the only method that detects also the sub-10-nm proteins with correct molar masses and concentrations (found in FCS 33mg/ml at 65 kDa and 120 kDa (corresponding to 4–5nm), attributed to BSA monomer and dimer), but in the ultrafine particle range the turbidity-AUC has its uncertainties

due to the Mie correction of intensities. X-Ray-AUC needs no such correction and detects selectively inorganic components, but requires exceedingly high concentrations of particles (~1%). Note that only accelerations above 1000g enable the detection of ultrafine components in sedimentation (fulfilled for X-ray-AUC fast (6000 rpm), not for slow (1500 rpm)) (Figure 2.6).

It is beyond the scope of this contribution to settle the size characterization issue. The results presented here suggest that DLS, laser diffraction and slow-speed sedimentation cannot determine whether an ultrafine fraction is present or not. Several valid methods confirm that FCS deagglomerates NPs to a significant fraction of ultrafine particles with low energy input by stirring only, independent from an often used ultrasound treatment.

The deagglomeration scales with the protein content. In Dulbecco's Modified Eagle's Medium (DMEM), all of the tested NPs were strongly agglomerated and no significant fraction of ultra fine particles could be determined (Figure 2.6). With increasing concentration of FCS, the mean particle size distribution (d_{50}) decreased, and a significant effect could be seen even in the presence of 5 % FCS. Also, large agglomerates were disintegrated, indicated by the declining d_{90} (data not shown).

The ZrO_2 used was stabilized and coated with an organic acid and well dispersible in ion free water, but agglomerated in DMEM, due to a change in pH. In 100 % FCS, the dispersion was as good as in pure water (Figure 2.7a). This behaviour was very similar to the dispersion pattern of carboxylated polystyrene particle: well dispersible in water, strong agglomeration in the presence of salts and dispersible again by addition of proteins. The naked TiO_2 B particle revealed a different dispersion pattern: hardly dispersible in water, wetted but still agglomerated in DMEM (Figure 2.7b). With increasing FCS-concentration, particles deagglomerated and at FCS-concentrations above 40 %, an ultrafine dispersion was reached. Two different dispersion patterns are evident: a) the naked NPs (CeO_2 C, TiO_2 B) and b) the particles modified with an organic acid (ZrO_2

and polystyrene latex). Dispersion patterns seem to depend mostly on the particle's surface modification, irrespective of the particle's bulk material.

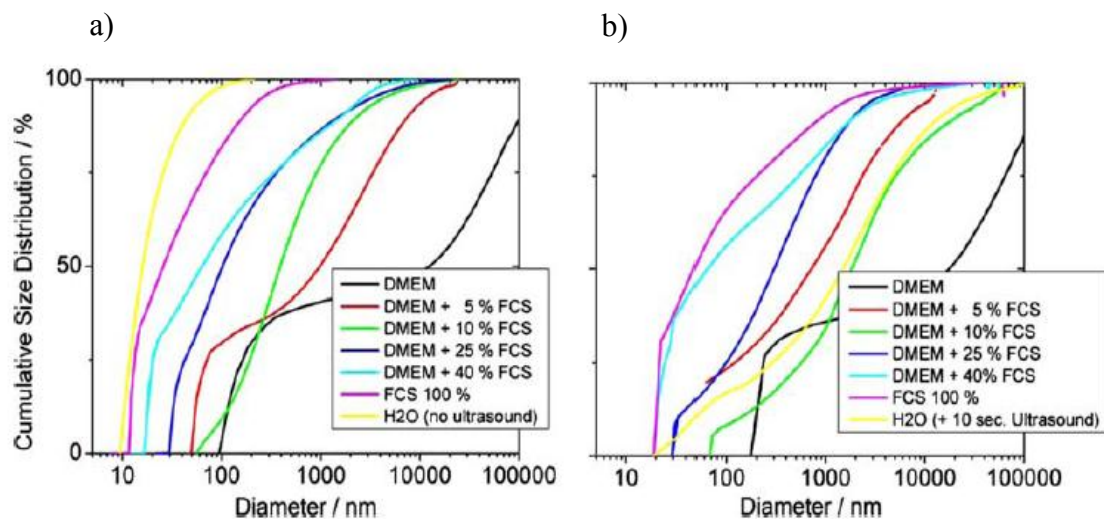


Figure 2.7. Size distribution of a) ZrO_2 (stabilized with an organic acid) and b) TiO_2 (unmodified) by turbidity-AUC. The ZrO_2 particle is well dispersible in water (yellow line) and strongly agglomerating in the high salt DMEM (black line), whereas the TiO_2 is hardly dispersible in water, at all. With increasing concentration of FCS, the particle sizes decrease at both particles.

It has been reported previously that metal oxide NPs mixed with a BSA solution showed a uniform ζ -potential, irrespective of their 'naked' chemical surface modification. This effect was thought to result from a BSA NP surface coverage [30]. Aqueous NP suspensions have been stabilized to prevent agglomeration by addition of BSA and FCS [31]. No systematic study on the effect of protein adsorption on the NP deagglomeration tendency has been published yet. Natural organic matter act as effective wetting and dispersing agents for carbon nanotubes, often more effective than synthetic head-tail surfactants [27]. The wetting and dispersing effect of interface-active proteins (among them HSA) has very recently been shown to be effective to debundle agglomerated single walled carbon nanotubes in aqueous suspension, which was technically a very demanding task before [29]. Similar to model nanoparticles, where direct evidence of both adsorption (Figure 2.6) and ensuing dispersion were pro-

vided (Figure 2.5), we identified adsorbed protein functioning as protection colloids as mechanism for the observed dispersion effect (Figures 2.2 to 2.4) [39]. Especially albumines are interface active and show at least five different binding sites for an entire variety of molecules (inorganic minerals, proteins, polar organic molecules, fats, and chiral centers) [46]. These findings are in agreement with and complementary to the previous reports of protein adsorption to NPs and carbon nanotubes.

Microbiological aspects. The dispersion of NPs in buffered solutions of proteins and nutrition allows the growth of contaminating microorganisms. Since these organisms as bacteria, yeast or other fungi and their metabolism products interfere with most standard toxicity test systems, NP preparations have to be sterilized.

For the optimization of the sterilization procedure the germ load of the used industrially produced and processed NPs was analyzed. Dispersions of ZrO_2 , TiO_2 B, and CeO_2 C were tested aerobically and anaerobically for sterility according standard procedures applying fluid and solid media under long-term cultivation [40]. The prominent bacteria identified were *Micrococcus luteus* [47, 48] and *Bacillus sp.* [48, 49]. *M. luteus* is a Gram positive, spherical, saprotrophic spore-forming bacterium that belongs to the *Micrococcaceae*. [50]. Bacteria of the genus *Bacillus* are Gram-positive, rod-shaped, spore-forming, and are either facultative or obligate anaerobes.

Due to the presence of microorganisms in the NPs analysed, different standard methods for sterilization of cell culture materials to aliquots of dispersed ZrO_2 , or TiO_2 B and CeO_2 C were applied. In order to reduce the microorganism burden of the particles, the addition of antibiotics/antimycotics, chemical sterilisation (sodiumazide, NaN_3), heat sterilisation (134 °C, 2,5 bar), and sterilisation by ionizing irradiation (30 Gy) was chosen. The sterilisation method should be effective to kill microorganisms without altering NP properties and without influencing the biological test systems.

NPs sterilized with the various methods were dispersed in cell culture medium and tested for contaminating microorganisms as described above. According to these standardized analyses, only γ irradiation was capable of eliminating all microorganisms identified in dispersions of untreated NPs. It has been shown that spores are often more resistant to γ irradiation than metabolically active bacteria [51], however, the underlying mechanism is still unclear [52]. The amount of endospores and the general level of contamination in the set-up appear to be sufficiently low to be eliminated by γ irradiation.

As γ rays have the capacity to ionise atoms, the effect of irradiation on nanomaterial properties was characterized. Irradiated and untreated dispersed ZrO_2 , or TiO_2 and CeO_2 C powders were analysed with regard to surface chemistry (ζ -potential and X-ray Photoelectron Spectroscopy, XPS), bulk structure (X-ray diffraction, XRD) and dispersion behaviour (AUC). None of the four methods detected any significant change after irradiation, hence γ -rays can serve as standard sterilisation procedure since neither surface nor the structure of our particles was altered.

Beside microorganism contamination itself test systems can also be affected by endotoxins, biologically highly active bacterial molecules often present in materials after a bacterial contamination. In 1894, endotoxin was first described as a heat-stable toxic substance that was released upon disruption of microbial envelopes [53]. Today, endotoxin is widely defined as component of the outer cell membrane of Gram negative bacteria being made up by lipopolysaccharides with lipid A being the bioactive component [54]. Inoue et al. (2006) have reported that endotoxins aggravate the inflammatory effect of carbon NPs in mice when applied simultaneously [55], on the one hand while nanometre sized TiO_2 B has been shown to adsorb endotoxins and cause proinflammatory reactions [56]. Furthermore, the determination of endotoxin concentration is a standard procedure in characterizing particulate matter or dust when studying health risks resulting from environmental [57] and work-place exposure.

To determine the endotoxin concentration of dispersed and powder NPs the Limulus amoebocyte lysate (LAL) test (Kinetic-QCL[®] Kinetic Chromogenic Assay; Lonza) was used. Dispersions of ZrO₂, TiO₂, and CeO₂ C (32 µg/ml) were first tested with and without added standard endotoxin concentrations to determine the influence of the nanomaterial on the enzymatic assay. The ZrO₂ organic surface modifier was tested likewise.

Nanoparticles reduced the measured endotoxin concentrations by more than 50% (TiO₂ B, CeO₂ C) or about 70% (ZrO₂, organically modified). As the particles do not decrease the measured absorption at 405 nm, this effect must be due to a partial inhibition of the enzymatic reaction (Figure 2.8). Also the ZrO₂ surface modifier (OM) contributes to the effect on the endotoxin test, as an amount of OM diluted in cell culture media equivalent to the amount present in the tested particle dispersions completely abolishes a detectable reaction. However, the particle bound surface modifier showed a minor effect on the endotoxin test system.

According to Friberg (1987), the average endotoxin concentration in human plasma is 6 pg/ml (0,07 EU/ml) which is half of the theoretical endotoxin concentration during a pyrogen reaction [58]. The endotoxin concentration measured in the particle dispersions is well below the detection limit of the assay (0,005 EU/ml \triangleq 0,5 pg/ml). Even taking into account the inhibitory effect of nanoparticles on the test system the endotoxin concentrations of NP dispersions were below a critical limit. This result was expected as we did not detect any gram⁻ bacteria in the particle dispersions.

Overall, we have identified γ irradiation as method of choice to efficiently sterilize dispersed and powder NPs for the use in physiological media without changing material properties and without disturbing the *in vitro* test systems.

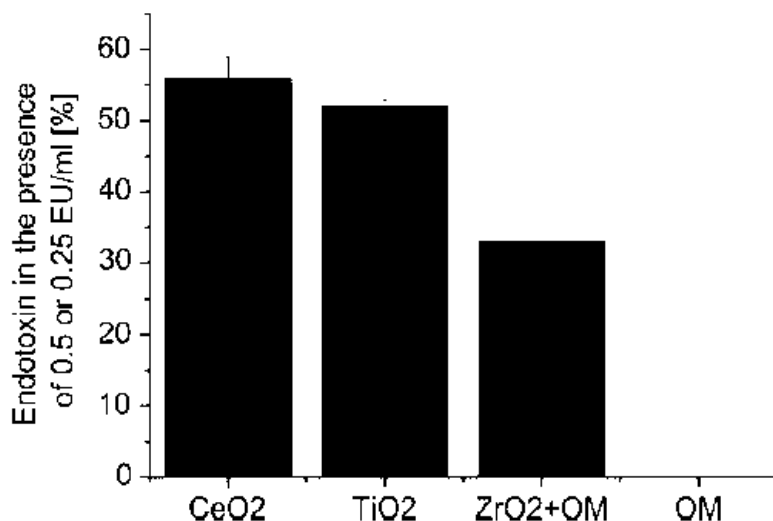


Figure 2.8. Influence of CeO₂ C, TiO₂ B and ZrO₂ (org. mod.) dispersions on the Kinetic QCL®-Assay; CeO₂, TiO₂, ZrO₂ (org. mod.) reduce the reaction rate to about one half to one third of the standard, the organic modifier (OM) applied to ZrO₂ particles completely inhibits the reaction when used in a concentration equivalent to the concentration in the ZrO₂ dispersion. 1 EU/ml \triangleq 0.1 ng/ml (*E. coli* 055:B05 endotoxin)

Furthermore, our data show that particles should be tested for endotoxins for *in vivo* and *in vitro* testing to prevent endotoxin dependent results of toxicity tests. The applied Kinetic-QCL endotoxin assay is suitable for measurement of NPs endotoxin concentration, however, the influence of NPs and possible surface modifiers on test results of the endotoxin assay needs to be considered when designing assays controls and interpreting absorption data. Based on these data and the relevant literature the use of NPs is recommended only if the endotoxin contamination is below 0,5 pg/ml, the detection limit of the assay.

The three nanomaterials tested in the frame of this study do not contain endotoxin in an extent detectable by the assay and exceeding the average concentration in human plasma and may therefore be used for *in vivo* and *in vitro* testing.

2.5 Conclusion

Many facets of preparation of nanoparticle dispersions have to be taken into account before physiological assays with NPs can be correctly interpreted. It is not sufficient to characterize the intrinsic properties of the nanomaterial – such as chemical composition and crystallinity, primary particle size and morphology, surface chemistry and charge, organic modification and water solubility.

The necessary information beyond intrinsic properties that one will need when working with NPs in physiological media is summarized in a checklist:

Dispersion issues

- dispersion protocol
- agglomerate size distribution and agglomeration state
- ζ -potential
- wettability and tendency to agglomerate/deagglomerate due to adsorption of solvent compounds
- adsorption of solvent compounds with possible influence on passivation, solubility, recognition.

Microbiological issues

- sterility
- endotoxin concentration
- endotoxin test reliability

By application of these topics characterized dispersions of particles for in vitro toxicity tests become available and reliable experiments can be performed.

To summarize the results, the drastic dispersing activity of fetal calf serum mixed with various types (polymer and metal oxide) of NPs that are either naked or organically modified was quantified. In pure serum, NPs were deagglomerated down to significantly nanosized dispersions, presumably by adsorption of proteins functioning as protection colloids. To complement this result, the first in-solution quantitative evidence of ad-

sorption of proteins on (polymeric) NPs with ensuing dispersing action was reported, in excellent agreement of several fractionating and integral methods.

Furthermore, evidence of inadvertent microbial contamination of standard NP test substances was provided, a source of false interpretation of supposed nano-effects. The γ irradiation as appropriate sterilization treatment was identified and used for further cell related testing. A comprehensive but feasible checklist to guarantee reproducible and reliable *in vitro* studies with inorganic NPs was proposed.

The recommendations expressed here are based on experimental findings and have implications for cell culture nanotoxicology. Do observed effects truly arise from the particle itself? With the above checklist, the pitfalls arising when dispersing NPs in physiological media to use them in *in vitro* assays can be overcome.

3 Intrinsic physico-chemical properties of CeO₂ nanoparticles do not mirror their biorelevant protein adsorption

The data presented in this chapter have been submitted partially as a research article in the journal ACS Nano:

Jens Schaefer, Christine Schulze, Elena E.J. Marxer, Ulrich F. Schaefer, Wendel Wohlleben, Udo Bakowsky, Claus-Michael Lehr: Intrinsic physico-chemical properties of CeO₂ nanoparticles do not mirror their biorelevant protein adsorption, ACS Nano, submitted

Contributions:

I performed the BCA assays, the corresponding mathematic modeling and prepared the manuscript.

Jens Schaefer, Elena Marxer and Udo Bakowsky from Philipps-University Marburg, Department of Pharmaceutics and Biopharmacy, Marburg, Germany, performed and interpreted the TEM, AFM and AFS measurements and helped to prepare the manuscript.

Wendel Wohlleben from BASF SE, Polymer Physics Research, Ludwigshafen, Germany, carried out the AUC experiments and the particle characterization.

Ulrich F. Schaefer and Claus-Michael Lehr helped to discuss and interpret the results and to prepare the manuscript.

3.1 Abstract

As engineered nanomaterials like CeO₂ particles reveal novel properties compared to the bulk material, also their toxicity is a major issue. Once they entered the body, they can interact with the physiological surroundings, i.e. also with proteins. This particle-protein interaction might lead to altered reactions concerning the particles, influencing their bio-persistence in the body. Hence, the investigation of protein adsorption onto those particles is of great importance. We investigated and compared the protein adsorption of Bovine Serum Albumin to three CeO₂ nanoparticles with only slightly different physico-chemical properties with Atomic Force Spectroscopy, Analytical Ultracentrifugation and BCA-assay. All adsorption processes could be fitted with a sigmoidal mathematic model, revealing differences in half-maximal adsorption for especially one of the three particles. Clearly, particles of the same bulk material do not necessarily reveal the same adsorption pattern for proteins, and the state of agglomeration must be taken into account to interpret the results correctly. We also showed that the protein might alter its shape during adsorption process specifically for the different particles tested. We conclude that even small differences concerning particle properties can lead to different protein adsorption and hence might provoke different reactions in the body. This means that testing of one particle of a bulk material as reference is not enough to determine the potential toxicity of nanomaterials.

3.2 Introduction

After proof of protein adsorption for a model particle and strong indications for protein adsorption on metal oxide particles, further investigations were performed to prove protein-particle interaction also for the metal oxide particles.

Only a small fraction of 1 % or less of an inhaled nanomaterial dose translocates into the blood stream [5], but due to bio-persistence issues that fraction also must be considered. Biopersistence may be influenced by protein adsorption of serum albumin after uptake into the blood system, and therefore this has to be investigated in the evaluation of toxic effects of nanoparticles.

The Dawson group has pioneered structure-property-relationships in protein coronas during the last few years [59, 60], and the biophysics of adsorbed proteins has been reviewed recently [61]. The majority of the few studies on metal oxides found adsorption of albumins (in serum) or humic acid (in soil), ensuing increased dispersibility [61, 62]. Cedervall et al. investigated the protein corona from serum, albumin and fibrinogen on polymeric nanoparticles using methods like microcalorimetry and surface plasmon resonance technique [33]. Recently Nienhaus and colleagues studied the adsorption of albumin in great detail, including on/off rates, adsorption affinity and monolayer saturation on inorganic fluorescent nanoparticles, using fluorescence correlation spectroscopy [63]. That match of material and method was powerful because it exploited the specific fluorescence properties of bespoke core-shell nanoparticles, but in general it is not applicable to industrially relevant nanomaterials.

Therefore, universally applicable methods were chosen and the extent of protein adsorption from Fetal Calf Serum (FCS) and from the dominating Bovine Serum Albumine (BSA) as the trigger of biokinetics and recognition with ensuing toxic effects were investigated intensively. Atomic Force Microscopy (AFM) was performed to directly analyze protein-particle interactions, as well as the Bicinchoninic Acid (BCA) protein quantification assay as an indirect method or Analytical Ultracentrifugation (AUC) to

examine the level of agglomeration correlated with the protein corona. We concentrated on three CeO₂ nanoparticles with very similar physico-chemical characteristics to see if those traits correlate to a specific protein adsorption pattern.

CeO₂ nanoparticles (CeO₂ NPs) are marketed as oxidative catalysts in self-cleaning surfaces in ovens [64], are being field-tested as catalytic diesel fuel additives [65] and find application as abrasive for chemical-mechanical polishing in electronic chip wafer production. The effect of CeO₂ particles from e.g. diesel fuel or from abrasion of CeO₂ containing coatings exposed to the environment was recently analyzed by van Hoecke et al. [66]. They investigated three different sizes (14, 20 and 29 nm) of CeO₂ particles in different aquatic toxicity tests. The differences in toxicity could not be explained by a direct effect of dissolved Ce-ions or CeO₂ nanoparticles uptake or by physical effects such as light restriction. Additionally they found that the particle properties - especially the higher surface area of smaller particles - have an influence on the toxicity of CeO₂ NPs.

3.3 Materials & Methods

Materials. Phenyltrimethoxysilane (Dynasylan® 9165) and 3-aminopropyl-triethoxysilane (Dynasylan® AMEO) were a gift from Degussa GmbH, Düsseldorf, Germany. N,N-Diisopropylethylamine, and Cyanuric Chloride were purchased from Sigma-Aldrich Chemie GmbH, Munich, Germany. Trichloromethane and methanol were purchased from Carl Roth GmbH + Co. KG, Karlsruhe, Germany. Water was double distilled prior to use. AFM tips CSC 37/noAl and NSC16/AIBS were purchased from Micromasch, Estonia. The BCA-Kit (Bicinchoninic Acid Kit for Protein Determination) and all Bovine Serum Albumin derivatives (Bovine Serum Albumin, purity 96 %, Bovine Serum Albumin, purity 99 %, Bovine Serum Albumin isothiocyanate conjugate) were purchased from Sigma Aldrich, Fetal Bovine Serum Gold came from PAA Laboratories GmbH, Cölbe, Germany.

Physicochemical characterisation of particles. The hydrodynamic diameters of metal oxide nanoparticles were determined by Dynamic Light Scattering (DLS) using a Zetasizer Nano ZS from Malvern Instruments (Herrenberg, Germany) equipped with a 10 mW HeNe laser at a wavelength of 633 nm at 25°C, essentially as described previously [67]. Scattered light was detected at a 173° angle with laser attenuation and measurement position adjusted automatically by the Malvern software. Values given are the means +/- standard deviation of three independent experiments with each experiment including three measurements of the same sample with at least 10 runs each, as determined by the zetasizer. The ζ -potential of the nanoparticles was determined by Laser Doppler Electrophoresis (LDE) using a folded capillary electrophoresis cell of the Zetasizer Nano ZS at 25°C, the light signal detected at a 17° angle. The average value was calculated with the data of three times 10 runs +/- standard deviation.

TEM-imaging. A carbon coated 300 mesh tem grid was dipped into a dispersion with a concentration of 0,1 mg/ml in isopropanol of the CeO₂ particles. The crystal structure and crystalline appearance was visualized using TEM-imaging on a Jeol JEM-3010 TEM (Jeol Ltd., Tokyo, Japan) with 300.000 V.

XRD crystallinity measurement. Crystallinity was determined by X-ray diffraction (XRD). The intensity of the diffracted x-ray beam was recorded by a D8 Advance (Fa. Bruker/AXS) as a function of the diffraction angle ($2^\circ < 2\theta < 150^\circ$). Quantitative phase analysis was performed using Rietveld refinement.

XPS detection of particle impurities and surface modifications. Impurities and surface modification were determined by X-ray photoelectron spectroscopy (XPS) with a Phi XPS 5500 system with 300 W monochromatic Al- K alpha radiation, pass energy for surveys 117 eV (measurement time of 45 min), detailed spectra at 23.5 eV (measurement time of 6 min). Evaluation was performed by CasaXPS 2.3.15, based on the Phi standard-sensitivity factors, with Shirley background subtraction and

peak shape fits as sum of 90 % Gaussian and 10 % Lorentzian. Information depth is limited to the surface 10 nm of the material. We performed two measurements per sample, each integrating over 0.5 mm². The results in % are derived from relative concentration of elements and their chemical bonds from line shape analyses.

TOF-SIMS characterization of particles. Static TOF-SIMS spectra were recorded using a TOF-SIMS V spectrometer (Iontof GmbH, Germany). A pulsed mass-filtered primary ion beam of 25 keV singly charged bismuth (Bi⁺) was used. This primary ion beam, resulting in a spot size of typically 5 μm on the sample surface, was raster scanned over an area of 250 x 250 μm to record spectra of positive and negative secondary ions. The rastered area integrates over more than 10⁶ particles. The primary ion dose density was always kept well below 10-12 ions cm⁻² and thus in the static SIMS regime. To prevent charging of the sample surface, a low-electron energy flood gun was used. The sample particle sediments were prepared for SIMS analysis by their placing on clean silicon wafers. On the thus prepared sample positions, no silicon wafer secondary ion mass signal could be detected any more, confirming that the sample layer thickness well exceeded the SIMS information depth of typically 1-3 nm.

Contact angel measurement. A thin planarized nanoparticle film of 1mm thickness was immobilized with a 100μm thick glue film on a PTFE-foil. After removal of the non immobilized powder the sample was treated with filtered nitrogen. The contact angles were measured with drops of water, formamide and diiodomethane. The drops were imaged onto a CCD and contact angles were extracted by standardized software.

AFM measurements. *AFM tip calibration.* AFM tips (CSC 37/noAl, MicroMasch, Estonia) were mounted to an atomic force microscope (Nanowizard®, JPK Instruments, Berlin, Germany). A force spectroscopy experiment was performed on purified glass to determine the sensitivity of the setup. For this, glass was presumed to be not indentable. The spring constants of the AFM tips were determined using the built-in algorithm which relies on a method described by Hutter et al. [68].

AFM tip modification. To remove production residues and contaminations, AFM tips were precleaned as described by Hinterdorfer et al. [69]. Briefly, they were consecutively incubated in peroxymonosulfuric acid and trichloromethane and dried in a dry air flow. Besides the cleaning effect, this method results in an enrichment of free silanol groups at the surface of the AFM tip. These silanol groups were used to facilitate silanization. First, a layer of Dynasylan 9165® was attached to the AFM tip by incubation in an organic solution of the silane (20 μ L / ml trichloromethane) for 30 min. Subsequently, the AFM tips were washed by dipping them into trichloromethane, methanol and water, consecutively. After this, the apex of the AFM tip was silanized with Dynasylan AMEO by 30 min incubation of the tips in an organic solution of the silane (20 μ L / ml trichloromethane). This was followed by washing the tips in trichloromethane, methanol and water, consecutively. AFM tips were heated to 105 °C for 1 h in a cabinet heater. Subsequently, the AFM tips were incubated in a solution of cyanuric chloride (1 mg/ml trichloromethane) containing 10 μ L N,N-Diisopropylethylamine for 2 h and washed by dipping them into trichloromethane and water. To attach BSA to the AFM tips, the pre-treated tips were incubated in an aqueous BSA solution (10mg/ml) for 12 h and afterwards washed with water.

As aromatic silane layers have been reported to be hydrophilic enough not to show repulsion when approached to a surface [70], Dynasylan 9165® was used to inactivate the side faces of the AFM tip. After removing the inactive a layer of Dynasylan AMEO® was applied to the cleaned apex, facilitating covalent coupling of the protein to the AFM tip.

Particle-protein interaction by atomic force spectroscopy. In an atomic force spectroscopy experiment, forces are determined as deflection (d) of the cantilever. With the spring constant (k_c) of the cantilever given, this applied force (F_{adh}) can be calculated from the detected deflection by Hooke's law (equation 1) [71]. For this, the exact determination of the spring constant and sensitivity of the cantilever, to which the AFM tip is mounted, are crucial prerequisites for reliable force spectroscopy experiments. For both, there is a proportional relation to the value of the force

measured in an experiment [72]. First, the sensitivity of the setup was determined three times. To determine the spring constant, the mean value of these experiments was used. Spring constants were determined three times for each tip and were all within the range of the manufacturer's specifications (SD<10 %). Prior to each experiment, the AFM sensitivity was determined again, because every change in the setup (e.g. position of the Laser on the backside of the cantilever) may change the sensitivity.

$$F_{adh} = k_c * d$$

Equation 1. Hooke's law; F_{adh} = force; k_c = spring constant; d = deflection

For each experiment a drop of the particle dispersion, pre-treated in a bath sonicator for 3 min, was dried onto a glass slide resulting in a thin homogeneous film of the particles. Films were visualized using NSC16/AlBS AFM tips in intermittent contact (air) mode.

In each experiment 64 adhesion measurements were performed on an area of 4 μm^2 with 0.5 μm z-length and a retract time of about 0.5 s. The experiments were done five times.

From these adhesion measurements the work of adhesion (W_{adh}) was calculated according to [73] using the formula:

$$W_A = \frac{3 * F_{adh}}{2 * \pi * R}$$

Equation 2. Work of adhesion, F_{adh} = force; R = tip radius

According to the JKR (Johnson, Kendall, Roberts) theory, R is the radius of the hemispherical point of contact. After each experiment the tip appearance was checked for dramatic changes. Using the formula:

$$\gamma_1 = \frac{W_{adh}^2}{4 * \gamma_2}$$

Equation 3. Surface free energy; Work of adhesion = W_{adh} ; γ_2 =surface free energy of tip

the surface free energy (γ_1) was calculated subsequently. Regarding to [73, 74] the surface free energy of the silicon tip determined using the contact angle technique range from approximately 41 mJm⁻² to 43 mJm⁻². In this study the value of the surface free energy of the silicon tips (γ_2) was fixed to 42 mJm⁻². The indentation of the particle deformation was calculated from the differences in the slope of the force-distance approach curve between glass as reference and the sample surface.

Agglomeration control by Analytical Ultracentrifugation (AUC). The particle size distribution was determined by analytical ultracentrifugation (AUC) of ~500 μ L of the test dispersion with a mass ratio of nanomaterial: FCS proteins = 2:1.

Simultaneous detection by synchronized interference optics (Beckmann, model XLI) quantified the amount and the diameter of each fraction independently from 1 nm up to several microns diameter [36, 75]. We can thus successively quantify in a single measurement the protein content, the protein molar mass, the nanomaterial content, and the nanomaterial state of agglomeration. When the retrieved concentration of proteins is less than 100 wt% at the expected molar mass, we assume that the remaining proteins have adsorbed to a particulate surface. When the retrieved concentration of nanomaterial is less than 100 wt% in the measurement interval, we assume that the remainder has agglomerated. The evaluation of the AUC raw data incorporated the loose packing of nanoparticle agglomerates by assigning to them a fractional dimension and using the fractal agglomerate sedimentation relation as specified in equation (6) of the reference [38]. We used a value of 2.1 for the fractional dimension, which is universal for the morphology of agglomerates from reaction limited colloidal association (RLCA, i.e. reversible agglomeration)

[38, 39]. A fractional dimension of 3 describes solid spheres, and is employed e.g. in routine DLS or PCCS evaluation, but is obviously wrong for agglomerates. The tabulated material's constant of refractive index allows the interference optics to linearly direct quantify the fraction that is dispersed to diameters below 100 nm in the actual test preparation, with the full size distributions. The value for the nanodispersed fraction is regarded as an upper limit, judging from the comparison of size determination methods with different physical measurement principles (chapter 2).

Determination of protein adsorption onto metal oxide nanoparticles indirectly via BCA-assay. Nanoparticles were dispersed with 2 ml of a corresponding protein solution (purified water with Bovine Serum Albumin, purity 96 %, Bovine Serum Albumin, purity 99 %, Bovine Serum Albumin isothiocyanate conjugate, or Fetal Bovine Serum Gold), leading to particle-protein ratios from 1:10 up to 100:1 (whereas not all ratios were tested for all protein solutions used). The resulting dispersions were stirred at room temperature for 1 h at 300 rpm, transferred into Eppendorf tubes and centrifuged at 23000 g for 45 min and 10 °C in a Hettich Universal 30 RF with rotor E1175 (Hettich Lab Technology, Tuttlingen, Germany). Afterwards, the supernatants were used for BCA-assay as described in the manual. A calibration curve with BSA (96 % purity) was prepared and the linear equation was calculated after subtracting the background noise (deionized water) to quantify the amount of protein in the supernatants. The resulting protein concentrations in the supernatants were subtracted from the original concentration and related to the negative control (centrifuged protein solution without particles). The protein concentration of the particle pellets could not be detected due to interactions of the particles with the test principle. Centrifugation of BSA/FCS solutions with the same protocol did not change the protein concentrations in the supernatant.

Sigmoidal fitting and determination of half-max values from the adsorption data. The protein adsorption data from BCA-assay were plotted

against the different particle-protein ratios (w/w) used and fitted with a heuristic sigmoidal model with the equation (equation 4):

$$y = A_1 + \frac{A_2 - A_1}{1 + 10^{(\log x_0 - x) \cdot p}}$$

Equation 4. sigmoidal fitting function

whereas A_1 is the initial value, A_2 the maximum of adsorption and x_0 equals to mass ratios at half-max adsorption. As the adsorption tends to 100 % with increasing particle-protein relation, A_2 was set and fixed at a value of 100 % and A_1 at a value of 0 %, the hillslope p , which is corresponding to the steepness of the curve, was kept variable. For the fits containing of 20 points set between A_1 and A_2 , left and right margin was set to 0 and 20 fit iterations were performed. From these sigmoidal fits, half-max values were read out. As the AUC data were performed only once due to the high costs and efforts, an error-related weighting of the data was disclaimed. All calculations were performed with the computer program Origin 6.0 (Microcal, Freiburg, Germany).

3.4 Results & Discussion

Physicochemical characterisation of particles. Intrinsic properties of the materials as pristine powder are essential to interpret the protein adsorption patterns in suspension. The results of the physicochemical characterization of the investigated particles are summarized in Table 3.1.

Visualization of CeO_2 particles was performed using AFM and TEM. The formulations tend to form aggregates as can be seen in figure 3.1. TEM images show square-cut crystalline particles for all batches. In contrast to particle sizes of about 20 nm in TEM images, AFM measurements result in primary particle diameters of 87 nm for CeO_2 B and C and 98 nm for CeO_2 A.

Performance of XRD revealed additional Cl for CeO₂ C for the otherwise very uniform particles. The particle surfaces also show no striking differences, only CeO₂ C shows an additional Li peak according to SIMS measurements.

Since adsorption should be governed by surface energy and polarity, we compared contact angles of a thin planarized powder film with drops of water, formamide and diiodomethane. The drops were imaged onto a CCD and contact angles were extracted by standardized software. After Owens-Wendt evaluation, all samples are hydrophilic, with total surface energies of 72.5 mN/m, 71.0 mN/m and 69.1 mN/m for CeO₂ A, B and C respectively. The disperse part of the surface energy (related to unspecific van-derWaals interactions) is lowest for CeO₂ C with 40.6 mN/m, against 41.1 mN/m and 42.3 mN/m for CeO₂ A and B.

To determine ζ -potential and the particle diameter with DLS, nanoparticles were dispersed in double distilled water with a concentration of 10mg/ml and incubated for 30 min in an ultrasonic water bath at room temperature. Sonication leads to a slight reduction of agglomeration of CeO₂ particles, with PDIs in the range of 0.2 to 0.3. The sizes of the different particles measured with DLS range from 170 nm for CeO₂ C to 190 nm for CeO₂ B. The ζ -potentials of all particles are positive with values of about +40 mV and comparable values to the manufacturer's reference data [35]. The pH of the particle dispersions in double distilled water was measured to be 5.9 for CeO₂ A/ CeO₂ C and 6.2 for CeO₂ B.

Table 3.1. Physical characterization of the tested nanoparticles with Dynamic Light Scattering (DLS), Atomic Force Microscopy (AFM) and laser Doppler Electrophoresis (LDE) (XRD, XPS, pH and BET surface data were adopted from [35]).

particle	AFM diameter \pm SD [nm]	TEM diameter \pm SD [nm]	XRD crystal-line phase & purity	XPS Surface chemistry [at%]	SIMS Surface organic contaminations	BET surface [m ² /g] [35]	DLS diameter \pm SD [nm] (PDI) *	Surface energy [mN/m] (Disperse + polar parts)	pH*	ζ -potential \pm SD [mV] *
CeO ₂ A	97.5 \pm 56.1	11.6 \pm 5.6	>99.97 % purity, cubic	O 57 Ce 25 C 18	Cerium-oxide-cluster, Na, organics	63	180.8 \pm 3.0 (0.257)	72.5 (41.4 + 31.1)	5.9	40.9 \pm 1.7
CeO ₂ B	87.0 \pm 49.7	22.6 \pm 5.7	>99.97 % purity, cubic	O 56 Ce 22 C 22	Cerium-oxide-cluster, Na, organics	44	189.2 \pm 1.4 (0.225)	71.0 (42.3 + 28.7)	6.2	38.3 \pm 4.8
CeO ₂ C	87.0 \pm 39.7	22.5 \pm 7.6	>99 % purity, Cerianite, cubic	O 53 Ce 26 C 20 Cl 0.6	Cerium-oxide-cluster, Na, organics, Li	33	170.4 \pm 2.1 (0.170)	69.1 (40.6 + 28.5)	5.9	31.5 \pm 3.5

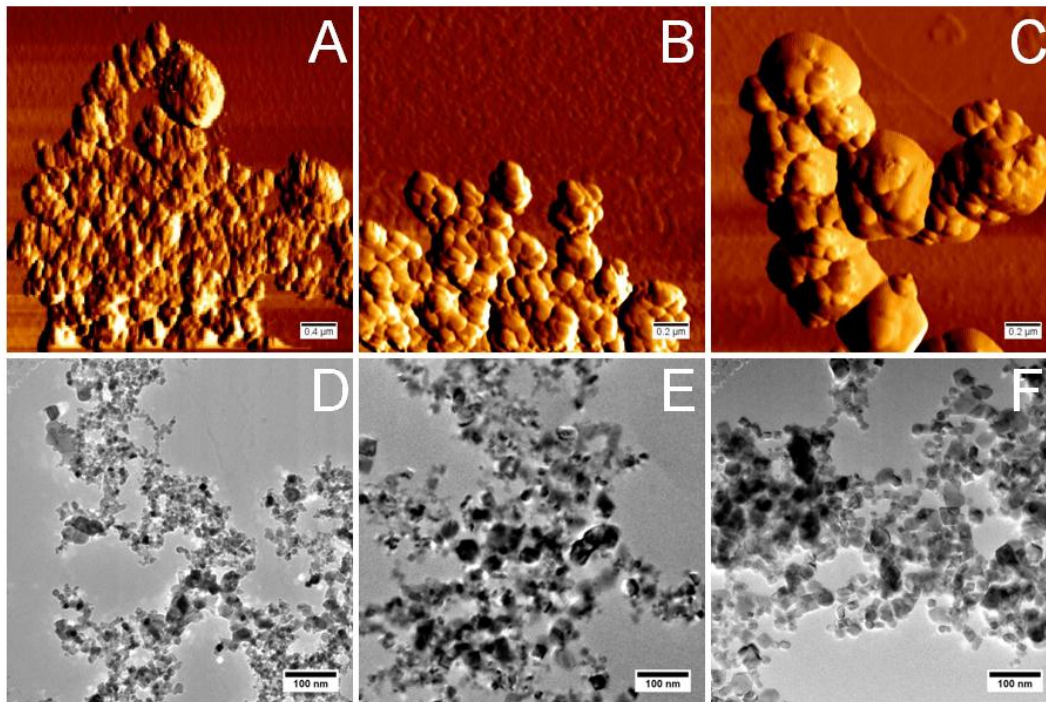


Figure 3.1. AFM and TEM images: A) amplitude image (4x4) of CeO₂ A particles; B) amplitude image (2x2) of CeO₂ B particles; C) amplitude image (2x2) of CeO₂ C particles; D) TEM image 25.000 x magnification (300.000 V) of CeO₂ A particles; E) TEM image 25.000x magnification of CeO₂ B particles and F) TEM image 25.000x magnification of CeO₂ C particles

Indirect measurement of protein adsorption with BCA-assay.

Different nanoparticle-protein relations lead to very different amounts of adsorbed protein: the higher the nanoparticle concentration in relation to the proteins, the higher the amount of protein adsorbed. Following incubation and removal of particles and adsorbed corona, the remaining (non-adsorbed) protein fraction in the supernatant was quantified a) by a protein-binding assay (BCA) and b) by mass-selective detection of BSA (AUC).

a) Plotting the amount of adsorbed protein from BCA-assay of supernatants to the nanoparticle-protein ratio leads to a sigmoid pattern for all particles tested (Figure 3.2). The adsorption isotherms for CeO₂ A and B are very similar, but CeO₂ C differs: The isotherms are shifted and higher particle/protein ratios are required to adsorb all proteins from BSA solu-

tion or FCS than for the other particles. This trend is more prominent for the adsorption of proteins from FCS.

By analyzing the sigmoid fits derived from BCA-assay with BSA, half-max values from 3.4 ± 0.3 up to 6.7 ± 0.3 could be calculated. As those values correspond to the particle-protein ratio at which 50 % of BSA is adsorbed, a low number means high protein affinity (see Table 3.2). Within this series the different types of CeO₂ show different affinity to BSA or protein from FCS, respectively, (see Figure 3.2) in descending order: from CeO₂ A, CeO₂ B to CeO₂ C.

b) The similarity of CeO₂ A and B is confirmed when we quantify the non-adsorbed BSA in the supernatant from interference detection during analytical ultracentrifugation (AUC). Again, sigmoid isotherms describe well the data, but quantitative half-max values nanoparticle-protein ratios disagree for especially CeO₂ C (Figure 3.2c). Note that BCA integrates all proteins in FCS-solution or BSA-solution, whereas AUC-measurements were performed with FCS solution, but only the mass-selected fraction 60–80 kDa and 100–140 kDa (assumed to represent BSA) was quantified. For CeO₂ A and CeO₂ B, the adsorbed BSA from FCS-solution (by AUC) agrees excellently with the adsorbed proteins in FCS-solution (by BCA-assay). Significantly fewer nanoparticles are required to deplete BSA from BSA-solution than from FCS-solution, since the adsorption isotherm is shifted to roughly 60% lower nanoparticle/protein values.

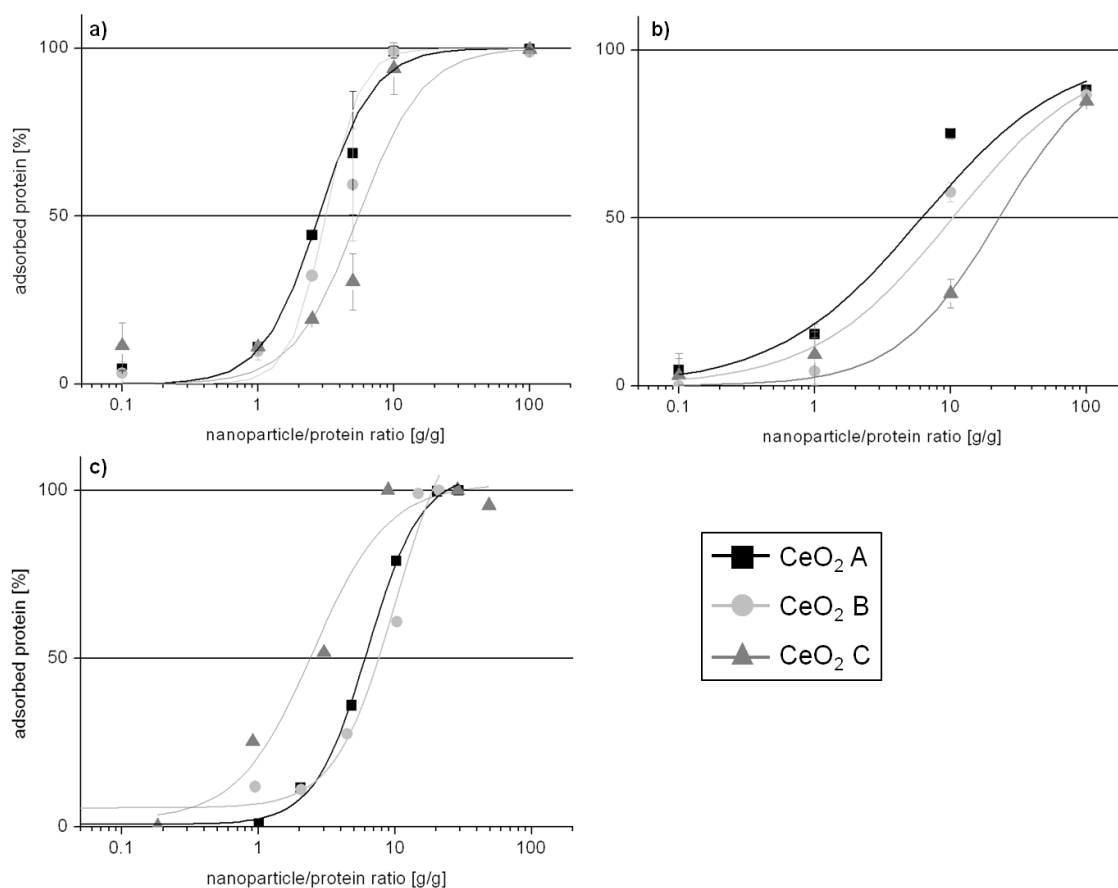


Figure 3.2. Adsorption isotherms for the different CeO₂ nanoparticles: a) adsorption of BSA from pure BSA solution from BCA-assay, b) overall protein adsorption from FCS solution from BCA-assay, c) adsorption of BSA from FCS solution, derived from AUC.

Table 3.2. Mass ratios at half-max for the adsorption of BSA and protein from FCS, gained by sigmoidal fitting of the data derived from BCA-assay and AUC (see figure 3.2). As these values correspond to particle-protein ratios, a high value means low particle-protein interaction ($R^2 > 0.97$ for all particles tested).

	CeO ₂ A	CeO ₂ B	CeO ₂ C
half-max BSA from BCA-assay [mg/mg]	3.4 ± 0.3	4.2 ± 0.2	6.7 ± 0.3
Half-max FCS from BCA-assay [mg/mg]	6.1 ± 0.3	10.3 ± 1	22.8 ± 2.8
half-max BSA from AUC [mg/mg]	6.3 ± 0.4	10 ± 3.8	2.5 ± 0.8

To compare the adsorption of different BSA derivatives and FCS, adsorption experiments with highly purified (BSA 99 %) and fluorescence labeled BSA (FITC-BSA) at a particle-protein ratio of 10:1 was performed (Figure 3.3). The protein adsorption of CeO₂ A and CeO₂ B differed significantly from that of CeO₂ C for FITC-BSA and FCS. In contrast, the adsorption of BSA 96 % and BSA 99 % was statistically equal for all particles tested. Protein-particle interaction for FCS proteins was significantly different for all particles tested. As the highly purified BSA 99 % does not differ significantly from the adsorption of BSA 96 %, a protein adsorption mediated by impurities cannot be demonstrated, although the adsorption for the highly purified BSA 99 % was higher for CeO₂ A and B. However, the different adsorption pattern for CeO₂ C strongly points to different adsorption mechanisms compared to CeO₂ A and B.

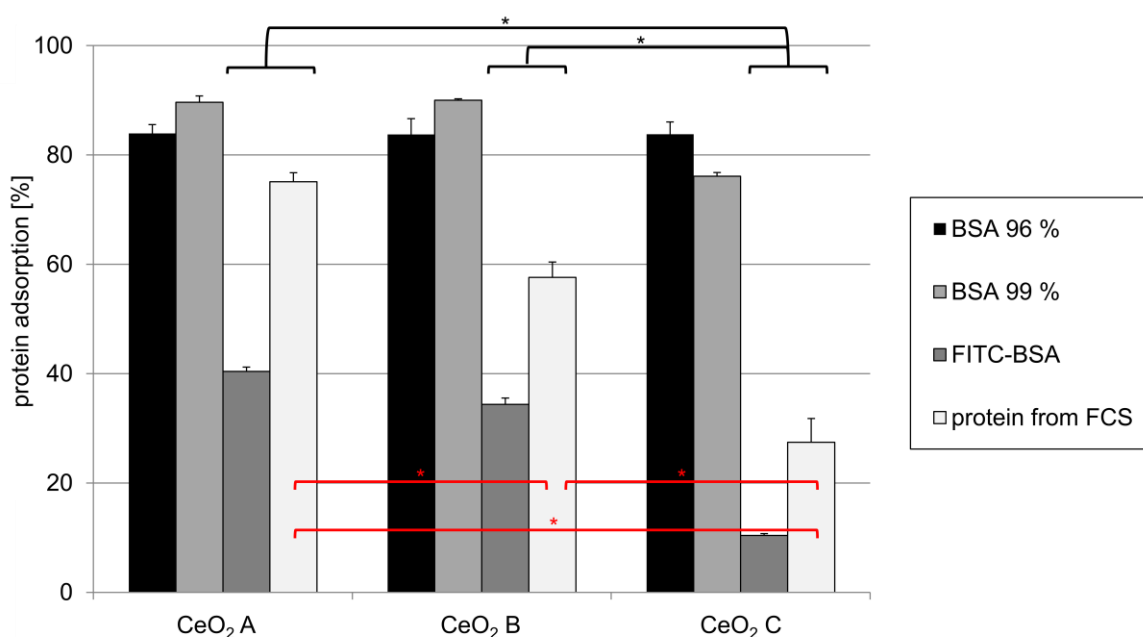


Figure 3.3. Protein adsorption from different BSA derivatives and FCS with a particle-protein relation of 10:1 (mean \pm sd, statistics: Kruskal-Wallis One-way Analysis of Variance on Ranks, followed by pairwise comparison procedure with Student-Newman-Keul-method, $p < 0.05$).

State of agglomeration with analytical ultracentrifugation (AUC). The interaction between colloids, and hence their tendency to agglomerate is

dictated by their surface properties – including the spontaneous change of surface properties due to protein adsorption. We characterized the state of agglomeration in FCS by AUC with interference detection. Since the signal height is directly linear with the concentration in the measurement interval, the ultrafine fraction (below 100 nm diameter) can be quantified. In Figure 3.4, the resulting particle size distributions are shown with logarithmic axes. For stabilized CeO₂ A and CeO₂ B in the presence of serum, significant ultrafine fractions were found, whereas CeO₂ C agglomerated stronger with two orders of magnitude less particles dispersed to 100 nm diameter or below. The two-peaked signal below 10 nm diameter is attributed to the serum proteins. The peaks can be converted from diameters to molar masses, giving 65 kDa and 120 kDa, in excellent agreement with BSA monomer and dimer. Again, the signal of the proteins is integrated and divided by the known protein refractive index increment $dn/dc = 0.18 \text{ cm}^3/\text{g}$ to provide an independent measurement of the actual concentration of the protein fraction that is not adsorbed on particles.

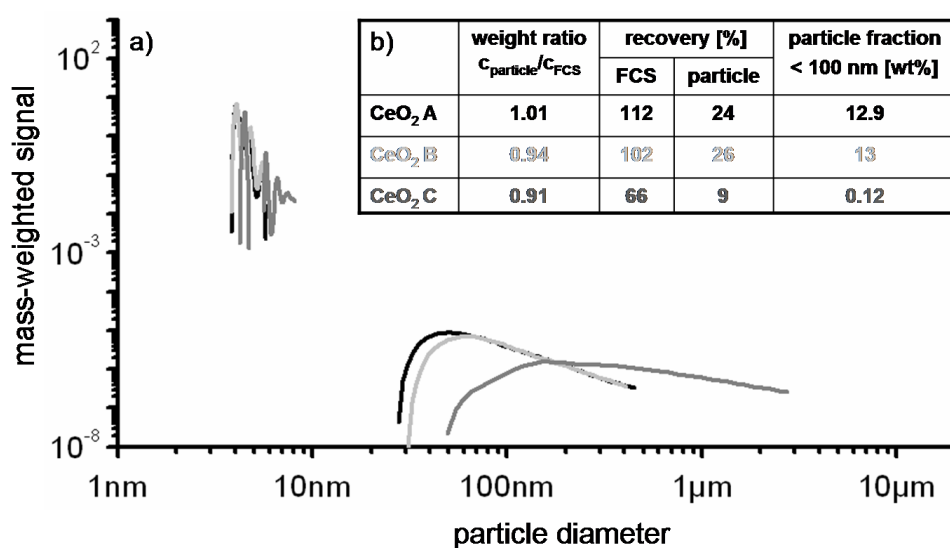


Figure 3.4. a) Size-distribution of the CeO₂ particles after dispersion in FCS-solution by AUC (particle-protein ratio of 1:1). The signal at 3-7 nm corresponds to the sizes of BSA monomer and dimer, respectively. b) table revealing the ultrafine fractions of the particles in numbers.

AFM force-distance measurements between proteins and particles.

Multiple preparations of adhesion force curves can be summarized to frequency distribution patterns. Measuring adhesion with an unmodified AFM tip clearly reveals similar hydrophilic properties in a normal adhesion force distribution for CeO₂ A and CeO₂ B (see Figure 3.5). CeO₂ C showed multiple unspecific interactions with the unmodified hydrophobic Si₃N₄-tip. The calculated main peak for measurements with unmodified tip was 2.2. nN for CeO₂ A (n=227), 3.3 nN for CeO₂ B (n=240) and 3.9 nN for CeO₂ C (n=283). The same experiments with covalent attached BSA at the apex of the tip caused lower interactions for CeO₂ C (peak at 2.6 nN of 258 measurements) and an increase up to 2.3 nN for CeO₂ A (n=229) and 3.4 nN for CeO₂ B (n=266). The broader distribution of the measured adhesion forces for CeO₂ C with an unmodified tip changed to a narrow distribution similar to the other two CeO₂ samples.

The results of adhesion measurements of each CeO₂ formulation are summarized in Table 3.3. There are only little differences in the calculated indentation depths for CeO₂ A and CeO₂ B particles with unmodified

AFM tips. They range from 3.4 nm for CeO₂ A to 3.5 nm for CeO₂ B. Lower values were obtained for the BSA modified tips, 3.0 nm for CeO₂ A, 3.3 nm for CeO₂ B. In contrast the indentation depth of the CeO₂ C increases from 1.5 nm to 2.8 nm.

The work of adhesion and surface free energy for the formulations using unmodified tips show an increasing order of the different particles. With unmodified tips CeO₂ C has the highest W_{adh} and CeO₂ A the lowest W_{adh} . BSA modification changed the W_{adh} for CeO₂ A and CeO₂ B, in contrast there is a major decrease for CeO₂ C particles.

Table 3.3. Atomic force measurements: indentation, force of adhesion, work of adhesion and surface free energy of all CeO₂ formulations with unmodified and BSA modified tips

formulation	Force of adhesion (F_{adh}) [nN]	Indentation [nm]	Work of adhesion (W_{adh}) [$mJ \cdot m^{-2}$]	Surface free energy (γ_2) [$mJ \cdot m^{-2}$]
CeO ₂ A	2.166	3.4	103	64
CeO ₂ A BSA modified tip	2.266	3.0	108	70
CeO ₂ B	3.262	3.5	156	144
CeO ₂ B BSA modified tip	3.435	3.3	164	160
CeO ₂ C	3.873	1.5	184	204
CeO ₂ C BSA modified tip	2.551	2.8	121	88

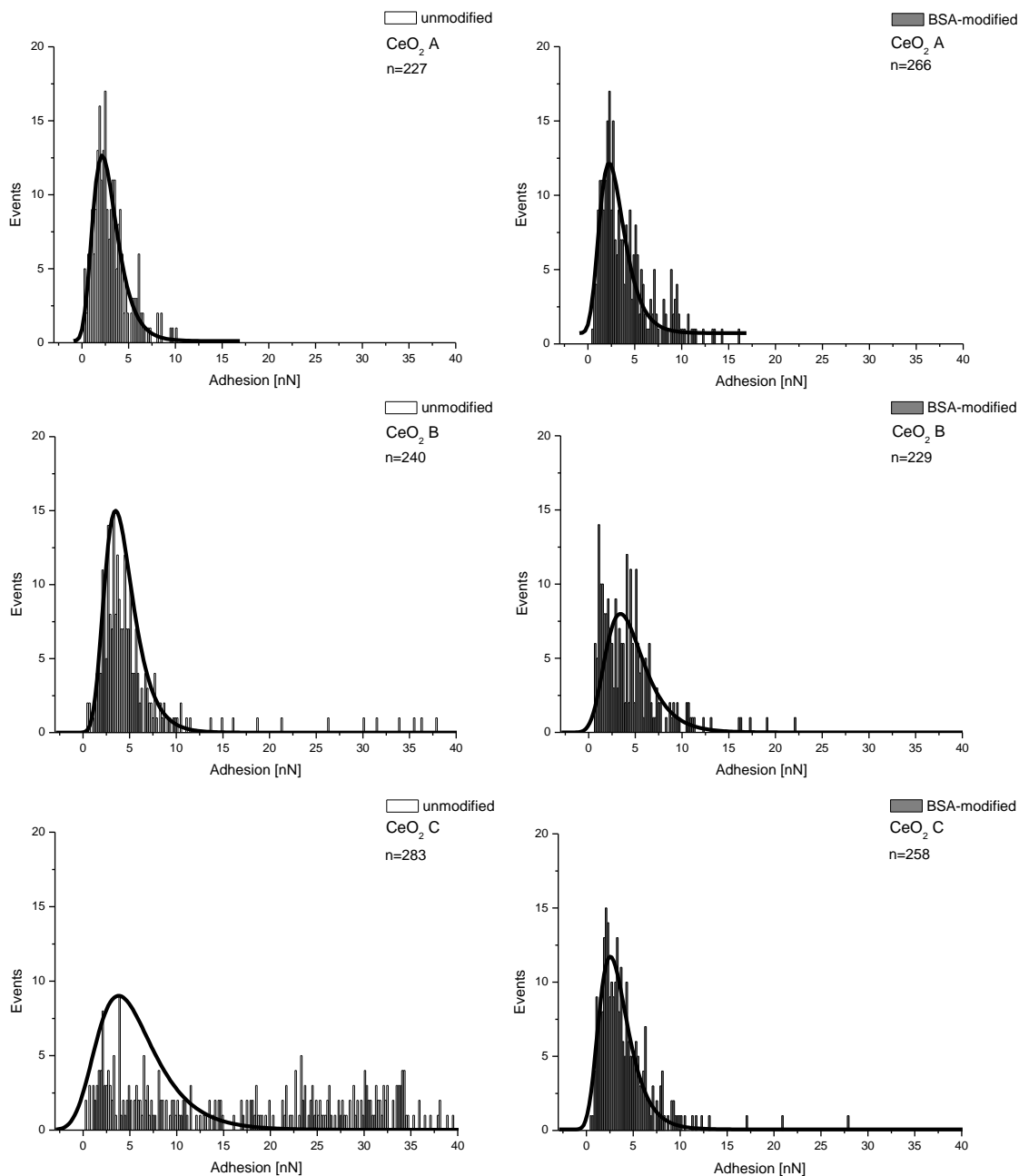


Figure 3.5. Frequency distribution of the adhesion values in the AFM force-distance curves: CeO₂ A, CeO₂ B and CeO₂ C particles.

Different particle characteristics are known to determine protein (e.g. BSA) adsorption onto nanoparticles, and in particular **hydrophobic interactions** tend to be the dominating feature [76-78]. Magnetic nanoparticles covered with thermo sensitive PNIPAM (Poly(N-isopropylacrylamide)) are hydrophobic above temperatures of 32°C. Shamim et al. could show

that BSA-adsorption was much higher at temperatures above 32 °C. Naked magnetic nanoparticles showed no increase in protein-adsorption with increasing temperature, i.e. protein adsorption is increasing with higher hydrophobicity [79]. Also, **electrostatic interactions** can play an important role [80, 81]. The amount of BSA adsorbed to magnetic nanoparticles covered with PNIPAM or chitosan increased with decreasing pH, whereas the maximum adsorption was near the isoelectric point of BSA (pI = 4.7) [79, 82]. There is strong evidence that the **size of the particle** may be another factor influencing protein adsorption. Nanoparticles of different sizes, but the same level of hydrophobicity show different degrees of Human Serum Albumin adsorption. Despite the fact that smaller nanoparticles reveal proportionally larger surface areas than larger ones, the adsorption surprisingly is in favor of the larger particles. Hence, it is speculated that the curvature of nanoparticles may suppress the protein adsorption at a particle size around 30 nm [33]. Clearly, not all proteins show the same adsorption patterns. Conditioning of different particles with complex protein mixtures, e.g. blood serum, leads to **different adsorption patterns for the protein fractions** [83, 84]. Under well-defined conditions, protein adsorption data can be used in established **mathematic models** involved: BSA-adsorption onto chitosan-coated magnetic nanoparticles could be fitted to Langmuir isotherms and hence quantified not only in terms of overall protein adsorption, but also in protein affinity [82]. Summarized, the protein adsorption onto particles depends on: hydrophobicity of the particle surface, pH, particle size and the protein(s) used, it might be fitted to Langmuir model under defined conditions. In this context, we interpreted the protein adsorption data generated with the CeO₂ nanoparticles.

Table 3.1 reveals close similarities in size, pH and ζ -potential for all three CeO₂ formulations. Contact Angle, XRD, XPS and SIMS measurements revealed only minimal differences in surface energy, surface chemistry or crystallinity.

Nevertheless, the frequency distributions of the adhesion measurements showed differences between the formulations. The adhesion forces between Si_3N_4 tip and CeO_2 A particles change only slightly by modifying the tip with BSA. Similar results with the AFM force measurements were obtained for CeO_2 B particles. Based on the force curves it could be seen, that a modification of the surface increases interactions, e.g. electrostatic attractive forces. This increase in the attractive forces between particle and tip is proportional to the snap-in of the force-distance curves. As it would be expected from size and ζ -potential, CeO_2 C should show a similar frequency distribution compared to CeO_2 A and CeO_2 B (Figure 3.5). However, in contrast CeO_2 C displays a very broad frequency distribution without a significant peak. The reason for that may be non-specific interactions. This behavior is totally changed when using a BSA modified contact tip. The more hydrophilic surface of the tip results in specific interactions thus leading to a narrow frequency distribution with a single pronounced peak.

It is known that proteins are flexible and that albumin changes its conformation on a surface in order to minimize interface energy. Gao et al. described a conformational changing of BSA molecules from α -helix to the more space requiring β -sheets [85]. These possible changes in the conformation of the structure of the adsorbed proteins can explain the different indentation values of CeO_2 C: Note that all indentation values (Table 3.3) are lower than the BSA hydrodynamic diameter of 4.5 nm. The indentation nearly doubles to 2.8 nm for BSA-modified tip for CeO_2 C compared to around 1.5 nm for the indentation with unmodified cantilever. It seems that BSA adsorbs in a stretched configuration as a flat layer on CeO_2 A and CeO_2 B, but stays extended on CeO_2 C. This is conform to the differences in adsorption for BSA 99 %, FITC-BSA and protein from FCS (Figure 3.3) and points to a lower affinity of BSA on CeO_2 C.

Similar results were obtained with Analytical Ultracentrifugation. At a 1:1 ratio of nanoparticles and proteins, the agglomerate diameter distributions of CeO_2 A and CeO_2 B, except for an insignificant shift in diameter, were almost identical and showed a low tendency to agglomerate with

more than 10 wt% of the particles added dispersed below 100 nm diameter. This low level of agglomeration is attributed to the presence of adsorbed proteins acting as protection colloids in steric stabilization. In contrast, the results for CeO₂ C deviate from the other two formulations. As shown in Figure 3.4, CeO₂ C forms agglomerates, which we interpret to be a result of the absence of adsorbed proteins.

All three formulations show different values in the protein adsorption derived from the BCA assay data (Figures 3.2 and 3.3, Table 3.2). As expected from force measurements and AUC data, CeO₂ A adsorbed more protein from pure BSA solution than CeO₂ B and CeO₂ C. The characteristics of the sigmoidal fits of the protein absorption at different particle-protein ratios are very similar for CeO₂ A and CeO₂ B.

Looking at the BCA data only, it seems that CeO₂ C might reveal the weakest affinity to BSA and FCS proteins in general. However, as provided by AUC measurements, CeO₂ C (Figure 3.4) shows a high tendency to agglomerate. This intense state of agglomeration could have led to a drastically decreased surface and hence to a lower overall protein adsorption. Presumably, the interaction between CeO₂ C particles was higher than that between protein and particle, which is supported by the large particle size distribution in FCS.

Our data could not be fitted to Langmuir isotherms, but had sigmoid patterns. We believe this is due to the correlation between the level of agglomeration and the protein concentration: The particulate surface that is available for adsorption is not independent of the protein concentration, as proteins can improve dispersion of the particles, which leads to smaller particle sizes (deagglomeration) and hence to a larger surface available for protein adsorption (see chapter 2, Figure 2.6). In well defined colloidal systems, such as stable polymer particle dispersions with uniform particle sizes, this problem is not occurring. Also, here the adsorption patterns are derived from a mixed influence of electrostatic and hydrophobic interactions (and maybe from different curvatures due to irregular particle shapes).

Protein adsorption does not necessarily occur directly to the particle, but can also be mediated by other substances. Here, the adsorption of the 96 % pure BSA seemed not to be mediated by impurities of the purchased protein but was a direct particle-protein interaction, as there was no significant difference in adsorption compared to highly pure BSA (Figure 3.3).

AUC quantified the adsorbed amount of specifically BSA in the FCS solution, whereas BCA-assay quantified the overall protein adsorption. Comparison of adsorption from FCS-solution by AUC and BCA-assay revealed a very good correlation for CeO₂ A and B, leading to the assumption that BSA must be dominating the corona. Hence, CeO₂ A and B seem to adsorb BSA from the FCS solution very specifically, in excellent accord with the small indentation depth in AFM, and hence extended configuration on the inorganic surface. Since differences for CeO₂ C between BSA-specific detection (AUC) and unspecific detection (BCA) persist, one can speculate about the formation of a secondary or soft corona at lower particle/protein ratios, which would indeed shift the BSA adsorption isotherm in the observed direction, supported also by the larger indentation depth. At present, this last detail remains open.

3.5 Conclusion

In this chapter, protein interactions of BSA with and adsorption of BSA or FCS as a complex protein mixture to nanoparticles was investigated. Clearly, generation as well as interpretation of protein adsorption or interaction data with metal oxide nanoparticles was difficult and methods from different physical, chemical and mathematical principles were necessary to succeed. It was demonstrated that nanoparticles from nominally the same inorganic material do not necessarily reveal the same adsorption patterns to proteins. As the state of agglomeration is depending on the protein concentration, the available particle surface and the protein adsorption influence each other, impeding the use of standard adsorption models as Langmuir. Also, the higher particle-particle interactions of

CeO₂ C may falsify the protein affinity due to a strong agglomeration tendency and decreased surface. The BSA adsorption detected in this work was a direct particle-protein interaction and not mediated by impurities. Finally, it was pointed out that CeO₂ A and B adsorbed BSA from a FCS-solution very specifically, and that BSA does change its conformation on the nanoparticle surface.

Particle-protein interaction could be proven for three different CeO₂ nanoparticles with similar physico-chemical characteristics. Based on our intention to determine structure-effect relations we proved that it is not sufficient to characterize intrinsic properties only, where only minute variations were detected. The variations were considerable in the next step of the biodistribution, namely in the adsorption of serum proteins albumin, mimicking the interaction after uptake into the blood system. The same must be expected in the lung for the interaction with surfactant proteins after inhalative exposure. In order to derive structure-effect relations, *in situ* or *as-tested* characterization, not *as-produced* is required, with implications for the discussion of 'Sameness' in the REACH Implementation Project on Nanomaterials.

4 Interaction of metal oxide nanoparticles with lung surfactant protein A

Many of the data presented in this chapter have been submitted as a research article in the European Journal of Pharmaceutics and Biopharmaceutics:

Christine Schulze, Ulrich F. Schaefer, Christian A. Ruge, Wendel Wohlleben, Claus-Michael Lehr: Interaction of metal oxide nanoparticles with lung surfactant protein A

Contributions:

Christine Schulze performed the BCA assays and SDS-PAGE in combination with immuno-blot, interpreted the results and wrote the manuscript.

Christian Ruge repeated the experiments and helped to interpret the data.

Wendel Wohlleben from BASF SE, Polymer Physics Research, Ludwigshafen, Germany, generated the AUC data and helped to interpret the results.

Ulrich F. Schaefer and Claus-Michael Lehr helped to interpret the results and to prepare the manuscript.

4.1 Abstract

The pulmonary surfactant, a major component of the Alveolar Lining Fluid (ALF) covering the respiratory epithelium of the deep lung is the first biological barrier encountered by nanoparticles after inhalation. We here report for the first time significant differences for metal oxide nanoparticles to the binding of Surfactant protein A, the predominant protein component of pulmonary surfactant. SP-A is a physiologically most relevant protein and provides important biological signals. Also, it is involved in the lung's immune defence, controlling e.g. particle binding, uptake or transcytosis by epithelial cells and macrophages. In our study, we could prove different particle-protein interaction for eight different nanoparticles, whereas particles of the same bulk material revealed different adsorption patterns. In contrast to other proteins as Bovine Serum Albumin (BSA), SP-A does not seem to significantly deagglomerate large agglomerates of particles, indicating different adsorption mechanisms as in the well-investigated model protein BSA. These findings may have important consequences for biological fate and toxicological effects of inhaled nanomaterials.

4.2 Introduction

As pointed out previously, the interactions of proteins and nanoparticles are of the utmost importance when they come in contact with biological systems. It is known that small particles are taken up in higher amounts than larger ones, so the level of particle uptake into cells could be altered due to protein coating of particles, which was proven to lead to deagglomeration (see chapter 2, Figure 2.6) and hence to smaller particle sizes. Also, it could be demonstrated that model protein BSA is adsorbing onto CeO₂ nanoparticles (see chapter 3, Figures 3.2 and 3.3, Table 3.2). There is also evidence that particles coated with proteins adsorbed onto endothelial cells in higher amounts as uncoated ones [84]. Hence, the phenomenon of protein adsorption onto nanoparticles entering biological systems could lead to significant toxicological consequences and must be investigated thoroughly.

The Dawson group has pioneered structure-property-relationships in protein coronas during the last few years using plasma proteins [59, 60, 86, 87]. However, there is general consensus in nanotoxicology that inhalation represents the most relevant route of exposure [61]. As stated previously, the first biological barrier that inhaled particles will encounter is the pulmonary surfactant (a component of the alveolar lining fluid (ALF)), an ultra thin liquid layer covering the respiratory epithelium towards the air side. The pulmonary surfactant consists of approximately 90% lipids (mainly phospholipids) and 10% proteins (so called surfactant proteins, Sp-X) by weight [20]. Concerning the interaction between the ALF and inhaled particles, we assume that especially the four so called lung surfactant proteins play a key role. Surfactant protein B and C are very lipophilic and improve the surface activity of surfactant phospholipids [88]. The more hydrophilic Surfactant proteins A and D (Sp-A, Sp-D) belong to the collectins recognizing, binding and facilitating the clearance of infectious particles from the lung [89]. As Sp-A is the most prominent of the four surfactant proteins and because of its major role in lung immune defence, a possible particle interaction with this protein is highly important to understand and to predict further biological responses. The

adsorption of ALF components has already been addressed in several studies for diesel soot, quartz and kaolin particles [90], as well as for gold [91], TiO₂ [92] and polystyrene particles [93], but they predominantly concentrated on the lipid fraction of ALF. Therefore, the interaction of metal oxide nanoparticles with lung surfactant proteins present in porcine Broncho-Alveolar Lavage Fluid (pBALF) was studied.

To investigate nanoparticles-protein interactions microcalorimetry and surface plasmon resonance technique were introduced by Cedervall et al. using co-polymer particles as model [33]. However, these techniques were not readily transferable to “real” nanomaterials, such as e.g. metal oxides, mainly due to rapid sedimentation. Hence, the colorimetric BCA-assay, gel-electrophoresis and immunoblotting was used to quantify and identify the interacting proteins. Also, the agglomeration behaviour of those particles in pBALF was investigated and compared to that of commonly used FCS.

4.3 Materials & Methods

Materials. The Bicinchoninic Acid Kit for Protein Determination (BCA assay), TRIS-HCl, glycerine, β -Mercaptoethanol, TWEEN 80, NaCl and MgCl₂ were purchased from Sigma-Aldrich Chemie GmbH, Munich, Germany. Acrylamid solution Rotiphorese Gel 40 (29:1), Temed, glycin and Ammoniumperoxodisulfate (APS) were from Carl Roth GmbH & Co., Karlsruhe, Germany. The nitrocellulose membranes (Whatman Protran BA 85 Nitrocellulose) were bought from Biometra, Goettingen, Germany. The protein marker was from Fermentas GmbH, St. Leon-Rot, Germany. The primary and secondary antibodies (Rabbit Anti-Surfactant Protein A and Alkaline Phosphatase conjugated goat anti-rabbit IgG) were purchased from Millipore GmbH, Schwalbach, Germany. The NTB/BCIP solution was bought from Roche Diagnostics GmbH, Mannheim, Germany. From SERVA Electrophoresis GmbH, Heidelberg, Germany, we used Sodium-dodecylsulfate (SDS). Methanol was HPLC grade from Fisher Scientific GmbH, Schwerte, Germany. Bromphenolblau was purchased from

Pharmacia Biotech AG, Duebendorf, Germany. The low-fat milk (1.5 %) was bought from a local dairy.

Determination of protein adsorption onto metal oxide nanoparticles via BCA-assay. 148 mg of nanoparticles were dispersed with 2 ml of a 1:10 diluted pBALF solution (leading to a protein concentration of 7.4 mg/ml), leading to particle-protein ratio of 10:1. The resulting dispersions were stirred at room temperature for 1 h at 300 rpm, transferred into Eppendorf tubes and centrifuged at 23000 g for 45 min and 10 °C in a Hettich Universal 30 RF with rotor E1175 (Hettich Lab Technology, Tuttlingen, Germany). Afterwards, the supernatants were used for BCA-assay as described in the manual. The resulting protein concentrations in the supernatants were subtracted from the original concentration and related to the negative control (centrifuged protein solution without particles).

Preparation of porcine Bronchoalveolar Lavage Fluid (pBALF). pBALF preparation was modified after [94]. In short, three porcine lungs, derived from a local butcher and removed in toto, were filled with cold (4 °C) purified water (Millipore GmbH, Schwalbach, Germany) and gently massaged for about 5 min. Then, the fluid was removed and collected; the fluid of all lungs was pooled and centrifuged at 1400 rpm for 4 min to remove cellular residues. The thus obtained volume of about 2 l of pBALF was freeze-dried in a Christ Alpha 2-4 LSC (Martin Christ Gefriertrocknungsanlagen GmbH, Osterode am Harz, Germany) lyophilisation device and rediluted in 200 ml of purified water in order to concentrate the proteins. The content of soluble compounds was determined gravimetrically to be 74,03 mg/ml. The content of Sp-A was proven by Westernblotting and Immunostaining as described later, in comparison to literature [95, 96] and a Sp-A reference. The pBALF was aliquoted and stored at -80 °C until use. The time frame between picking up the lungs and preparation of the pBALF was about 45 min. During the whole transportation process, the lungs were cooled on ice to preserve the tissue. After they arrived in the laboratory, we started pBALF preparation immediately.

SDS-PAGE, Western Blotting and Immunostaining. The contents and preparation of all buffers and solutions are summarized in Table 4.1.

After incubation with the nanoparticles in a particle-protein relation of 10:1 and centrifugation, the supernatants were removed, the pellets rinsed 3 times with purified water and resuspended with 0.5 ml of purified water. 0.1 ml of the supernatants and pellet dispersions respectively were mixed with 0.1 ml of 2x sample buffer and denatured for 5 min at 95 °C to detach the proteins from the particles. Then, 20 µl of each sample was pipetted into the pockets of a 12 % Polyacrylamide gel (4.5 ml of purified water, 2.5 ml of separation gel buffer, 3 ml of Acrylamid solution (Rotiphorese Gel 40 (29:1)), 0.05 ml of Ammoniumperoxodisulfate (APS) 0.005 ml of Temed), covered with a 4 % stacking gel (2.5 ml of purified water, 0.95 ml of stacking gel buffer, 0.4 ml of Acrylamid solution, 0.0225 ml of APS, 0.0075 ml of Temed) and run, soaked in running buffer, for 110 min at 100 V in a MiniProtean II (Bio-Rad Laboratories GmbH, Munich, Germany).

The stacking gels were removed and the separation gels covered with nitrocellulose membranes, sandwiched in filter paper and soaked in blotting buffer. After removing air bubbles from the layer interspaces, the blotting sandwiches were transferred into a Mini Trans-blot Cell (Bio-Rad Laboratories GmbH, Munich, Germany) and tank-blotted in blotting buffer at 300 mA for 90 min. As the protein marker was prestained, there was no need to check the protein transfer by Ponceau staining.

The membranes were blocked for 2 h in blocking buffer, then they were incubated with Rabbit Anti-Surfactant Protein A at a dilution of 1:2500 in blocking buffer (Anti-Surfactant Protein A) for 2 h under gentle luffing. The blots were washed 3 times with TBS buffer for 10 min prior to incubation with Alkaline Phosphatase conjugated goat anti-rabbit IgG (Goat anti-Rabbit IgG, Alkaline Phosphatase Conjugated), diluted 1:5000 in blocking buffer. After washing 3 times for 10 min with TBS buffer, the blots were developed in 10 ml of NBT-BCIP dying solution for several minutes. Finally, the blots were scanned and saved as .tiff files.

Table 4.1: Buffers and solutions needed for SDS-PAGE, Westernblotting and Immunostaining.

	components	concentration
stacking gel buffer	Tris-HCl SDS adjust to pH 6.8	0.5 M 0.4 % (w/v)
separation gel buffer	Tris-HCl SDS adjust to pH 8.8	1.5 M 0.4 % (w/v)
2x sample buffer	Tris-HCl SDS Glycerin β -Mercaptoethanol Bromphenolblau adjust to pH 6.8	0.12 M 8 % (w/v) 20 % (w/v) 10 % (v/v) 0.1 % (w/v)
running buffer	Tris Glycin SDS	0.025 M 0.192 M 0.1 % (w/v)
blotting buffer	Tris-HCl Glycin Methanol pH 8.3	0.025 M 0.192 M 20 % (v/v)
TBS buffer	Tris-HCl NaCl pH 7.5	0.02 M 0.15 M
blocking solution	low-fat milk (1.5 %) TWEEN 80 in TBS buffer	10 % (v/v) 0.1 % (v/v)
buffer for NTB/BCIP dying solution	Tris-HCl NaCl MgCl ₂ pH 9.5	0.1 M 0.1 M 0.05 M
NTB/BCIP dying solution	NTB/BCIP stock solution in buffer for NTB/BCIP dying solu- tion	0.2 %

Agglomeration control by Analytical Ultracentrifugation (AUC). The particle size distribution was determined by analytical ultracentrifugation (AUC) of ~500 μ L of the test dispersion with a mass ratio of nanomaterial : BALF proteins = 2:1. This ratio corresponds to around 10 mg/cm² protein mass concentration / nanomaterial specific surface in the solution and it was chosen because this situation is close to a particulate contamination in the lung: Only a small part of the available protein mass has adsorbed.

Simultaneous detection by synchronized interference optics (Beckmann, model XLI) quantified the amount and the diameter of each fraction independently from 1 nm up to several microns in diameter [36, 37, 61]. We can thus successively quantify in a single measurement both the protein content, the protein molar mass, the nanomaterial content, and the nanomaterial state of agglomeration, presented as double-logarithmic plot in Figure 4.3. When the retrieved concentration of proteins is less than 100wt% at the expected molar mass, we assume that the remaining proteins have adsorbed to a particulate surface. When the retrieved concentration of nanomaterial is less than 100wt% in the measurement interval, we assume that the remainder has agglomerated. The evaluation of the AUC raw data incorporated the fractal morphology of nanoparticle agglomerates and applied the fractional dimension of 2.1 together with the sedimentation relation as specified in Eq. (6) of the reference [38]. This value of the fractional dimension has been shown to be universal for all reaction-limited colloid agglomerates [38, 39]. The tabulated material's constant of refractive index allows the interference optics to linearly direct quantify the fraction that is dispersed to diameters below 100 nm in the actual test preparation, with the full size distributions shown in the integrated table in Figure 4.3. The value for the nanodispersed fraction is regarded as an upper limit, judging from the comparison of size determination methods with different physical measurement principles (see chapter 2, Figure 2.6).

Nanoparticles. To be able to interpret the protein adsorption patterns and to show the high variability of the particles we were dealing with, we tried to characterize the nanoparticles we worked with (see Table 4.2 and Figure 4.1).

Table 4.2: Physico-chemical properties of the nanoparticles tested (the data are adopted from [35])

sample	chemical composition, crystallinity	mean primary particle size, morphology	surface area [m ² /g]	surface chemistry [At%]	organic modification	pH [#]
BaSO ₄	56,5 % Ba 38.6 % SO ₄ orthorhombic	38 nm irregular but globular	41,4	Ba 13 S 11 O 52 C 17	yes	8.6
AlOOH	82.7 % AlOOH; impurities: C, Na, Fe, Si, Li, B	40 nm, irregular but spherical	47	O 62 Al 32 C 7	none	4.3
TiO ₂ A	O 58 % Ti 41 % Cl > 1 % anatase 95 %, rutile 5 %	17 nm irregular but spherical	117	O 53 Ti 21 C 25 Cl 1	yes	5.4
TiO ₂ B	>99.5 % TiO ₂ rutile and anatase, tetragonal	27 nm irregular but globular	52	O 58 Ti 26 C 14 N 0.5 Cl 1	none	6.1
CeO ₂ A	> 99.97 % purity	14 nm cubic, aggregated	63	O 57 Ce 25 C 18	none	5.9
CeO ₂ B	> 99.97 % purity	20 nm, aggregated	44	O 56 Ce 22 C 22	none	6.2
CeO ₂ C	>99 % CeO ₂ Cerianite, cubic	70 nm irregular but globular	33	O 53 Ce 26 C 20 Cl 0.6	none	5.9
Carbon black	n.d.	16 nm, aggregated	340	n.d.	none	5

[#]10 mg/ml of nanoparticle in purified water
n.d. not determined

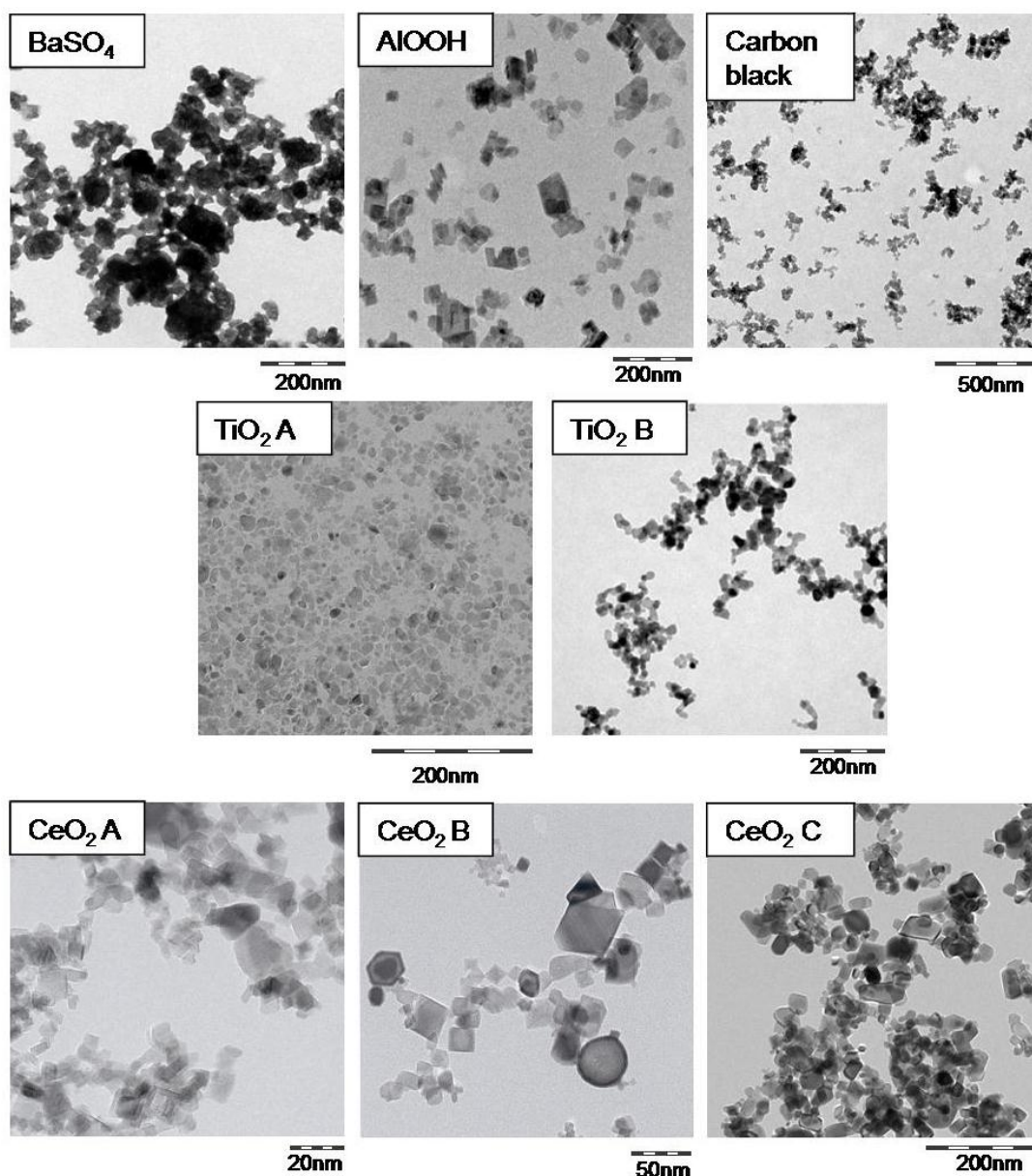


Figure 4.1. TEM pictures of the different nanoparticles tested for protein adsorption. The particles were dispersed in isopropanol and dried before use.

4.4 Results & Discussion

Direct and indirect analysis of SP-A adsorption onto metal oxide nanoparticles. The protein adsorption on nanoparticles was determined by measuring the protein content in the supernatant (BCA-assay) and expressed as a percentage of the protein content in a similarly treated

pBALF sample without nanoparticles. Clearly, different particles show a different protein adsorption (see Figure 4.2a), BaSO₄ and TiO₂ A generally adsorbing much less protein than the rest of the particles tested. Also, different particles of the same bulk material reveal different adsorption patterns, as could be shown for CeO₂ A and B compared to CeO₂ C and for the two TiO₂ particles.

The pulmonary surfactant is a complex mixture of lipids, phospholipids and proteins important for normal respiratory function [97]. Among the four lung surfactant proteins known, i.e. Sp-A, Sp-B, Sp-C and Sp-D, Sp-A is by far the most abundant (approximately 90 %) [96, 98, 99] and specific antibodies are commercially available, hence, we decided to focus our further experiments on Sp-A. Sp-A consists of eight trimers, each of those trimers including a long triple helical collagenous stem, a flexible hinge, a helical bundle connector and a globular head [100-102]. This globular structure contains Carbohydrate Recognition Domains (CRDs), and as Sp-A is a member of the collectin protein family, it recognizes and binds carbohydrates in a Ca²⁺-dependent process as a part of the immune defence system [97, 103]. Also, Sp-A is able to bind multiple ligands as sugars, Ca²⁺ and phospholipids in a cooperative manner [100], allowing Sp-A to bind to the surface of multiple pathogens like bacteria, viruses and funghi [89], but also associates with the lipid fraction of pulmonary surfactant via those globular structures [104, 105].

To measure the binding of SP-A onto the metal oxide nanoparticles, samples of both the supernatant and the pellet of the previously described adsorption experiment were each analyzed by SDS-PAGE under reducing conditions, followed by Western blot and immunostaining (Figure 4.2b).

TiO₂ A and BaSO₄ showed relatively low overall protein adsorption (30 % and 5 %, resp.), but nevertheless high Sp-A interaction as suggested by a strong SP-A signal in the pellet and a weak (TiO₂ A) or no (BaSO₄) signal in the supernatant. Obviously, those particles are adsorbing Sp-A very specifically. For the model protein BSA protein adsorption has been reported to be pH dependent, the maximum being near its isoelectric point [79, 82]. This, however, might not be transferable to the adsorption of Sp-

A to BaSO₄, as the pH of the BaSO₄ dispersion of 8.6 differs from the pI of Sp-A of 4.4-5.6. Interestingly, according to the manufacturer's specifications, both TiO₂ A and BaSO₄ bear some organic modifications (Table 4.2). As pBALF is not Ca²⁺-free, an ion-mediated adsorption to the organic groups of the two particles via the CRD domain of Sp-A may be possible, similarly as has been suspected by Salvador-Morales and Co-workers for accidental organic modifications of carbonanotubes [106].

AlOOH and CeO₂ C show an intermediate overall binding of pBALF proteins (Figure 4.2a). In contrast, binding of Sp-A to CeO₂ C was only weak, as indicated by the fact that the strongest signal was found in the supernatant and the weaker signal in the pellet. For AlOOH, Sp-A was only detected in the pellet, similar as for BaSO₄.

Strongest (~ 100 %) overall protein binding in pBALF was observed with TiO₂ B, CeO₂ A and B and carbon black. For neither of those particles any SP-A signal could be detected in the supernatant. For TiO₂ B and CeO₂ B, similar Sp-A adsorption to the nanoparticles was observed (intermediate Sp-A signal in the pellet). Only a very weak Sp-A signal was found for the CeO₂ A pellet, whereas carbon black revealed no Sp-A signal at all. The reason might be an extremely strong binding of the Sp-A to the surface of those types of nanoparticles, even resisting the conditions of the desorption protocol used in this study. As we stated previously, the globular domains of SP-A do not only bind to carbohydrates, but also to phospholipids. Although this interaction is considered superficial, it has hydrophobic and polar contributions [100]. As carbon black is very hydrophobic, a hydrophobic interaction between carbon black and the globular side of Sp-A might be speculated, boosted by the largest BET surface of all particles tested (340 m²/g). This also adds to the high affinity of overall protein binding, causing failure of the desorption protocol and hence empty lanes on the gels for both supernatant and pellet.

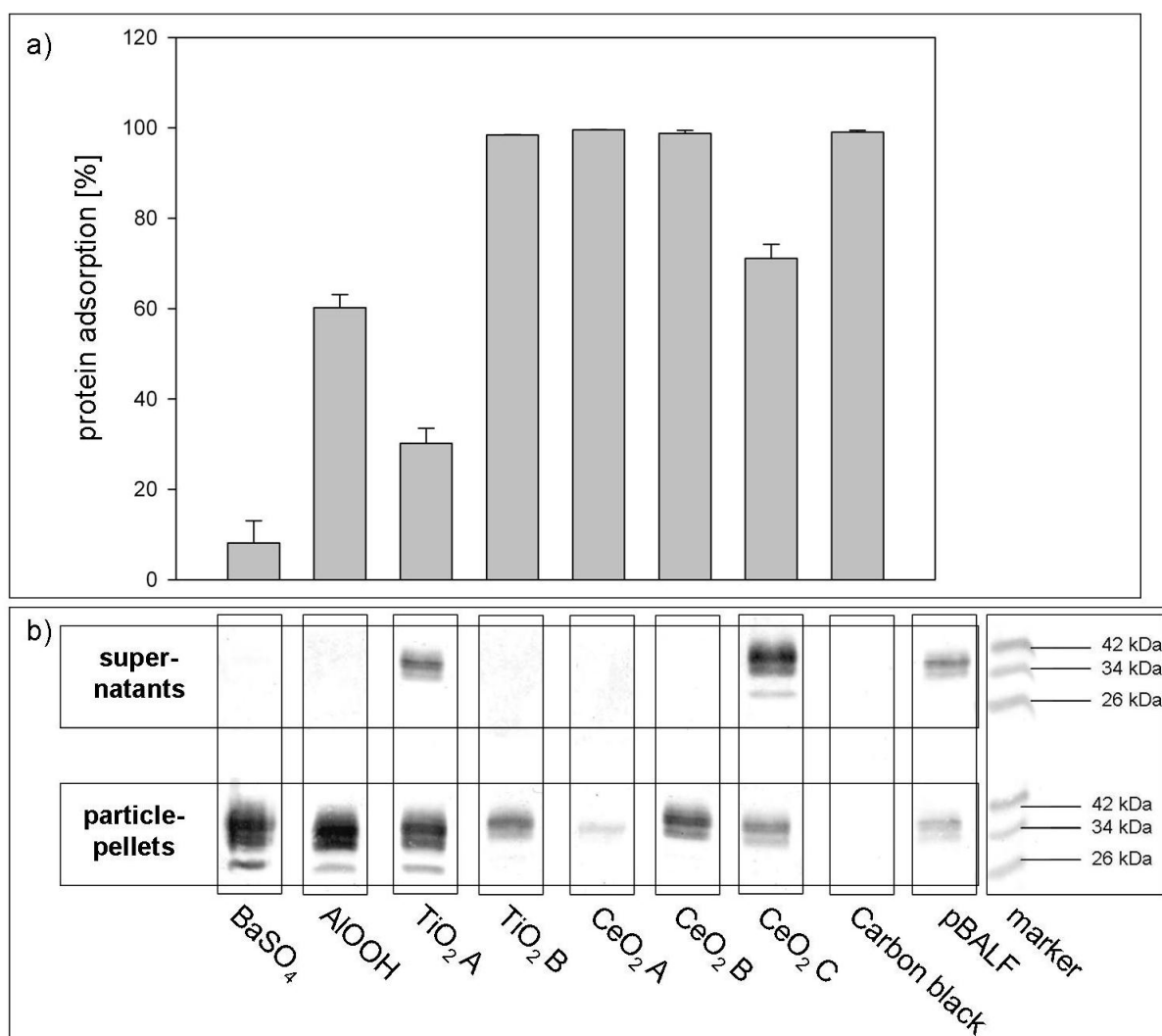


Figure 4.2. Adsorption of proteins from pBALF at a nanoparticle/protein ratio of 10:1. a) Total protein adsorption (BCA assay): The particles show striking differences, even when derived from the same bulk material. All values were related to the pBALF-supernatant after nanoparticle separation by centrifugation (mean + standard deviation; n=3). b) Immunoblot of Sp-A from supernatant and pelleted nanoparticles after conditioning in pBALF (Sp-A monomer: 36 kDa). As control, pBALF 1:10 diluted was used.

It is known that protein adsorption is depending on the hydrophobicity of the particle surface [76-78]. As stated previously, 90 wt% of ALF are (phospho)lipids and we cannot exclude the possibility of at least a partially washout of this lipid fraction into our pBALF. Hence, an indirect ad-

sorption mechanism, mediated or influenced by those lipids, is most likely.

Comparing the binding of pBALF proteins and in particular SP-A to the different nanomaterials in this study, no striking differences could be observed, even for nanoparticles made of the same material (e.g. CeO₂ A versus B or C; TiO₂ A versus B). There was no obvious correlation to physico-chemical data such as the mean primary particle size, surface area, etc. (Table 4.2), which would allow a prediction of protein binding from such data.

Investigation of deagglomeration capacity of pBALF. Complementary to protein binding, also the agglomeration behaviour of the same particles in pBALF was studied, as this is the second property that decides about a nanoparticle's trafficking in the body. Analytical Ultracentrifugation (AUC) with interference detection provides a signal that is directly linear with the concentration in the measurement interval [61]. The ultrafine fraction (below 100 nm diameter) can be quantified. In Figure 4.3, the resulting particle size distributions are shown with logarithmic axes. Only TiO₂ A and BaSO₄ are dispersible by stirring in water with 40 wt% and 0.5 wt% ultrafine fraction, respectively. For the more hydrophobic materials (carbon black, unfunctionalized metal oxides), less than 0.01 wt% ultrafine fraction is found in water, but media with serum or Sp-X enhance wetting and lower the degree of agglomeration. The detailed size distributions (Figure 4.3) indicate that agglomeration tendency in pBALF is significantly stronger than in Fetal Calf Serum (FCS; Figure 4.3, inserted table), which is widely used in cell culture media. Several studies have hinted at the dispersing power of albumin and other interface-active serum components on CNTs [29, 107, 108], metal carbide nanoparticles [109, 110] and metal oxide nanoparticles [109-112]. For mouse BALF, the degree of agglomeration of metal oxide nanoparticles was reported to be comparable with a buffer containing BSA and dipalmitoyl phosphatidyl choline [113] and in a BAL-mimicking dispersion medium [114], but only after 10 min. ultrasonication. Obviously, the anticipated interface activity

of Sp-X is in general not sufficiently strong to overcome the agglomeration tendency due to other components in complete pBALF. This result is in good agreement with histological studies of lung slices after inhalation exposure of rodents, where the particulate material that was deposited on the lung surface is found in the form of agglomerates [114].

The differences in protein adsorption of FCS compared to pBALF can also be seen in Figure 4.4: For six of the eight particles tested, there was a significant difference in protein adsorption for FCS at a particle-protein ratio of 10:1.

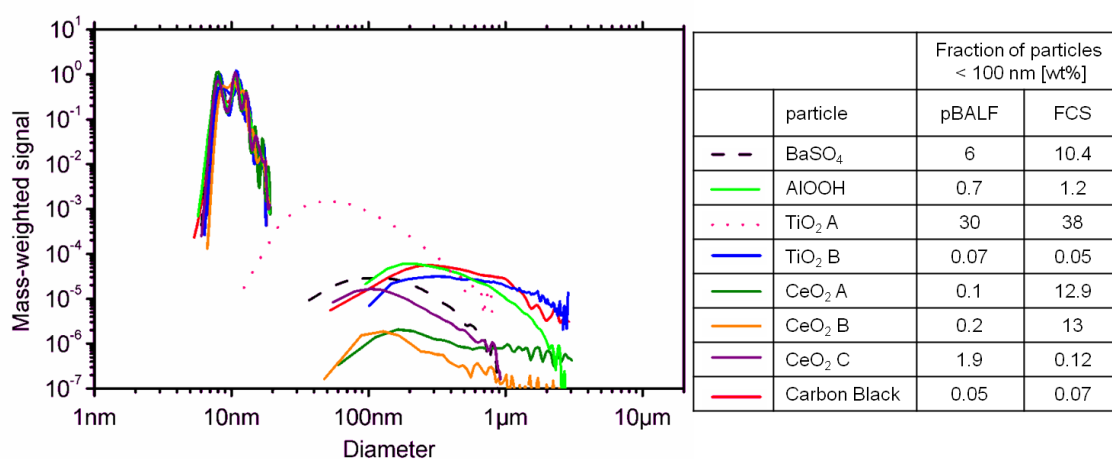


Figure 4.3. Full particle size distribution of nanoparticles in diluted pBALF (from interference-AUC). The table shows the initial weight ratio and the protein and particle concentrations within the shown size interval as well as the resultant ultra fine fraction of the particle suspension.

After inhalation and deposition in the deep lung, i.e. ALF, particles with a diameter of 1-6 μm are wetted and sink into the aqueous phase [23], whereas this mechanism is independent of shape, surface topography and surface free energy [115-118]. This process becomes even more efficient with decreasing particle size and this is expected to occur with nanoparticles, too [119]. As SP-A is integrated into the lipid structure of ALF, the tested nanoparticles most likely come in contact with SP-A *in vivo*.

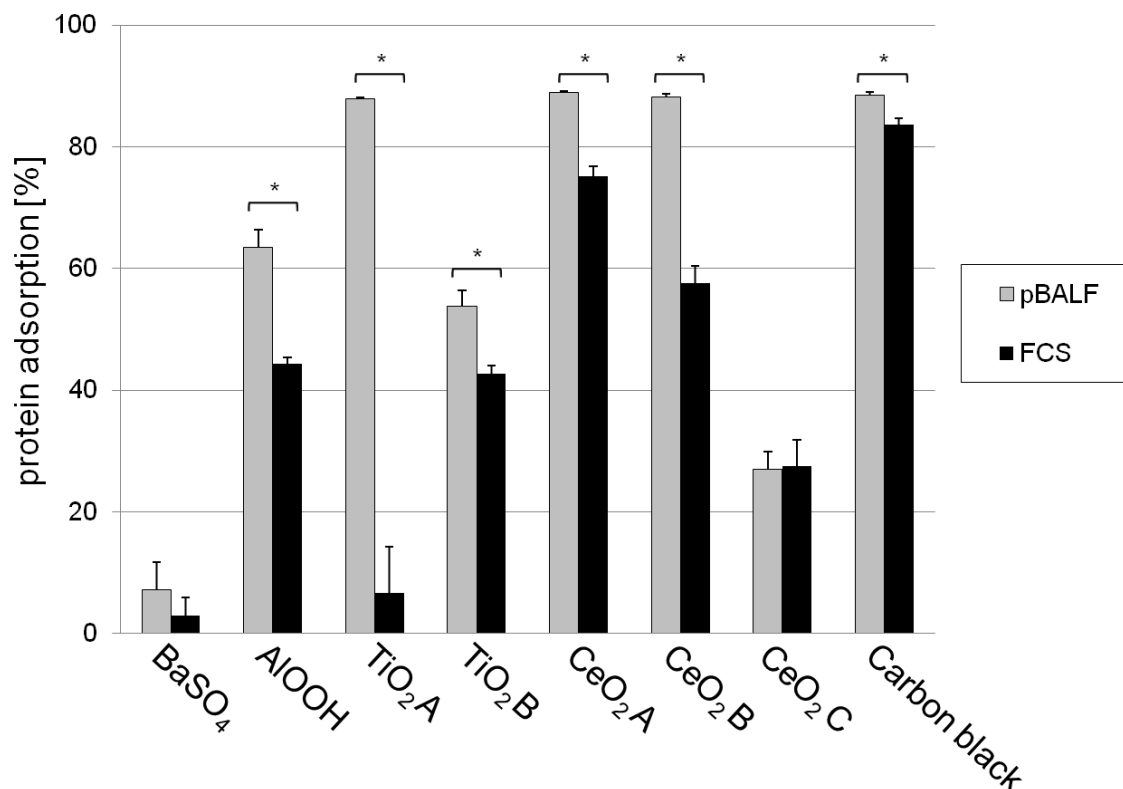


Figure 4.4. Comparison of pBALF and FCS adsorption onto metal oxide nanoparticles at a particle-protein relation of 10:1, determined with BCA-assay (statistics: Kruskal-Wallis One-way Analysis of Variance on Ranks, followed by pairwise comparison procedure with Student-Newman-Keul-method, $p < 0.05$).

The results clearly show that there are specific differences in the binding and interaction of metal oxide nanoparticles with Sp-A. A major biological role of Sp-A is to bind to inhaled particulate matter (e.g. microorganisms, dust, etc) to enhance their phagocytic clearance by macrophages [106, 120, 121]. In this way, SP-A plays an important role in limiting pulmonary infection, lung allergy and inflammation [95]. On the one hand, the binding pattern of Sp-A and other lung surfactant proteins may be decisive whether inhaled particles will be phagocytosed by macrophages and hence cleared from the deep lung to the airways. Although Geiser and colleagues found that the lung surface macrophages do not efficiently phagocytose these ultrafines but take them up in a rather sporadic and

unspecific way [122], most of our particles were highly agglomerated and thus still large enough for this clearance pathway. On the other hand, uptake and hence translocation of particles might be facilitated, as Type II cells, which cover the majority of the alveolar region, have Sp-A receptors that cause Phospholipid uptake [123]. Nanoparticles could be taken up "accidentally" via this surfactant trafficking. This theory is supported by data from *in vivo* experiments that also indicate nanoparticle uptake into epithelia of the respiratory tract via transcytosis and translocation into the lymphatic system or the blood stream [25].

In another way, the interaction of Sp-A with inhaled metal oxide nanoparticles could be important, as a relative Sp-A deficiency could occur due to its accumulation onto particles. Sp-A knockout mice are less effective in clearing lung pathogens and therefore these mice are more susceptible to lung infection. Sp-A deficient animals also present decreased phagocytosis and oxidant metabolism in response to instilled Group B streptococci [124]. There are even a few publications indicating disease correlation with lowered levels of Sp-A in humans. These include association of lowered SP-A levels with asthma and allergen-induced bronchial inflammation [97, 103]. Obviously, there are strong reasons to assume that the binding to Sp-A, and probably other lung surfactant proteins as well, can alter the toxicological properties of particulate matter, such as metal oxide nanoparticles, reaching the deep lung after inhalation drastically.

Strikingly, only the two particles that were organically functionalized with synthetic polymers (BaSO₄ powder and TiO₂ A) did not almost completely agglomerate after pBALF exposure. These are the same particles that differentiated by low overall protein adsorption, but strong Sp-A interaction (see Figure 4.2). This points again to the decisive role of the surface chemistry in nanotoxicology, and opens routes to control the fate of nanomaterials in the lung.

4.5 Conclusion

In this study, for the first time, differences in the interaction of industrially relevant metal oxide nanoparticles with physiologically relevant lung surfactant protein A were demonstrated. Attempts to correlate the adsorption patterns of Sp-A to those of commonly used model proteins failed, underscoring the need to apply sufficiently specific and sensitive analytical methods. In the future, further adsorption experiments with all four surfactant proteins must be performed to find out more about the structure activity relations between particles and their binding of lung surfactant proteins. Also, the effects of lung surfactant protein adsorption onto particles and their biological properties, in particular lung clearance by macrophages and translocation across the alveolar epithelium, must be investigated.

5 Transport of metal oxide nanoparticles across an in vitro air-blood barrier model: adaptations and results

Contributions:

Except particle characterization and metal oxide nanoparticle quantification, I performed all experiments, interpreted the data and prepared the manuscript.

Matthias Voetz (Bayer Technology Services GmbH, PT-MT-Materials Characterization & Testing, Leverkusen, Germany), Wendel Wohlleben (BASF SE, Polymer Physics Research, Ludwigshafen, Germany) and Cornel Venzago (AQura GmbH, Hanau-Wolfgang, Germany) quantified the metal oxide particles for the transport experiments.

Ulrich F. Schaefer and Claus-Michael Lehr helped interpreting the results and preparing the manuscript.

5.1 Abstract

As inhalation is the major exposure route for nanoparticles, the question if inhaled particles can overcome the alveolar barrier and hence enter the body is of great interest. Here, we adapted the for soluble substances well established Calu-3 in vitro air-blood barrier model to the use of nanoparticle transport testing. As the usually used filter supports hindered particle transport due to their small pore size, supports with a pore size of 3 μm had to be used. On those filters, barrier and transport characteristics of the cells were tested and culture conditions changed to gain optimal conditions. Functionality was confirmed with transport experiments with polystyrene model particles prior to testing of industrially relevant engineered metal oxide particles. Except for CeO_2 nanoparticles, no transport across the epithelial barrier model could be detected. For ZrO_2 nanoparticles, a compromised barrier function could be detected.

5.2 Introduction

As mentioned before, inhalation of nanoparticles into the lung is probably the most important route for nanoparticle exposure, especially as translocation of nanoparticles over the air-blood barrier into secondary target organs was recently proven in rats for iridium and carbon nanoparticles [125]. Overcoming the alveolar epithelium to access the blood stream might bear some risks: Instillation experiments with rats showed an increased carcinogenicity for TiO₂ and carbon black nanoparticles [126]. Also, numerous publications report cytotoxic effects or the provocation of oxidative stress in *in vitro* assays for silver [127, 128], iron oxide and manganese oxide [129] and silica nanoparticles [130]. Hence, the safety of nanoparticles is a major issue that needs attention and further investigation. Some *in vivo* inhalation and instillation experiments have been performed, mostly in rats, already. But for broad testing, *in vitro* assays were simpler, less time consuming, cheaper and ethically unproblematic. Grown on so called Transwell® filter devices, Calu-3 cells develop a tight monolayer, mimicking the alveolar air-blood barrier. In contrast to other *in vitro* lung models like the cell line A549, they develop tight junctions, which are the prerequisite for an intact barrier function and selective transport procedures [131]. Transport of substances from one side to the other can be due to different mechanisms: on one hand, the substance can be actively taken up into the cell, be transported through it and then released on the other side again (transcellular transport). On the other hand, opening of the tight junctions can occur, whereas either the substance per se or the cell itself can trigger this opening (paracellular transport). This model is well-known and characterized for soluble substances, e.g. pharmaceutically relevant chemicals, already [132-137]. However, to this type of experiments the pores of the support membrane for the cells has normally a diameter of 0.4 µm, which is in the range of the nanoparticles in use. Therefore, the model had to be tested and adopted for the use of those metal oxide nanoparticles, i.e. the filter inserts have to be replaced by inserts with a larger pore size of 3 µm. As those filter inserts reveal different properties (see Figure 5.1), the cells

might not be cultivated on those inserts, or they could grow through the pores and clog them, negating particle transport.

In this chapter, the necessary adaptations to the Calu-3 air-blood barrier model are reported, as well as characterized and compared to standard procedure. The functionality was proven by transport assays with polystyrene model particles prior of using this model for transport experiments with commercially available ZrO_2 , $AlOOH$ and two different TiO_2 and CeO_2 nanoparticles.

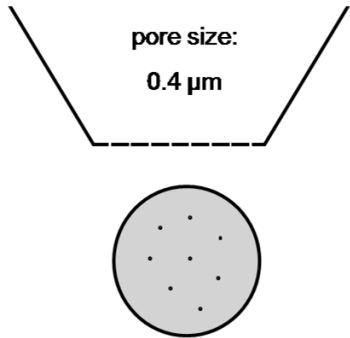
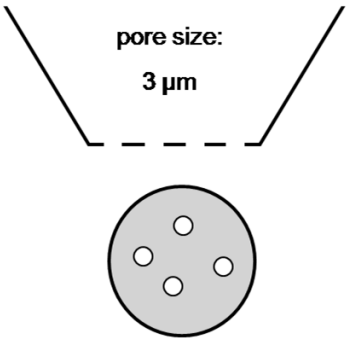
	<p>a)</p>  <p>pore size: 0.4 μm</p>	<p>b)</p>  <p>pore size: 3 μm</p>
pores/cm ² :	4·10 ⁶	2·10 ⁶
pore area/total filter area:	1:200	1:7
problem:	NP may not pass filter due to their size (50-200 nm)	cells may grow through the pores

Figure 5.1. Comparison of Transwell[®] filter systems for use in transport assays: a) System for dissolved drugs, b) adapted system for nanoparticle transport.

5.3 Materials & Methods

Materials. Polystyrene nanoparticles were purchased from Polysciences Europe GmbH, Eppelheim, Germany. All ingredients for Krebs-Ringer

buffer (KRB; 114.2 mM NaCl, 3 mM KCl, 1.5 mM $K_2HPO_4 \times 3 H_2O$, 10 mM HEPES, 4 mM D-Glucose, 1.4 mM $CaCl_2$, 2.56 mM $MgCl_2$) and PBS (137 mM NaCl, 8.1 mM $Na_2HPO_4 \times H_2O$, 2.7 mM KCl, 1.5 mM KH_2PO_4 , pH 7.4), as well as Bovine Serum Albumin, Na-Fluorescein, Triton X and Paraformaldehyde were from Sigma-Aldrich Chemie GmbH, Munich, Germany. The Transwell filter systems with a pore size of 0.4 μm and 3 μm were bought from Corning Inc., Corning, USA. RPMI 1650 medium and Fetal Calf Serum Gold (FCS Gold) were from PAA Laboratories GmbH, Cölbe, Germany, Na-Pyruvate solution from Cambrex GmbH, Taufkirchen, Germany. Xylol, alcian blue, Kernechtrot and Roti-Histokitt were purchased from Carl Roth GmbH + Co. KG, Karlsruhe, Germany. Propranolol-Hydrochloride was from Synopharm, Barsbuettel, Germany. Leica Histowax paraffin was bought from Leica Microsystems Inc, Bannockburn, USA.

Permeation of polystyrene nanoparticles through filters of different pore sizes without cells. Polystyrene nanoparticles with a diameter of 0.05 μm , 0.1 μm or 0.2 μm , carboxylated or plain, were dispersed in KRB + 1 % Bovine Serum Albumin in a concentration of 224 $\mu g/ml$ (corresponding to a concentration of 100 $\mu g/cm^2$). The apical compartments of the Corning Transwell systems with a pore diameter of 0.4 μm or 3 μm were filled with 0.5 ml of particle dispersion. The basolateral side was filled with KRB + 1 % BSA and incubated under shaking at 200 rpm for 6 h at 37 °C in an incubator. After 6 h, samples from apical as well as from the basolateral compartments were taken and fluorescence read out (λ_{ex} = 485/20 nm; λ_{em} = 530/30 nm, Multiwell Plate Reader from Tecan Group Ltd., Maennedorf, Switzerland) to quantify the amount of particles in each compartment. Total recovery was determined as the amount of nanoparticles in the apical and basolateral compartment in comparison to the initially applied amount and was found as $100 \pm 10 \%$.

Calu-3 cell culture. Calu-3 cells from American Type Culture Collection, Manassas, USA, were grown in RPMI 1650 medium with a supplement of 5 ml of Na-Pyruvate and 10 % FCS Gold up to 90 % of confluence and

splitting once a week in a ratio of 1:5 to 1:7. The passages from 28 to 50 were used for experiments.

For the preparation of transport assays, 10^5 cells/well were seeded in Transwell inserts and cultured for 7-10 days prior to use. Only cell monolayers with TEER values of $> 800 \Omega\text{cm}^2$ were used for experiments.

Cross sections and staining of Calu-3 cells on filters with different pore sizes. Cell layers grown on filters with $0.4 \mu\text{m}$ or $3 \mu\text{m}$ were cut off from the Transwell system including the filter membrane at day 10 or 7 respectively and fixed in 4 % Paraformaldehyde in PBS. The filters were embedded into paraffin (Leica Histowax), cut in $4 \mu\text{m}$ slices and collected on glass slides. After prewarming them for 15 min at 37°C , the samples were incubated in xylol for 5 min prior to incubation in a descending isopropanol series for 5 min for each alcohol concentration (100 %, 96 % and 70 % in deionized water). After rinsing in deionized water for 5 min, the samples were dyed with alcian blue (in 3 % acetic acid) for 30 min prior to rinsing with deionized water. Then, the samples were incubated with Kernechtrot and rinsed with deionized water again. After incubation in an ascending isopropanol series (conversely to the descending series) the samples were kept in xylol for 5 min and covered with Roti-Histokitt.

TEER profile of Calu-3 cells grown on filter inserts with different pore sizes. The cells were cultured as described above and seeded into the filter inserts with a density of $0.75 \cdot 10^5$, $1 \cdot 10^5$ or $1.25 \cdot 10^5$ cells/well. TEER values were measured with a voltohmmeter equipped with STX-2 chopstick electrodes (Evom from World Precision Instruments, Berlin, Germany) directly after seeding and then before every change of medium, until the TEER values clearly have passed their maximum.

Transport assays with model substances Na-Fluorescein and Propranolol. The test substances were dissolved in KRB in a concentration of $30 \mu\text{M}$ and added to the apical side. Samples were taken from the basolateral compartment directly after application, after 15 min, 30 min, 45 min, 60 min, 90 min and 120 min, the volume was refilled with pre-warmed KRB. Propranolol-Hydrochloride was quantified with High Pres-

sure Liquid Chromatography as described previously by Becker and colleagues [138], Na-Fluorescein with a Tecan Multiwell reader ($\lambda_{\text{ex}}= 485/20$ nm; $\lambda_{\text{em}}= 530/30$ nm).

Transport assays without cells were performed in the same way for both substances, except the sampling intervals were shortened to 2 min, 5 min, 7 min, 10 min and 15 min.

Transport experiments with polystyrene model particles. The particles used for permeability experiments of the blank filters were also used for transport experiments with Calu-3 cells. The cells were incubated with 224 $\mu\text{g}/\text{ml}$ of particle dispersed in KRB + 1 % BSA for 6 h. The quantification was performed as described above and the amount of particles transported was calculated in relation to the initial amount of particles used.

Transport experiments with metal oxide nanoparticles. Prior to use, the particles were sterilized by γ -irradiation as described earlier (see chapter 2.3) to avoid contamination of the cells during the transport assay. Also, the snap-on lid glasses and magnetic stirrers were sterilized as described in chapter 2.3 and particle dispersions prepared under sterile conditions. Cells were grown on filter inserts with a pore size of 3 μm and cultured for 7-10 days. Only cells that reached TEER values of 800 Ωcm^2 or more were used. The preparation of the particle dispersion was following the protocol of the project NanoCare we described earlier (see chapter 2.3). In a concentration of 224 $\mu\text{g}/\text{ml}$ (corresponding to 100 $\mu\text{g}/\text{cm}^2$), the particles were dispersed in RPMI 1650 medium + 10 % FCS Gold. The incubation time was 6 or 24 h at 37 C° under gentle shaking (200 rpm). Before incubation, 0.1 ml from each compartment was taken and diluted in 9.9 ml of the dispersion medium. At the end of the experiment, TEER was checked. The apical as well as the basolateral compartment were extracted and washed 3 times with dispersion medium (apical compartments with 0.5 ml, basolateral compartments with 1.5 ml). The samples of each compartment were pooled in a test tube and filled up to a volume of 10 ml, leading to a dilution of 1:20 for the apical and 1:6.7 for the basolateral compartments. For determination of the amount of nanoparticle

in the cell layer and filter membrane, the Transwells were immersed with 4 ml of dispersion medium + 1 % Triton X and incubated for 0.5 h at 37 °C under gentle shaking. Finally, those 4 ml were withdrawn by suction and pooled with the dispersion medium from two washing steps (2 x 3 ml of dispersion medium + 1 % Triton X, leading to a total volume of 10 ml). All samples were frozen at -80 °C until quantification of the metal with Inductively coupled Plasma Mass Spectrometry (ICP-MS) or Inductively coupled plasma optical emission spectrometry (ICP-OES).

Quantification of metal oxide nanoparticles. Only the metal ion was quantified and afterwards related by means of atomic mass to the nanoparticle oxides. Furthermore, all dilution factors were taken into account.

Quantification of ZrO₂ and AlOOH with inductively coupled plasma optical emission spectrometry (ICP-OES). *ZrO₂.* Standard Zr solutions in 3 % HCl in H₂O (200 ppm, 100 ppm, 20 ppm, 10 ppm, 2 ppm, 1 ppm) were prepared and diluted 1:10 in RPMI medium + 10 % FCS to prepare a calibration line. The accuracy of the calibration line was controlled by comparison to the Zr-specific signals at 343.823 nm and 339.198 nm. Measurements were performed with a Spektro Flame D with a Crossflow vaporizer and a flow of 1.6-1.8 ml/min (high frequency generator 1200 W). At the sample injector equilibrium was established by a higher flow rate for 15 s. Samples were measured and compared to the calibration line to quantify the Zr concentration of the samples. After 15-20 measurements, the optics were repositioned and the calibration line remeasured before further sample investigation. The resulting Zr concentrations were converted to the corresponding ZrO₂ amount. The limit of detection was 0.5 ppm for the Zr ions.

AlOOH. 200 ppm of AlOOH was solubilized in concentrated H₂SO₄ prior to dilution in 1 % H₂SO₄ to a calibration line (concentrations 50 ppm, 20 ppm, 10 ppm, 2 ppm, 1 ppm). The calibration line was controlled by measurement of an Al standard solution (1 mg/ml) at 394.401 nm and 396.152 nm. Sample measurement was performed analogue to Zr and

also converted to the corresponding AlOOH amount. Also here, the limit of detection was 0.5 ppm.

Quantification of CeO₂ A and C as well as TiO₂ A and B with Inductively Coupled Plasma Mass Spectrometry (ICP-MS). *CeO₂ A and C.*

After disintegration of the particles with nitric acid, the Cerium content of the solution was determined with ICP-MS (Agilent 7500a, with a Meinhardt vaporizer and a 1300 W generator). As an internal standard, ⁴⁵Sc was used; the limit of detection was 0.1 ppm for the metal ion.

TiO₂ A and B. Thawed and homogenized samples were disintegrated with nitric acid and hydrofluoric acid by means of pressurized vessel digestion in a microwave autoclave (UltraClave III, Milestone, Leutkirch, Germany). Measurement was performed by ICP-MS (ThermoFisher, X-Series-2, Bremen, Germany). The instrument was equipped with a microconcentric nebulizer (AHF, Tübingen, Germany) and run at a generator power of 1300 W. Indium was used as internal standard at a concentration of 1 µg/l. ⁴⁹Ti was used as the analyte isotope for the evaluation of the results. According to the lowest calibration point the limit of quantification was estimated at 0.5µg/ml.

Physico-chemical characterization of the metal oxide nanoparticles.

For detailed characteristics of the particles, see Table 5.1. The particles were varying in their bulk material, although we investigated two TiO₂ particles, with or without organic modification. Also, we used two CeO₂ particles, whereas the CeO₂ A particles had a smaller primary particle size, a much bigger surface and were slightly less acidic than CeO₂ C. For details on the methodologies for particle characterization, see chapter 3.3.

Table 5.1. Characteristics of the used metal oxide nanoparticles (data adopted from [35]; n.d.: not determined).

sample	chemical composition, crystallinity	mean primary particle size, morphology	BET surface area [m ² /g]	surface chemistry [At%]	organic modification	pH#	solubility in water [ppm]
ZrO₂	ZrO ₂ monoclinic Baddelyite tetragonal	14 nm, irregular but globular	122	O 55 Zr 21 C 24 Cl 0.6	Organic acid with mass = 180 g/mol	3.7	190
AlOOH	82.7 % AlOOH; impurities: C, Na, Fe, Si, Li, B	40 nm, irregular but spherical	47	O 62 Al 32 C 7	none	4.3	n.d.
TiO₂ A	O 58 % Ti 41 % Cl > 1 % anatase 95 %, rutile 5 %	17 nm irregular but spherical	117	O 53 Ti 21 C 25 Cl 1	yes	5.4	10
TiO₂ B	>99.5 % TiO ₂ rutile and anatase, tetragonal	27 nm irregular but globular	52	O 58 Ti 26 C 14 N 0.5 Cl 1	none	6.1	130
CeO₂ A	> 99.97 % purity	14 nm cubic, aggregated	63	O 57 Ce 25 C 18	none	5.9	n.d.
CeO₂ C	>99 % CeO ₂ Cerianite, cubic	70 nm irregular but globular	33	O 53 Ce 26 C 20 Cl 0.6	none	5.9	> 1

5.4 Results & Discussion

Adaptations of the Calu-3 air-blood barrier model to nanoparticles.

Normally, filters with a pore size of 0.4 μm are used within the Transwell system, but as shown in Figure 5.2, this filter material even used without a cell layer provided a significant barrier to particles up to 200 nm. Hence, filters with a pore size of 3 μm were tested. Clearly, this change revealed a transport of up to 100 % of the theoretical equilibrium concentration in the acceptor after an incubation period of 6 hours only, which is a prerequisite for further studies with cell layers.

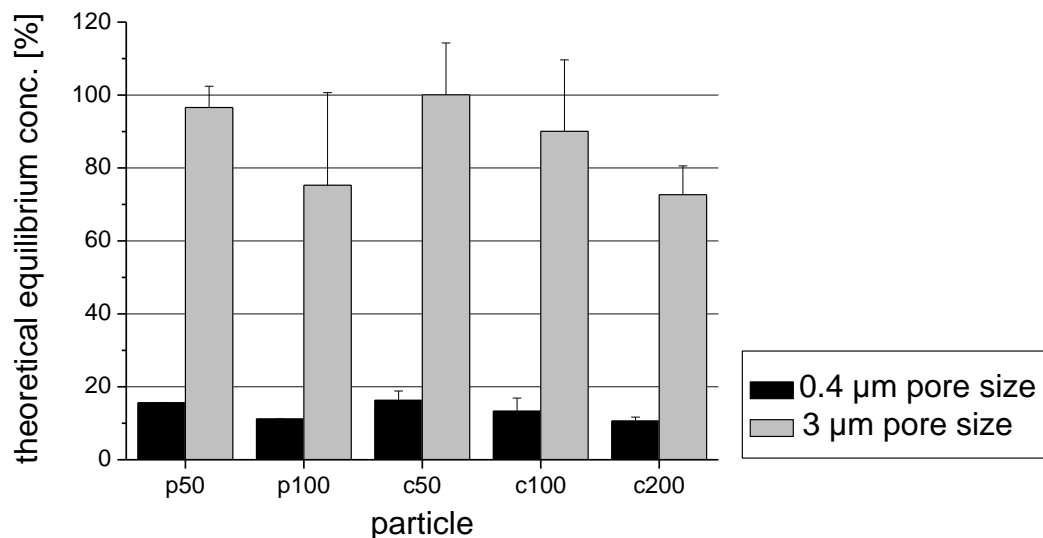


Figure 5.2. Permeation of model particles through blank filters with different pore sizes: After 6 h of incubation, up to total concentration equilibrium was achieved for particles permeated through the filter with the large pores, whereas a pore size of 0.4 μm was a significant barrier for particle permeation (c=carboxylated; p=plain; the number corresponds to the particle diameter; shaking rate 200 rpm; mean + sd).

These results indicated that the use of filter inserts with a pore size of 3 μm is needed to perform particle-related transport assays without taking the likelihood of wrong negative results.

Since the larger pore size is very big relative to the cells used, the relevant cell characteristics had to be investigated. As mentioned in Figure 5.1, the cells could grow into the pores or even on both sides of the filters, leading to reinforcement of the barrier and hence falsification of permeation rates. Comparison of cross sections of Calu-3 cells on filter inserts with 0.4 μm or 3 μm pore size respectively did not reveal any visible difference in morphology (Figure 5.3). Also, the cells did grow only on the surface of the filters, no invasion into the pores or even growth on both sides of the filters occurred.

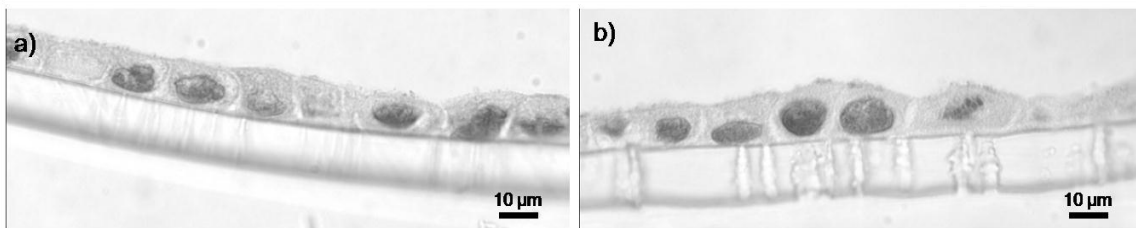


Figure 5.3. Calu-3 cell monolayers on filter inserts with different pore sizes: a) pore size of 0.4 μm , Calu-3 cells at day 7; b) pore size of 3 μm , Calu-3 cells at day 10. Clearly, the different size of the pores can be recognized. Both pictures show a confluent cell monolayer without intercellular spaces. Hence, no differences in morphology can be seen for both monolayers. (seeding density 10^5 cells/ cm^2 ; TEER values $> 800 \Omega\text{cm}^2$; magnification 100x)

Still, similar morphologies alone are no sufficient indicator for analogous barrier properties. Hence, we investigated the integrity of the monolayer by measuring the TEER profile. As can be seen in Figure 5.4, Calu-3 cells grown on filter inserts with both pore sizes reached TEER values of more than $1000 \Omega\text{cm}^2$, but the maximum for cells grown on the filters with 3 μm pores was lower than for the smaller pore size. Also, the time frame in which the cells kept up these high TEER values was for the larger pore size much shorter (4 days) than for the cells on the smaller pores (up to 9

days). For Calu-3 cells on filters with 0.4 μm pores, a seeding density of $7.5 \cdot 10^4$ cells per well (equals an area of 1.12 cm^2) was sufficient, whereas the optimal seeding density for growth on larger pores should be increased to 10^5 cells/well, as less cells lead to a slower increase of TEER values and a shortened time period for experiments (Figure 5.4). In literature, TEER values from 400 to 600 Ωcm^2 , but also from 700 up to 2500 Ωcm^2 were reported [139-141]. Geys and colleagues postulated the Calu-3 monolayers to be tight at a TEER of 575 Ωcm^2 for the 0.4 μm pores and at 420 Ωcm^2 for filters with 3 μm pore size [142]. Although differences in the TEER profile could be detected, an intact barrier function seemed to be given also with filters of the larger pore size.

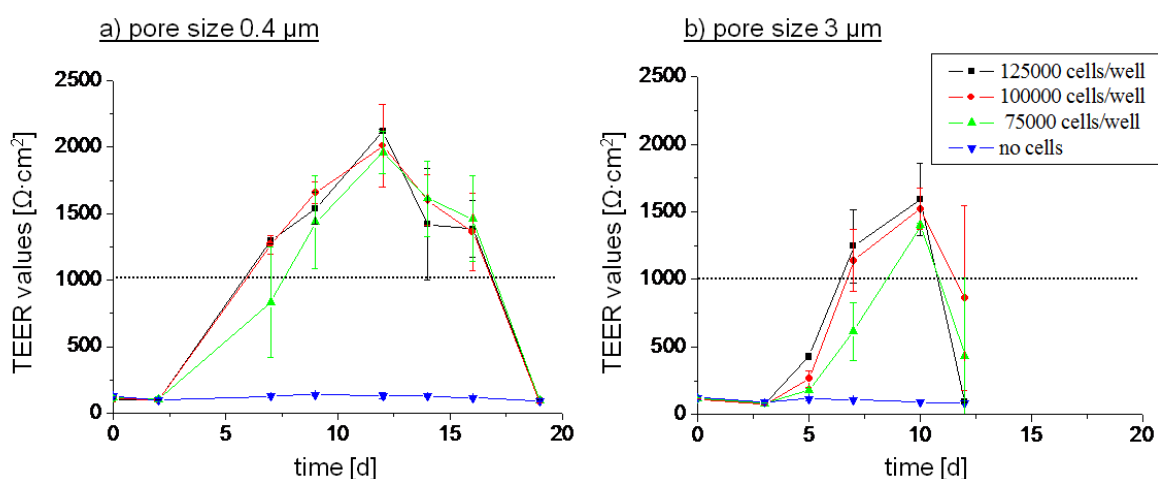


Figure 5.4. TEER profiles of Calu-3 cells grown on filter inserts with different pore sizes: Both pore sizes lead to TEER values of more than 1000 Ωcm^2 , although the time line are varying. For Calu-3 cells on filters with a pore size of 3 μm the maximum is lower and is reached earlier than on filters with the smaller pore size. Also, the time frame for experiments is with 4 days for the larger pores size shorter than 9-10 days, respectively (mean \pm sd, n=9).

Although the integrity of the monolayer could be proven, the bigger pore size still might have an influence on transport patterns. We calculated

the total “pore area” of both filters to be $5 \cdot 10^{-3} \text{ cm}^2$ (0.4 μm pore size) or 0.14 cm^2 (3 μm pore size), respectively. This results in the much higher relation of this “pore area” compared with total filter area, although both filters have equal dimensions (see Figure 5.1). A larger pore area means also more contact of the cells with the basolateral compartment, hence, an altered transport pattern of the cells due to this fact had to be checked. Transport assays with well characterized soluble model substances were performed with filter inserts of both pore sizes with and without cell monolayers and compared. As high permeability marker the lipophilic drug propranolol was used, the hydrophilic sodium-fluorescein was the model substance for low permeation. Clearly, the cell monolayer with its lipophilic membrane is only a weak barrier to propranolol, and no significant difference in permeation could be detected for both pore sizes. Also, there was no difference between the two filters without the cells, suggesting permeation not only through the pores, but through the whole filter area. It might be speculated that diffusion not only occurs through the pores, but also through the PET membrane, diminishing the effect of the larger pore area/filter area ratio of the filters with the 3 μm pore size. For the filters with the smaller pores, the P_{app} value for the low permeation marker sodium fluorescein was in very good agreement with literature [143]. However, the P_{app} value for sodium-fluorescein was about five times higher for the larger pore size, but experiments without cells clearly confirm this to be due to the larger diffusion area in favour of the filters with 3 μm pores, as the same ratio occurred in experiments without cells (see Table 5.2). In contrast to propranolol, the filter material seems to be an effective barrier and permeation occurs through the pores only. These results confirm that no change in transport patterns occurred; the higher P_{app} -value for the low permeability marker was caused by simple physics.

Table 5.2. P_{app} values for propranolol as high and sodium-fluorescein as low permeability marker, tested with and without cell monolayers, to confirm similar transport patterns for Calu-3 cells on both filter inserts (TEER for experiments containing Calu-3 cells $> 800 \Omega\text{cm}^2$ before and after transport assays; mean \pm sd, n=3).

	P_{app} high permeability marker (Propranolol-HCl) [cm/s]		P_{app} low permeability marker (Sodium-Fluorescein) [cm/s]	
	filter only	cell monolayer	filter only	cell monolayer
pore size				
0.4 μm	$7.34 \pm 1.19 \cdot 10^{-5}$	$3.13 \pm 0.22 \cdot 10^{-5}$	$3.83 \pm 0.09 \cdot 10^{-5}$	$1.61 \pm 0.05 \cdot 10^{-7}$
3 μm	$7.2 \pm 0.25 \cdot 10^{-5}$	$4.86 \pm 0.35 \cdot 10^{-5}$	$20.6 \pm 0.5 \cdot 10^{-5}$	$9.37 \pm 0.38 \cdot 10^{-7}$
ratio 3 $\mu\text{m}/0.4 \mu\text{m}$	1	1.5	5.4	5.82

Transport experiments with polystyrene model particles. As proof of the functionality of the adapted barrier model, transport experiments with polystyrene model particles with a size range from 50 to 200 nm were performed. Clearly, a particle transport of up to 4 % after 24 h of incubation could be seen (Figure 5.5), which is corresponding well to the transport rates found in literature for Calu-3 cells [142]. Smaller particles seem to be transported in higher amounts than the larger 200 nm particles, but only the plain 50 nm particle showed a significantly higher transport rate compared to the larger particles. A generally increased transport for the plain particles cannot be confirmed. To rule out transport of the fluorescent dye only after cleavage from the particle, the presence of particles in basolateral samples was tested via Dynamic Light Scattering. In all samples, particles could be detected of the same size as applied in the apical compartment.

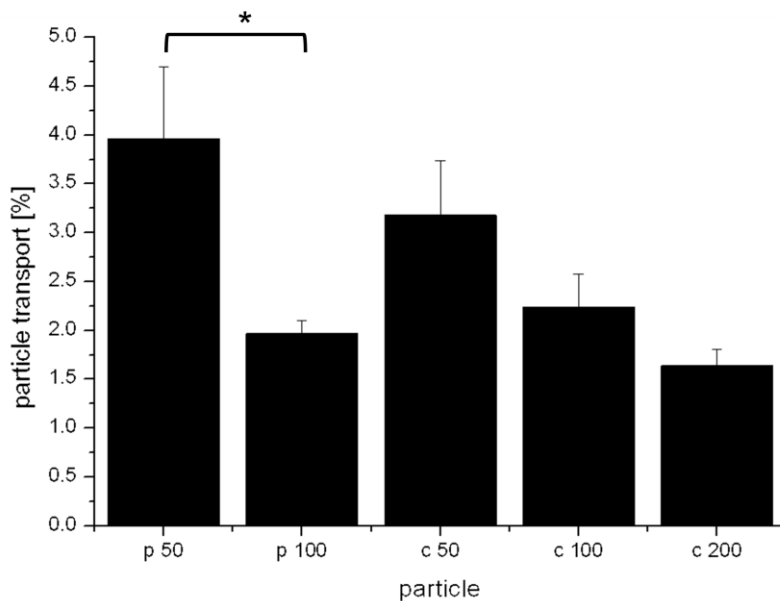


Figure 5.5. Transport of model polystyrene particles over Calu-3-cell monolayers grown on supports with 3 μm pore size from apical to basolateral side after an incubation time of 24 h. The TEER for the Calu-3 cells exceeded 800 Ωcm^2 before and after transport assays. Significant differences are marked with a (*) (p=plain particle without surface modifications, c=carboxylated surface; numbers represent the diameter of the particle; mean + sd; n=3; statistics: One way ANOVA, followed by pair wise multiple comparison with Holm-Sidak-method, $p < 0.05$).

Transport of metal oxide nanoparticles. The transport assays with metal oxide nanoparticles were performed with a particle concentration of 100 $\mu\text{g}/\text{cm}^2$ (=224 $\mu\text{g}/\text{ml}$) for 6 and 24 h of incubation under sterile conditions. The transport results are summarized in Table 5.3: All of the particles tested permeated through the naked filter, i.e. the filter pores were no significant obstacle for particle permeation. For ZrO_2 , AlOOH and both TiO_2 particles neither a transport nor particle uptake into the cell or adhesion onto the cell surface could be detected. This is in good agreement with *in vivo* short and long-term inhalation studies performed with the very same TiO_2 and AlOOH particles, as no translocation into liver, kidney, spleen or basal brain with olfactory bulb could be detected [35, 144]. In those inhalation studies, also CeO_2 C was tested negative for translocation into the mentioned organs. This is in contrast to our findings, as

we could prove a particle transport similar to that of the carboxylated 100 nm model particle (see Figure 5.5). Also, cerium could be detected in the cell lysates and filter washout samples, indicating a transcellular transport of the CeO₂ particles. The particle concentrations for CeO₂ C in the in vivo assay was with a maximum concentration of 10 mg/m³ (= 0.01 µg/ml) much lower than the concentration tested here (100 µg/cm²= 224 µg/ml). Therefore, an overload effect may be a plausible explanation for the transport detected. Still, a decrease in concentration was not possible due to the detection limits of ICP-MS.

Table 5.3. Summary of transport assays performed with metal oxide nanoparticles after an incubation time of 24 h; Except for both CeO₂ particles, no transport could be detected (n=3; mean ± sd).

nano-particle	theoretical equilibrium conc. through naked filter [%]	transport through cells after 24 h [%]	cellular uptake & filter washout after 24 h [%]
ZrO ₂	54.6 ± 5.8	0	0
AlOOH	62.2 ± 25.5	0	0
TiO ₂ A	27 ± 4.9	0	0
TiO ₂ B	46.4 ± 5.4	0	0
CeO ₂ A	31.9 ± 5.6	3.5 ± 1.3	3.5 ± 1.3
CeO ₂ C	75.9 ± 50.2	3.2 ± 0.1	5.5 ± 2.1

The TEER value is an indicator of an intact epithelial cell monolayer with proper barrier functions. Hence, when the monolayer is compromised, the TEER is decreasing. Controlling of the TEER before and after the incubation with ZrO₂ particles revealed a significant decrease of TEER after 24 h compared to the negative control (Table 5.4). Although the barrier seemed to be compromised, no ZrO₂ translocation could be detected. In all experiments, also the negative controls, TEER (treated with dispersion

medium instead of particle dispersion) decreased after 24 h. The same ZrO₂ particles (concentrations of 0.1 -10 µg/cm²) tested on MDCK II and NRK52E cells had no effect on TEER [35]. Hence, the TEER decrease for ZrO₂ is more likely to be due to the experimental procedure or also an overload effect.

Table 5.4. TEER values of the cells after 6 or 24 h of incubation with (=samples) or without nanoparticles (=negative contr.). The data are relative to the TEER measurements taken immediately before incubation (mean ± sd). The only particle revealing a significant decrease in barrier function is ZrO₂ after an incubation of 24 h (grey cells; P=0.95).

	TEER after 6 h incubation [%]		TEER after 24 h incubation [%]	
	sample	negative contr.	sample	negative contr.
ZrO₂	79.7 ± 9.7	86.6 ± 2	47.4 ± 6.8	69.8 ± 3.5
AlOOH	58.5 ± 10.6	47.7 ± 3.4	29.6 ± 1.3	49.8 ± 16.3
TiO₂ A	82.9 ± 5.1	68.1 ± 6.4	29.6 ± 3.7	23.8 ± 3.7
TiO₂ B	85.1 ± 2.3	83.6 ± 5	21.1 ± 0.2	21.4 ± 1.3
CeO₂ A	104.3 ± 26.2	74 ± 17.8	39 ± 8.9	34.4 ± 9.6
CeO₂ C	54.9 ± 17.3	46.3 ± 6.8	43.3 ± 5.9	37.4 ± 6.2

5.5 Conclusion

To test the transport of nanoparticles with the air-blood barrier model Calu-3, the model had to be adapted by adjusting the pore size of the filter inserts the cells are grown on. Clearly, this change did not influence the transport patterns of the cells, although the seeding density as well as the time frame for experiments had to be adjusted. The functionality of the model was proven with polystyrene model particles prior to experiments with much more complicated to handle metal oxide nanoparticles. Although the TEER values decreased in all experiments, no translocation

was detected for ZrO_2 , TiO_2 A and B and for $AlOOH$. Only CeO_2 A and C revealed a transport. As metal oxide nanoparticles are not easily detected and quantified, determination of transport rates is a challenging task, whereas the optimal experimental setup is still to be improved.

Summary and outlook

Industrial nanoparticles are not developed to be compatible with *in vitro* cell culture assays which are carried out in isotonic solutions at physiological pH and often in the presence of proteins. The tendency of nanoparticles to deagglomerate or agglomerate is strongly sensitive to these parameters. The state of agglomeration and the protein corona bear an important influence on the level of toxic effects via the change of transport mechanisms and surface coating. Here the interaction of nanoparticles with physiological media for *in-vitro* nanotoxicology experiments was rigorously characterized. Beyond adsorption of proteins on metal oxide and polymeric nanoparticles, nanoparticle deagglomeration due to adsorbing proteins acting as protection colloids was quantified. Previously neglected, but indispensable testing of sterility and measures to ensure it were reported. These findings resulted in a checklist of pre-requirements for dispersion of nanoparticles in physiological media and for reliable attribution of potential toxic effects.

Once nanoparticles have entered the body, they can interact with the physiological surroundings, i.e. also with proteins. This particle-protein interaction might lead to altered reactions concerning the particles, influencing their bio-persistence in the body. Hence, the investigation of protein adsorption onto those particles is of great importance. Here, the protein adsorption of Bovine Serum Albumin to three CeO₂ nanoparticles with only slightly different physico-chemical properties were investigated and compared with Atomic Force Spectroscopy, Analytical Ultracentrifugation and BCA-assay. All adsorption processes could be fitted with a sigmoid mathematic model, revealing differences in half-maximal adsorption for especially one of the three particles. Clearly, particles of the same bulk material do not necessarily reveal the same adsorption pattern for proteins, and the state of agglomeration must be taken into account to interpret the results correctly. Also, it was shown that the protein might

alter its shape during adsorption process specifically for the different particles tested. It can be concluded that even small differences concerning particle properties can lead to different protein adsorption and hence might provoke different reactions in the body. This means that testing of one particle of a bulk material as reference is not enough to determine the potential toxicity of nanomaterials.

After inhalation, the Alveolar Lining Fluid (ALF) covering the respiratory epithelium of the deep lung is the first biological barrier encountered by nanoparticles. Hence, the adsorption of Surfactant protein A, the predominant protein component of pulmonary surfactant (an integral part of ALF), was investigated. For the first time significant differences for metal oxide nanoparticles to the binding of Sp-A were reported. Sp-A is a physiologically most relevant protein and provides important biological signals. Also, it is involved in the lung's immune defense, controlling e.g. particle binding, uptake or transcytosis by epithelial cells and macrophages. In this work, different particle-protein interactions for eight different nanoparticles were proven, whereas particles of the same bulk material revealed different adsorption patterns. In contrast to other proteins as Bovine Serum Albumin (BSA), Sp-A does not seem to significantly deagglomerate large agglomerates of particles, indicating different adsorption mechanisms as in the well-investigated model protein BSA. These findings may have important consequences for biological fate and toxicological effects of inhaled nanomaterials.

Inhaled nanoparticles could not only adsorb physiologically relevant Surfactant components, but also translocate over the air-blood barrier. The for soluble substances well established Calu-3 *in vitro* air-blood barrier model was adapted to the use of nanoparticle transport testing. As the usually used filter supports hindered particle transport due to their small pore size, supports with a pore size of 3 μm had to be used. On those filters, barrier and transport characteristics of the cells were tested and culture conditions changed to gain optimal conditions. Functionality was confirmed with transport experiments with polystyrene model particles

prior to testing of industrially relevant engineered metal oxide particles. Except for two different CeO₂ nanoparticles, no transport across the epithelial barrier model could be detected. For ZrO₂ nanoparticles, a compromised barrier function could be seen.

In chapter 5, we mentioned the possible transport routes for nanoparticles over our epithelial model. As we have proven for polystyrene model particles, some nanomaterials can be transported via those routes. However, an expansion of the epithelial model to a triple cell culture, containing macrophages on the apical and Dendritic cells on the basal side [145-147], reveals more possibilities of overcoming the epithelial barrier. Blank and colleagues. could show that polystyrene particles with a size of 1 μm were rarely taken up by the epithelial cells, but by the macrophages and the Dendritic cells, either by extensions or total migration of the Dendritic cells through the epithelium. Also, particle transport between Dendritic cells and between Macrophages and Dendritic cells could be shown [148]. This particle transport is not disrupting the integrity of the epithelial layer [149]. Those transport routes might be relevant for the tested particles, too, i.e. a negative result with our “epithelium only” model does not guarantee no transport is happening at all. In the future, further investigations with those triple cell cultures, mimicking reality more closely, might bring new insights in the transport pattern of metal oxide particles. Furthermore, after thorough comparison, it might be possible to use this extended triple cell culture model to eventually replace animal testing under certain circumstances.

Also, the impact of protein adsorption, especially of physiologically relevant proteins like Sp-A, must be investigated more intensely. After refinement of the pBALF generation protocol, protein conditioned nanoparticles of the same material, but with different physical properties, i.e. ζ -potential or hydrophobicity, have to be investigated to correlate Sp-X adsorption to specific particle properties. Although we demonstrated articulate differences in protein adsorption on nanoparticles with similar properties, at least a rough estimate on protein adsorption mechanisms might be possible.

Conditioning with Sp-X might have some influence on the reaction of the cells at the air-blood barrier. Hence, an influence on the particle transport and other cell reactions after conditioning should be investigated. For this purpose, aerosolized conditioned particles could be deposited on the before mentioned triple cell culture to compare particle transport with or without Sp-A coating.

Zusammenfassung und Ausblick

Aufgrund des Herstellungsprozesses industriell gefertigter Nanopartikel, wie sie hier verwendet wurden, sind die Partikel nicht kompatibel mit *in vitro* Testsystemen. Diese Arten von Versuchen müssen, um zellverträglich zu sein, mit Medien im physiologischen pH-Bereich, isotoner Salzlaster und oft auch unter Anwesenheit von Proteinen durchgeführt werden. Diese Parameter sind für die Stabilität der Partikeldispersionen von essentieller Bedeutung, und schon kleine Änderungen können zu Agglomeration, aber auch zu Deagglomeration führen. Die tatsächliche Partikelgröße sowie die Belegung der Partikel mit Proteinen (Ausbildung einer sog. Proteincorona) sind für die Abschätzung der Toxizität der Partikel von bedeutender Wichtigkeit, da sie einerseits die Aufnahme in den Körper, andererseits die Oberflächeneigenschaften der Partikel verändern. Daher wurden die Wechselwirkungen zwischen Metalloxid-Nanopartikeln und physiologischen Medien, wie sie in *in vitro* nanotoxikologischen Tests verwendet werden, intensiv charakterisiert. Neben der Adsorption von Proteinen an Modell- und Metalloxid-Partikel wurde die Deagglomeration der Nanopartikel durch Proteine als Schutzkolloide quantifiziert. Für *in vitro* Langzeitversuche sind außerdem die Sterilität sowie der Endotoxingehalt der Partikel von immenser Bedeutung. Daher wurde eine Möglichkeit der Sterilisierung der Partikel als auch Parameter aufgedeckt, die bei der Bestimmung des Endotoxingehalts beachtet werden müssen. Die Ergebnisse gipfeln in einer Checkliste, die die Voraussetzungen zur Dispersion der Partikel in physiologischen Medien aufzeigt, um belastbare Daten zur Nanotoxizität von Nanomaterialien zu gewinnen.

Sobald Nanopartikel in den Körper eindringen, können sie mit der Umgebung, d.h. auch mit Proteinen, interagieren. Diese Interaktion kann zu veränderten Reaktionen der Körperbarrieren auf die Partikel führen und damit die Verweildauer im Körper beeinflussen. Mit Analytischer Ultrazentrifugation, Rasterkraft-Spektroskopie und BCA-Protein-

Quantifizierung wurden die Adsorption von Bovinem Serumalbumin (BSA) an drei CeO₂-Partikel mit ähnlichen physikalisch-chemischen Eigenschaften sowie der Agglomerationsgrad der Partikel untersucht. Die Proteinadsorption konnte mit einem sigmoidalen mathematischen Modell beschrieben werden und zeigte vor allem bei einem der drei Partikel eindeutige Unterschiede in der halbmaximalen Adsorption. Es zeigte sich eindeutig, dass Partikel aus gleichem Material und mit sehr ähnlichen physikalisch-chemischen Eigenschaften nicht unbedingt auch die gleichen Proteinadsorptionsmuster zeigen und dass der Agglomerationsgrad in die Beurteilung mit einfließen muss, um die Ergebnisse korrekt zu interpretieren. Des Weiteren fanden sich eindeutige Hinweise darauf, dass BSA in unterschiedlicher Konformation an die getesteten Partikel adsorbiert. Dies bedeutet, dass auch kleine Unterschiede in den Eigenschaften der Partikel zu unterschiedlicher Proteinadsorption führen und damit verschiedene Reaktionen im Körper hervorrufen kann. Deshalb ist es nicht ausreichend, nur einen Partikel eines Materials als Referenz zu testen und davon auszugehen, dass Partikel mit ähnlichen Eigenschaften das gleiche Adsorptionsverhalten und damit auch ein ähnliches nanotoxikologisches Potential aufweisen.

Nach Inhalation ist die erste Barriere, auf die ein Nanopartikel trifft, das Alveolar Lining Fluid (ALF), welches die Lungenbläschen zur Luftseite hin auskleidet. Deshalb war der nächste konsequente Schritt die Untersuchung der Proteinadsorption mit physiologisch relevantem Surfactant-Protein A (Sp-A), der vorherrschenden Proteinkomponente des pulmonalen Surfactant (integraler Bestandteil des ALF). Zum ersten Mal überhaupt konnten Unterschiede in der Proteinadsorption verschiedener industriell gefertigter Metalloxid-Nanopartikel gefunden werden. Sp-A ist ein physiologisch hochrelevantes Protein, das einerseits Signalkaskaden innerhalb der Epithelzelle auslöst, andererseits auch immunologische Funktion hat: Es opsonisiert Bakterien und andere Pathogene, damit sie von Macrophagen erkannt und phagozytiert werden können. Demnach könnte eine Adsorption von Sp-A an Nanopartikel eine gesteigerte Auf-

nahme in Macrophagen als auch ins Alveolarepithel bedeuten. Eine solche Partikel-Protein-Interaktion konnte für acht Nanopartikel bewiesen werden, wobei Partikel aus gleichem Material auch hier unterschiedliche Adsorption zeigten. Im Gegensatz zu BSA scheint Sp-A keine signifikante Deagglomeration der Partikel hervorzurufen, was auf unterschiedliche Adsorptionsmechanismen hinweist. Diese Ergebnisse könnten wichtige Konsequenzen bezüglich des Verbleibs im Körper als auch des direkten toxikologischen Effekts inhalierter Nanomaterialien haben.

Inhalierete Nanopartikel könnten jedoch nicht nur physiologisch relevantes Sp-A adsorbieren, sondern auch die Blut-Luft-Schranke überwinden, sodass sie in den Blutkreislauf und somit in den Körper gelangen. Um den Partikeltransport über diese Körperbarriere *in vitro* zu testen, wurde das für lösliche Substanzen seit längerem etablierte Calu-3 Modell auf Transwell-Filtern an die Besonderheiten von Nanopartikeln angepasst. Da die üblicherweise benutzten Filter mit einer Porengröße von 0,4 μm eine deutliche Barriere für die Partikel darstellten, musste auf eine Porengröße von 3 μm gewechselt werden. Um optimale Versuchskonditionen zu erreichen, mussten die Kulturbedingungen an die größeren Poren angepasst werden. Außerdem wurden die Barriere- sowie Transporteigenschaften auf diesen Filtern bestätigt. Die Funktionalität des veränderten Modells wurde vor Durchführung von Transportversuchen mit Metalloxid-Partikeln mittels Polystyren-Modellpartikeln verifiziert. Mit Ausnahme von beiden getesteten CeO_2 -Partikeln konnte für keinen der Metalloxid-Partikel weder eine Aufnahme in die Zelle noch ein Transport über die epitheliale Barriere bestimmt werden. ZrO_2 -Partikel schienen eine Beeinträchtigung der Barriereigenschaften zu verursachen, was jedoch wahrscheinlich ein Overload-Effekt gewesen ist.

Mögliche Transportwege für Nanopartikel über epitheliale Barrieren wurden in Kapitel 5 bereits erwähnt. Wie hier mit den Polystyren-Modellpartikeln gezeigt werden konnte, kann Partikeltransport über einen dieser Wege funktionieren. Mit einer Ausweitung des Barrieremodells mit zusätzlichen Macrophagen auf der apikalen und Dendritischen Zellen auf der basalen Seite [145-147] konnten bereits weitere Möglichkeiten,

die epitheliale Barriere zu überwinden, aufgezeigt werden: Blank und Mitarbeiter haben gezeigt, dass Partikel mit einem Durchmesser von 1 μm zwar kaum von den Epithelzellen eines solchen Modells, jedoch von den Macrophagen und Dendritischen Zellen aufgenommen werden, entweder durch Ausbildung von Ausläufern oder durch komplette Wanderung der Dendritischen Zellen durch das Epithel auf die apikale Seite. Außerdem konnte ein Partikelaustausch zwischen den Macrophagen und Dendritischen Zellen beobachtet werden [148], der die Barriereeigenschaften der Epithelzellen nicht beeinflusste [149]. Auch diese Transportrouten könnten für den in der Realität stattfindenden Partikeltransport relevant sein, daher ist ein negatives Ergebnis aus Transportversuchen mit Modellen, die ausschließlich aus Epithelzellen besteht, nicht ausreichend. Eine Übernahme eines solchen Tripelzellkultur-Modells könnte neue Einsichten auch in den Transport von Metalloxid-Nanopartikeln bringen, da diese die Realität besser widerspiegeln. Nach ausführlichem Vergleich mit *in vivo* Versuchen könnte es somit sogar möglich sein, dies unter gewissen Umständen als Ersatzmodell für Tierversuche zu nutzen. Der Einfluss der Proteinadsorption, besonders der von physiologisch relevanten Proteinen wie Sp-A, muss weiter intensiv untersucht werden, um das toxikologische Potential von Nanopartikeln besser abschätzen zu können. Nachdem das Protokoll zur BALF-Gewinnung weiter verfeinert wurde, könnten Adsorptionsversuche mit Partikeln aus gleichem Material, jedoch mit unterschiedlichen physikalischen Eigenschaften, z.B. ζ -Potential oder Hydrophobizität, helfen, diese Eigenschaften einer bestimmten Sp-A-Adsorption zuzuordnen. Obwohl in Kapitel 3 gezeigt wurde, dass auch Partikel mit ähnlichen physikalisch-chemischen Eigenschaften unterschiedliche Proteinadsorption zeigen können, wäre eventuell wenigstens eine grobe Abschätzung der Proteinadsorptionsmechanismen möglich.

Konditionierung mit Surfactant-Proteinen kann, wie bereits erwähnt, einen Einfluss auf die zelluläre Reaktion an der Blut-Luft-Schranke haben. Deshalb sollte der Einfluss der Porencorona auf Partikelaufnahme und –

Transport untersucht werden. Zu diesem Zweck könnten aerosolisierte, mit Proteinen konditionierte Nanopartikel auf das o.g. Tripelzellkultur-Modell deponiert und mit dem Transportverhalten unkonditionierter Partikel verglichen werden.

Abbreviations

ALF	Alveolar lining fluid
AlOOH	Aluminumoxide-Hydroxide
APS	Ammoniumpolysulfate
AUC	Analytical Ultracentrifugation
BaSO ₄	Bariumsulfate
BCA-assay	Bicinchoninic Acid assay
BET surface	Brunauer, Emmett, Teller surface
BMBF	Bundesministerium für Bildung und Forschung
BSA	Bovine serum albumin
c50, c100, c 200	carboxylated Polystyrene nanoparticles with a diameter of 50, 100 or 200 nm
CNTs	Carbonanotubes
DLS	Dynamic Light scattering
DMEM	Dulbecco's Modified Eagle Medium
FCS	Fetal Calf Serum
FITC-BSA	BSA, labelled with Fluorescein-Isothiocyanate
HSA	Human serum albumin
ICP-MS	Inductively Coupled Plasma Mass Spectrometry
ICP-OES	inductively coupled plasma optical emission spectrometry
KRB	Krebs-Ringer buffer
LAL	Limulus amebocyte lysate
CeO ₂	Ceriumdioxide
NP(s)	nanoparticle(s)
NTB/BCIP	Nitro blue tetrazolium chloride/ 5-Bromo-4-chloro-3-indolyl phosphate,toluidine salt
OM	surface modifier
p50, p100	plain Polystyrene nanoparticles with a diameter of 50 or 100 nm
PB	Phosphate buffer

pBALF	porcine Bronchoalveolar Lavage Fluid
PNIPAM	Poly(N-isopropylacrylamide)
REACH	Registration, Evaluation, Authorization and Restriction of Chemicals
rpm	rounds per minute
SDS-(PAGE)	Sodiumdodecylsulfate-Polyacrylamid-Gelelectrophoresis
Sp-A, B, C, & D	Surfactant protein A, B, C, & D
Sp-X	collective term for Surfactant proteins A to D
TBS	Tris-buffered saline
TEM	transmission electron microscopy
TEER	Transepithelial Electrical Resistance
TiO ₂	Titaniumdioxide
TOF-SIMS	time of flight secondary ion mass spectrometry
TRIS-HCl	Tris(hydroxymethyl)-aminomethan-hydrochloric acid
TWEEN 80	Polysorbate 80
XPS	X-ray photoelectron spectroscopy
XRD	X-ray diffraction
ZrO ₂	Zirconiumdioxide

References

1. Adlakha-Hutcheon G, Khaydarov R, Korenstein R, Varma R, Vaseashta A, Stamm H: **Nanomaterials, nanotechnology: Applications, consumer products, and benefits.** *Nanomaterials: Risks and Benefits* 2009:195-207.
2. Savolainen K, Alenius H, Norppa H, Pylkkänen L, Tuomi T, Kasper G: **Risk assessment of engineered nanomaterials and nanotechnologies-A review.** *Toxicology* 2010, **269**:92-104.
3. *Lux Research. Profiting from International Nanotechnology.* New York: Lux Research Inc.; 2006.
4. Maynard AD, Aitken RJ, Butz T, Colvin V, Donaldson K, Oberdörster G, Philbert MA, Ryan J, Seaton A, Stone V, et al: **Safe handling of nanotechnology.** *Nature* 2006, **444**:267-269.
5. **SCENIHR (Scientific Committee on Emerging and Newly Identified Health Risks)**; 19 January 2009.
6. Borm PJ, Kreyling W: **Toxicological hazards of inhaled nanoparticles--potential implications for drug delivery.** *J Nanosci Nanotechnol* 2004, **4**:521-531.
7. Buzea C, Pacheco Blandino, I.I., Robbie, K. : **Nanomaterials and nanoparticles: Sources and toxicity.** *Biointerphases* 2007, **2**:MR17-MR172.
8. **Foresight Guidelines for Responsible Nanotechnology Development,** <http://www.foresight.org/guidelines/current.html>
9. Bower KN, Choularton TW, Flynn MJ, Swietliki E, Martinsson B: **Observations of the interaction of an urban plume with cloud.** *Journal of Aerosol Science* 2000, **31**:S66-S67.
10. Kuhlbusch TAJ, Neumann S, Fissan H: **Number size distribution, mass concentration, and particle composition of PM1 PM2.5, and PM10 in bag filling areas of carbon black production.** *Journal of Occupational and Environmental Hygiene* 2004, **1**:660-671.
11. Williams SG, Carmel-Harel O, Manning PA: **A functional homolog of Escherichia coli NhaR in Vibrio cholerae.** *J Bacteriol* 1998, **180**:762-765.

12. Oberdorster G, Ferin J, Gelein R, Soderholm SC, Finkelstein J: **Role of the alveolar macrophage in lung injury: Studies with ultrafine particles.** *Environmental Health Perspectives* 1992, **97**:193-199.
13. Gehr P, Bachofen M, Weibel ER: **The normal human lung: ultrastructure and morphometric estimation of diffusion capacity.** *Respir Physiol* 1978, **32**:121-140.
14. Weibel ER: **Morphometry of the human lung: the state of the art after two decades.** *Bull Eur Physiopathol Respir* 1979, **15**:999-1013.
15. Patton JS: **Mechanisms of macromolecule absorption by the lungs.** *Advanced Drug Delivery Reviews* 1996, **19**:3-36.
16. Gehr P, Green FH, Geiser M, Im Hof V, Lee MM, Schurch S: **Airway surfactant, a primary defense barrier: mechanical and immunological aspects.** *J Aerosol Med* 1996, **9**:163-181.
17. Crapo JD, Barry BE, Gehr P: **Cell number and cell characteristics of the normal human lung.** *American Review of Respiratory Disease* 1982, **126**:332-337.
18. Yang W, Peters JI, Williams Iii RO: **Inhaled nanoparticles-A current review.** *International Journal of Pharmaceutics* 2008, **356**:239-247.
19. Goerke J, Clemens, JA (Ed.). **Handbook of Physiology.** Washington, DC: American Physiological Society; 1986.
20. Goerke J: **Pulmonary surfactant: functions and molecular composition.** *Biochim Biophys Acta* 1998, **1408**:79-89.
21. Perez-Gil J: **Structure of pulmonary surfactant membranes and films: the role of proteins and lipid-protein interactions.** *Biochim Biophys Acta* 2008, **1778**:1676-1695.
22. White MK, Strayer DS: **Surfactant protein A regulates pulmonary surfactant secretion via activation of phosphatidylinositol 3-kinase in type II alveolar cells.** *Exp Cell Res* 2000, **255**:67-76.
23. Kreyling WG, Geiser, M: **Dosimetry of Inhaled Nanoparticles.** In *Nanoparticles in Medicine and Environment, Inhalation and Health Effects*; Edited by Marijnissen JC, Gradon, L. Berlin: Springer; 2009: 145-171
24. Hoet PHM, Brüske-Hohlfeld I, Salata OV: **Nanoparticles - Known and unknown health risks.** *Journal of Nanobiotechnology* 2004, **2**.

25. Oberdörster G, Oberdörster E, Oberdörster J: **Nanotoxicology: An Emerging Discipline Evolving from Studies of Ultrafine particles.** *Environ Health Perspect* 2005, **113**:823-839.
26. Courrier HM, Butz N, Vandamme TF: **Pulmonary drug delivery systems: Recent developments and prospects.** *Critical Reviews in Therapeutic Drug Carrier Systems* 2002, **19**:425-498.
27. Hyung H, Fortner JD, Hughes JB, Kim JH: **Natural organic matter stabilizes carbon nanotubes in the aqueous phase.** *Environ Sci Technol* 2007, **41**:179-184.
28. Limbach LK, Li Y, Grass RN, Brunner TJ, Hintermann MA, Muller M, Gunther D, Stark WJ: **Oxide nanoparticle uptake in human lung fibroblasts: effects of particle size, agglomeration, and diffusion at low concentrations.** *Environ Sci Technol* 2005, **39**:9370-9376.
29. Nepal D, Geckeler KE: **Proteins and carbon nanotubes: close encounter in water.** *Small* 2007, **3**:1259-1265.
30. Patil S, Sandberg A, Heckert E, Self W, Seal S: **Protein adsorption and cellular uptake of cerium oxide nanoparticles as a function of zeta potential.** *Biomaterials* 2007, **28**:4600-4607.
31. Richter V, Potthoff, A, Pompe, W, Gelinsky M, Ikonomidou, H, Bastian, S, Schirmer, K, Scholz, S, Hofinger, J: **BMBF-project INOS - evaluation of nanoparticles - a contribution to sustainable development of nanotechnology.** In *EuroNanoForum*. pp. 145-147; 2007:145-147.
32. Wick P, Manser P, Limbach LK, Dettlaff-Weglikowska U, Krumeich F, Roth S, Stark WJ, Bruinink A: **The degree and kind of agglomeration affect carbon nanotube cytotoxicity.** *Toxicology Letters* 2007, **168**:121-131.
33. Cedervall T, Lynch I, Lindman S, Berggard T, Thulin E, Nilsson H, Dawson KA, Linse S: **Understanding the nanoparticle-protein corona using methods to quantify exchange rates and affinities of proteins for nanoparticles.** *Proceedings of the National Academy of Sciences of the United States of America* 2007, **104**:2050-2055.
34. Powers KW, Palazuelos M, Moudgil BM, Roberts SM: **Characterization of the size, shape, and state of dispersion of nanoparticles for toxicological studies.** *Nanotoxicology* 2007, **1**:42-51.

35. Kuhlbusch TAJ, Krug, HF, Nau, K (Ed.). **NanoCare, Health related Aspects of Nanomaterials, Final Scientific Report**, 1st edition. Frankfurt a.M.: DECHEMA e.V.; 2009.
36. Cölfen H: *Analytical ultracentrifugation of nanoparticles*. Valencia, California: American Scientific Publishers; 2004.
37. Mächtle W, Börger L. : *Analytical Ultracentrifugation of Polymers and Nanoparticles*. Berlin: Springer; 2006.
38. Lin MY, Lindsay HM, Weitz DA, Ball RC, Klein R, Meakin P: **Universal reaction-limited colloid aggregation**. *Phys Rev A* 1990, **41**:2005-2020.
39. Evans DF, Wennerström H: *The Colloidal Domain: Where Physics, Chemistry, Biology, and Technology Meet*. 2nd edn. New York: Wiley-VCH; 1999.
40. Murray PR, Baron E J, Jorgensen JH, Pfaller MA and Tenover FC: *Manual of Clinical Microbiology, Volumes 1 & 2*. Washington, D. C.: ASM Press; 2003.
41. Lucocq JM, Baschong W: **Preparation of protein colloidal gold complexes in the presence of commonly used buffers**. *Eur J Cell Biol* 1986, **42**:332-337.
42. Martin-Rodriguez A, Cabrerizo-Vilchez MA, Hidalgo-Alvarez R: **A comparative study on the electrokinetic behavior of bovine serum albumin molecules adsorbed onto different polymer colloids**. *Colloids and Surfaces A: Physicochemical and Engineering Aspects* 1994, **92**:113-119.
43. Deschaume O, Shafran KL, Perry CC: **Interactions of bovine serum albumin with aluminum polyoxocations and aluminum hydroxide**. *Langmuir* 2006, **22**:10078-10088.
44. Lindl T, Bauer, J: *Zell- und Gewebekultur*. 2. edn. Stuttgart, New York: Gustav Fischer Verlag; 1989.
45. Renwick LC, Brown D, Clouter A, Donaldson K: **Increased inflammation and altered macrophage chemotactic responses caused by two ultrafine particle types**. *Occup Environ Med* 2004, **61**:442-447.
46. Kragh-Hansen U: **Structure and ligand binding properties of human serum albumin**. *Dan Med Bull* 1990, **37**:57-84.
47. Schroeter J (in Cohn F): *Beitrage zur Biologie der Pflanzen* 1872 (1875):109-126.
48. Skerman VBD, McGowan, V., and Sneath, P.H.A. (editors): **Approved lists of bacterial names**. *Med J Aust* 1980, **2**:3-4.
49. Cohn F: *Beitrage zur Biologie der Pflanzen* 1872, **1**:127-224.

50. Madigan MT, Martinko JM, Dunlap PV and Clark DP: Brock: **Biology of Microorganisms**. New Jersey: Prentice Hall; 2005
51. Roberts TA, Hitchins AD: *Resistance of spores*. New York: Academic Press; 1969.
52. Nicholson WL, Munakata N, Horneck G, Melosh HJ, Setlow P: **Resistance of Bacillus endospores to extreme terrestrial and extraterrestrial environments**. *Microbiol Mol Biol Rev* 2000, **64**:548-572.
53. Pfeiffer R: **Weitere Untersuchungen über das Wesen der Choleraimmunität und über spezifisch bacterizide Prozesse**. *Z Hyg* 1894:1-16.
54. Bishop RE: **Fundamentals of endotoxin structure and function**. *Contrib Microbiol* 2005, **12**:1-27.
55. Inoue K, Takano H, Yanagisawa R, Hirano S, Sakurai M, Shimada A, Yoshikawa T: **Effects of airway exposure to nanoparticles on lung inflammation induced by bacterial endotoxin in mice**. *Environ Health Perspect* 2006, **114**:1325-1330.
56. Ashwood P, Thompson RP, Powell JJ: **Fine particles that adsorb lipopolysaccharide via bridging calcium cations may mimic bacterial pathogenicity towards cells**. *Exp Biol Med (Maywood)* 2007, **232**:107-117.
57. Rylander R: **Endotoxin in the environment-exposure and effects**. *J Endotoxin Res* 2002, **8**:241-252.
58. Friberg P: **Use of Quantitative Assay in Endotoxin Testing**. In *Detection of Bacterial Endotoxins with the Limulus Amebocyte Lysate Test* Edited by Stanley W. Watson JL, Thomas J. Novitsky. New York: Alan R. Liss; 1987: 149-169
59. Lindman S, Lynch I, Thulin E, Nilsson H, Dawson KA, Linse S: **Systematic investigation of the thermodynamics of HSA adsorption to N-isopropylacrylamide/N-tert-butylacrylamide copolymer nanoparticles. Effects of particle size and hydrophobicity**. *Nano Lett* 2007, **7**:914-920.
60. Lundqvist M, Stigler J, Elia G, Lynch I, Cedervall T, Dawson KA: **Nanoparticle size and surface properties determine the protein corona with possible implications for biological impacts**. *Proc Natl Acad Sci U S A* 2008, **105**:14265-14270.
61. Landsiedel R, Ma-Hock, L, Kroll A, Schnekenburger J, Wiench K, Wohlleben W: **Testing metal-oxide nanomaterials for human safety**. *Adv Mater* 2010, **in press**.

62. Yang K, Lin D, Xing B: **Interactions of humic acid with nanosized inorganic oxides.** *Langmuir* 2009, **25**:3571-3576.
63. Rucker C, Potzl M, Zhang F, Parak WJ, Nienhaus GU: **A quantitative fluorescence study of protein monolayer formation on colloidal nanoparticles.** *Nat Nanotechnol* 2009, **4**:577-580.
64. Palmisano P, Faraldi P, Fino D, Russo N: **Household oven self-cleaning surfaces via catalytic thermal oxidation.** *Chemical Engineering Journal*, **in press, corrected proof.**
65. Jung H, Kittelson DB, Zachariah MR: **The influence of a cerium additive on ultrafine diesel particle emissions and kinetics of oxidation.** *Combustion and Flame* 2005, **142(3)**:276-288.
66. Van Hoecke K, Quick J, Mankiewicz-Boczek J, De Schampheleere K, Elsaesser A, Van der Meeren P, Barnes C, McKerr G, Howard C, Van der Meent D, Rydzynski K, Dawson K, Salvati A, Lesniak A, Lynch I, Silversmit G, De Samber B, Vincze L, Janssen C: **Fate and effects of CeO₂ nanoparticles in aquatic ecotoxicity tests.** *Environ Sci Technol* 2009, **43**:4537-4546.
67. Höbel S, Prinz R, Malek A, Urban-Klein B, Sitterberg J, Bakowsky U, Czubayko F, Aigner A: **Polyethylenimine PEI F25-LMW allows long-term storage of frozen complexes as fully active reagents in si-RNA-mediated gene targeting and DNA delivery.** *Eur J Pharm Biopharm* 2008, **70**:29-41.
68. Hutter JL, Bechhoefer, J: **Calibration of atomic-force microscope tips.** *Review of Scientific Instruments* 1993, **64**:1868.
69. Hinterdorfer P, Baumgartner W, Gruber HJ, Schilcher K, Schindler H: **Detection and localization of individual antibody-antigen recognition events by atomic force microscopy.** *Proc Natl Acad Sci U S A* 1996, **93**:3477-3481.
70. Vakarelski I, Higashitani K.: **Single-nanoparticle-mediated tips for scanning probe microscopy.** *Langmuir* 2006, **22(7)**:2931-2934.
71. Butt H-H, Cappella B, Kappl M: **Force measurements with the atomic force microscope: Technique, interpretation and applications.** *Surface Science Reports* 2005, **59(1-6)**:1-152.
72. Leite FL, Herrmann PSP: **Application of atomic force spectroscopy (AFS) to studies of adhesion phenomena: a review.** *Journal of Adhesion Science and Technology* 2005, **19**:365-405.

73. James J, Crean B, Davies M, Toon R, Jinks P, Roberts CJ: **The surface characterisation and comparison of two potential sub-micron, sugar bulking excipients for use in low-dose, suspension formulations in metered dose inhalers.** *Int J Pharm* 2008, **361**:209-221.
74. Davies M, Brindley A, Chen X, Marlow M, Doughty SW, Shrubbs I, Roberts CJ: **Characterization of drug particle surface energetics and young's modulus by atomic force microscopy and inverse gas chromatography.** *Pharm Res* 2005, **22**:1158-1166.
75. Colfen H: W. Machtle and L. Borger (Eds.) **Analytical Ultracentrifugation of Polymers and Nanoparticles.** *Anal Bioanal Chem* 2006.
76. Gessner A, Waicz R, Lieske A, Paulke B, Mader K, Muller RH: **Nanoparticles with decreasing surface hydrophobicities: influence on plasma protein adsorption.** *Int J Pharm* 2000, **196**:245-249.
77. Israelachvili JN, Pashley RM: **Measurement of the Hydrophobic Interaction between Two Hydrophobic Surfaces in Aqueous Electrolyte Solutions.** *Journal of Colloid and Interface Science* 1984, **98**:500-514.
78. Luck M, Paulke BR, Schroder W, Blunk T, Muller RH: **Analysis of plasma protein adsorption on polymeric nanoparticles with different surface characteristics.** *J Biomed Mater Res* 1998, **39**:478-485.
79. Shamim N, Hong L, Hidajat K, Uddin MS: **Thermosensitive-polymer-coated magnetic nanoparticles: adsorption and desorption of bovine serum albumin.** *J Colloid Interface Sci* 2006, **304**:1-8.
80. Koutsoukos PG, Mumme-Young CA, Norde W, Lyklema J: **Effect of the nature of the substrate on the adsorption of human plasma albumin.** *Colloids and Surfaces* 1982, **5**:93-104.
81. Yoon J-Y, Kim J-H, Kim W-S: **The relationship of interaction forces in the protein adsorption onto polymeric microspheres.** *Colloids and Surfaces A: Physicochemical and Engineering Aspects* 1999, **153**:413-419.
82. Liang Y-Y, Zhang L-M, Li W, Chen R-F: **Polysaccharide-modified iron oxide nanoparticles as an effective magnetic affinity adsorbent for bovine serum albumin.** *Colloid Polym Sci* 2007, **285**:1193-1199.
83. Cedervall T, Lynch I, Foy M, Berggard T, Donnelly SC, Cagney G, Linse S, Dawson KA: **Detailed identification of plasma proteins adsorbed on copolymer nanoparticles.** *Angew Chem Int Ed Engl* 2007, **46**:5754-5756.

84. Ehrenberg MS, Friedman AE, Finkelstein JN, Oberdorster G, McGrath JL: **The influence of protein adsorption on nanoparticle association with cultured endothelial cells.** *Biomaterials* 2009, **30**:603-610.
85. Gao H, Geng XP, Wang BH, Zhou Y: **Studies on the conformational change of adsorbed BSA onto a moderately hydrophobic surface at different denaturant concentrations and surface coverages.** *J Colloid Interface Sci* 2010, **344**:468-474.
86. Lynch I, Cedervall T, Lundqvist M, Cabaleiro-Lago C, Linse S, Dawson KA: **The nanoparticle-protein complex as a biological entity; a complex fluids and surface science challenge for the 21st century.** *Advances in Colloid and Interface Science* 2007, **134-135**:167-174.
87. Lynch I, Dawson KA: **Protein-nanoparticle interactions.** *Nano Today* 2008, **3**:40-47.
88. Bissinger RL, Carlson CA: **Surfactant.** *Newborn and Infant Nursing Reviews Pulmonary Issues* 2006, **6**:87-93.
89. Kingma PS, Whitsett JA: **In defense of the lung: surfactant protein A and surfactant protein D.** *Current Opinion in Pharmacology* 2006, **6**:277-283.
90. Wallace WE, Keane MJ, Murray DK, Chisholm WP, Maynard AD, Ong TM: **Phospholipid lung surfactant and nanoparticle surface toxicity: Lessons from diesel soots and silicate dusts.** *Journal of Nanoparticle Research* 2007, **9**:23-38.
91. Bakshi MS, Zhao L, Smith R, Possmayer F, Petersen NO: **Metal nanoparticle pollutants interfere with pulmonary surfactant function in vitro.** *Biophys J* 2008, **94**:855-868.
92. Schleh C, Muhlfield C, Pulskamp K, Schmiedl A, Nassimi M, Lauenstein HD, Braun A, Krug N, Erpenbeck VJ, Hohlfeld JM: **The effect of titanium dioxide nanoparticles on pulmonary surfactant function and ultrastructure.** *Respir Res* 2009, **10**:90.
93. Schleh C, Hohlfeld JM: **Interaction of nanoparticles with the pulmonary surfactant system.** *Inhal Toxicol* 2009, **21 Suppl 1**:97-103.
94. Tausch HW, de la Serna JB, Perez-Gil J, Alonso C, Zasadzinski JA: **Inactivation of pulmonary surfactant due to serum-inhibited adsorption and reversal by hydrophilic polymers: experimental.** *Biophys J* 2005, **89**:1769-1779.

95. Kishore U, Bernal AL, Kamran MF, Saxena S, Singh M, Sarma PU, Madan T, Chakraborty T: **Surfactant proteins SP-A and SP-D in human health and disease.** *Arch Immunol Ther Exp (Warsz)* 2005, **53**:399-417.
96. McCormack FX: **Structure, processing and properties of surfactant protein A.** *Biochim Biophys Acta* 1998, **1408**:109-131.
97. Hickling TP, Clark H, Malhotra R, Sim RB: **Collectins and their role in lung immunity.** *J Leukoc Biol* 2004, **75**:27-33.
98. Matalon S, Hickman-Davis JM, Wright JR, Geoffrey JL, Steven DS: **SURFACTANT | Surfactant Protein A (SP-A).** In *Encyclopedia of Respiratory Medicine*. Oxford: Academic Press; 2006: 143-148
99. Notter RH, Chess PR, Wang Z, Geoffrey JL, Steven DS: **SURFACTANT | Overview.** In *Encyclopedia of Respiratory Medicine*. Oxford: Academic Press; 2006: 135-143
100. Casals C: **Role of surfactant protein A (SP-A)/lipid interactions for SP-A functions in the lung.** *Pediatric Pathology and Molecular Medicine* 2001, **20**:249-268.
101. Haagsman HP, Diemel RV: **Surfactant-associated proteins: functions and structural variation.** *Comparative Biochemistry and Physiology - Part A: Molecular & Integrative Physiology* 2001, **129**:91-108.
102. Heinrich S, Hartl D, Griese M: **Surfactant protein A - From genes to human lung diseases.** *Current Medicinal Chemistry* 2006, **13**:3239-3252.
103. Hohlfeld JM: **The role of surfactant in asthma.** *Respir Res* 2002, **3**:4.
104. Palaniyar N, Ikegami M, Korfhagen T, Whittsett J, McCormack FX: **Domains of surfactant protein A that affect protein oligomerization, lipid structure and surface tension.** *Comparative Biochemistry and Physiology - Part A: Molecular & Integrative Physiology* 2001, **129**:109-127.
105. Palaniyar N, Ridsdale RA, Possmayer F, Harauz G: **Surfactant protein A (SP-A) forms a novel supraquaternary structure in the form of fibers.** *Biochemical and Biophysical Research Communications* 1998, **250**:131-136.
106. Salvador-Morales C, Townsend P, Flahaut E, Venien-Bryan C, Vlandas A, Green MLH, Sim RB: **Binding of pulmonary surfactant proteins to carbon nanotubes; potential for damage to lung immune defense mechanisms.** *Carbon* 2007, **45**:607-617.

107. Lacerda L, Herrero MA, Venner K, Bianco A, Prato M, Kostarelos K: **Carbon-nanotube shape and individualization critical for renal excretion.** *Small* 2008, **4**:1130-1132.
108. Lin D, Xing B: **Tannic acid adsorption and its role for stabilizing carbon nanotube suspensions.** *Environ Sci Technol* 2008, **42**:5917-5923.
109. Bastian S, Busch W, Kuhnel D, Springer A, Meissner T, Holke R, Scholz S, Iwe M, Pompe W, Gelinsky M, et al: **Toxicity of tungsten carbide and cobalt-doped tungsten carbide nanoparticles in mammalian cells in vitro.** *Environ Health Perspect* 2009, **117**:530-536.
110. Meissner T, Potthoff A, Richter V: **Suspension characterization as important key for toxicological investigations;** *Journal of Physics: Conference Series* 2009, **170**:6pp.
111. Bihari P, Vippola M, Schultes S, Praetner M, Khandoga AG, Reichel CA, Coester C, Tuomi T, Rehberg M, Krombach F: **Optimized dispersion of nanoparticles for biological in vitro and in vivo studies.** *Particle and Fibre Toxicology* 2008, **5**.
112. Sayes CM, Reed KL, Warheit DB: **Assessing toxicity of fine and nanoparticles: comparing in vitro measurements to in vivo pulmonary toxicity profiles.** *Toxicol Sci* 2007, **97**:163-180.
113. Sager TM, Porter DW, Robinson VA, Lindsley WG, Schwegler-Berry DE, Castranova V: **Improved method to disperse nanoparticles for in vitro and in vivo investigation of toxicity.** *Nanotoxicology* 2007, **1**:118-129.
114. Ma-Hock L, Burkhardt S, Strauss V, Gamer AO, Wiench K, van Ravenzwaay B, Landsiedel R: **Development of a short-term inhalation test in the rat using nano-titanium dioxide as a model substance.** *Inhal Toxicol* 2009, **21**:102-118.
115. Gehr P, Schürch S, Berthiaume Y, Im Hof V, Geiser M: **Particle Retention in Airways by Surfactant.** *Journal of Aerosol Medicine* 2009, **3**:27-43.
116. Geiser M, Matter M, Maye I, Im Hof V, Gehr P, Schurch S: **Influence of airspace geometry and surfactant on the retention of man-made vitreous fibers (MMVF 10a).** *Environ Health Perspect* 2003, **111**:895-901.
117. Geiser M, Schurch S, Gehr P: **Influence of surface chemistry and topography of particles on their immersion into the lung's surface-lining layer.** *J Appl Physiol* 2003, **94**:1793-1801.

118. Schurch S, Gehr P, Im Hof V, Geiser M, Green F: **Surfactant displaces particles toward the epithelium in airways and alveoli.** *Respir Physiol* 1990, **80**:17-32.
119. Geiser M, Kreyling WG: **Deposition and biokinetics of inhaled nanoparticles.** *Part Fibre Toxicol* 2010, **7**:2.
120. Hartshorn KL, Crouch E, White MR, Colamussi ML, Kakkanatt A, Tauber B, Shepherd V, Sastry KN: **Pulmonary surfactant proteins A and D enhance neutrophil uptake of bacteria.** *Am J Physiol* 1998, **274**:L958-969.
121. Kishore U, Greenhough TJ, Waters P, Shrive AK, Ghai R, Kamran MF, Bernal AL, Reid KBM, Madan T, Chakraborty T: **Surfactant proteins SP-A and SP-D: Structure, function and receptors.** *Molecular Immunology* 2006, **43**:1293-1315.
122. Geiser M, Casaulta M, Kupferschmid B, Schulz H, Semmler-Behnke M, Kreyling W: **The role of macrophages in the clearance of inhaled ultrafine titanium dioxide particles.** *Am J Respir Cell Mol Biol* 2008, **38**:371-376.
123. Stevens PA, Wissel H, Sieger D, Meienreis-Sudau V, Rustow B: **Identification of a new surfactant protein A binding protein at the cell membrane of rat type II pneumocytes.** *Biochem J* 1995, **308**:77-81.
124. Korfhagen TR, LeVine AM, Whitsett JA: **Surfactant protein A (SP-A) gene targeted mice.** *Biochim Biophys Acta* 1998, **1408**:296-302.
125. Kreyling WG, Semmler-Behnke M, Seitz J, Scymczak W, Wenk A, Mayer P, Takenaka S, Oberdorster G: **Size dependence of the translocation of inhaled iridium and carbon nanoparticle aggregates from the lung of rats to the blood and secondary target organs.** *Inhal Toxicol* 2009, **21 Suppl 1**:55-60.
126. Roller M: **Carcinogenicity of inhaled nanoparticles.** *Inhal Toxicol* 2009, **21 Suppl 1**:144-157.
127. AshaRani PV, Low Kah Mun G, Hande MP, Valiyaveetil S: **Cytotoxicity and genotoxicity of silver nanoparticles in human cells.** *ACS Nano* 2009, **3**:279-290.
128. Carlson C, Hussain SM, Schrand AM, Braydich-Stolle LK, Hess KL, Jones RL, Schlager JJ: **Unique cellular interaction of silver nanoparticles: size-dependent generation of reactive oxygen species.** *J Phys Chem B* 2008, **112**:13608-13619.
129. Choi JY, Lee SH, Na HB, An K, Hyeon T, Seo TS: **In vitro cytotoxicity screening of water-dispersible metal oxide nanoparticles in human cell lines.** *Bioprocess Biosyst Eng* 2009.

130. Wahl B, Daum N, Ohrem HL, Lehr CM: **Novel luminescence assay offers new possibilities for the risk assessment of silica nanoparticles.** *Nanotoxicology* 2008, **2**:243-251.
131. Forbes B, Ehrhardt C: **Human respiratory epithelial cell culture for drug delivery applications.** *Eur J Pharm Biopharm* 2005, **60**:193-205.
132. Florea BI, Cassara ML, Junginger HE, Borchard G: **Drug transport and metabolism characteristics of the human airway epithelial cell line Calu-3.** *J Control Release* 2003, **87**:131-138.
133. Forbes B: **Human airway epithelial cell lines for in vitro drug transport and metabolism studies.** *Pharmaceutical Science & Technology Today* 2000, **3**:18-27.
134. Lehr CM, Bur M, Schaefer UF: **Cell culture models of the air-blood barrier for the evaluation of aerosol medicines.** *Altex* 2006, **23 Suppl**:259-264.
135. Mathias NR, Yamashita F, Lee VHL: **Respiratory epithelial cell culture models for evaluation of ion and drug transport.** *Advanced Drug Delivery Reviews* 1996, **22**:215-249.
136. Sakagami M: **In vivo, in vitro and ex vivo models to assess pulmonary absorption and disposition of inhaled therapeutics for systemic delivery.** *Adv Drug Deliv Rev* 2006, **58**:1030-1060.
137. Wan H, Winton HL, Soeller C, Stewart GA, Thompson PJ, Gruenert DC, Cannell MB, Garrod DR, Robinson C: **Tight junction properties of the immortalized human bronchial epithelial cell lines Calu-3 and 16HBE14o.** *Eur Respir J* 2000, **15**:1058-1068.
138. Becker U, Ehrhardt C, Schneider M, Muys L, Gross D, Eschmann K, Schaefer UF, Lehr CM: **A comparative evaluation of corneal epithelial cell cultures for assessing ocular permeability.** *ATLA Alternatives to Laboratory Animals* 2008, **36**:33-44.
139. Foster KA, Avery ML, Yazdanian M, Audus KL: **Characterization of the Calu-3 cell line as a tool to screen pulmonary drug delivery.** *Int J Pharm* 2000, **208**:1-11.
140. Furuse M, Itoh M, Hirase T, Nagafuchi A, Yonemura S, Tsukita S: **Direct association of occludin with ZO-1 and its possible involvement in the localization of occludin at tight junctions.** *J Cell Biol* 1994, **127**:1617-1626.

141. Loman S, Radl J, Jansen HM, Out TA, Lutter R: **Vectorial transcytosis of dimeric IgA by the Calu-3 human lung epithelial cell line: upregulation by IFN-gamma** *Am J Physiol* 1997, **272**:L951-L958.
142. Geys J, Coenegrachts L, Vercammen J, Engelborghs Y, Nemmar A, Nemery B, Hoet PH: **In vitro study of the pulmonary translocation of nanoparticles: a preliminary study.** *Toxicol Lett* 2006, **160**:218-226.
143. Mathias NR, Timoszyk J, Stetsko PI, Megill JR, Smith RL, Wall DA: **Permeability characteristics of Calu-3 human bronchial epithelial cells: in vitro–in vivo correlation to predict lung absorption in rats.** *J Drug Target* 2002, **10**:31-40.
144. Pauluhn J: **Pulmonary toxicity and fate of agglomerated 10 and 40 nm aluminum oxyhydroxides following 4-week inhalation exposure of rats: toxic effects are determined by agglomerated, not primary particle size.** *Toxicol Sci* 2009, **109**:152-167.
145. Blank F, Rothen-Rutishauser BM, Schurch S, Gehr P: **An optimized in vitro model of the respiratory tract wall to study particle cell interactions.** *J Aerosol Med* 2006, **19**:392-405.
146. Rothen-Rutishauser B, Müller L, Blank F, Brandenberger C, Mühlfeld C, Gehr P: **A newly developed in vitro model of the human epithelial airway barrier to study the toxic potential of nanoparticles.** *Altex* 2008, **25**:191-196.
147. Rothen-Rutishauser BM, Kiama SC, Gehr P: **A three-dimensional cellular model of the human respiratory tract to study the interaction with particles.** *American Journal of Respiratory Cell and Molecular Biology* 2005, **32**:281-289.
148. Blank F, Rothen-Rutishauser B, Gehr P: **Dendritic cells and macrophages form a transepithelial network against foreign particulate antigens.** *American Journal of Respiratory Cell and Molecular Biology* 2007, **36**:669-677.
149. Blank F, Wehrli M, Baum O, Gehr P, Rothen-Rutishauser B: **The epithelial integrity is preserved during particle exchange across the epithelium by macrophages and dendritic cells.** *European Respiratory Review* 2008, **17**:78-80.

Publication List

Publications

- Schulze, C., Kroll, A., Lehr, C-M., Schaefer, U.F., Becker, K., Schnekenburger, J., Schulze Isfort, C., Landsiedel, R., Wohlleben, W.: Not ready to use - Overcoming pitfalls when dispersing nanoparticles in physiological media. *Nanotoxicology* 2008, 2:51-61
- Schaefer, J., Schulze, C., Marxer, E.J., Schaefer, U.F., Wohlleben, W., Bakowsky, U., Lehr, C-M.: Intrinsic physico-chemical properties of CeO₂ nanoparticles do not mirror their biorelevant protein adsorption, *ACS Nano*, submitted
- Schulze, C., Schaefer, U.F., Ruge, C.A., Wohlleben, W., Lehr, C-M.: Interaction of metal oxide nanoparticles with lung surfactant protein A, *European Journal of Pharmaceutics and Biopharmaceutics*, submitted

Oral Presentations

- Schulze, C., Schaefer, U.F., Lehr, C.-M., Optimizing experimental conditions for epithelial cell culture models to study uptake and transport of nanoparticles, Congress on “Alternative Test Methods In Inhalation Toxicology”, May 7-9, 2007, Berlin, Germany

Poster Presentations

- Schulze, C., Schaefer, U.F., Lehr, C.-M., Schneider, M., Born, K., Dzeyk, K., Parlitz, R., Detection of Protein Binding to Metaloxide Nanomaterial using High Resolution Ultrasound Technology, 6th

World Meeting of Pharmaceutics, Biopharmacy and Pharmaceutical Technology, April 7-10, 2008, Barcelona, Spain

- Schulze, C., Lehr, C.-M., Schaefer, U.F., Wohlleben, W., Detection of Protein Binding to Metaloxide Nanomaterial, Congress „Nano-Tox“, September 7-10, 2008, Zurich, Switzerland
- Schulze, C., Schaefer, U.F., Lehr, C.-M., Protein adsorption onto nanoparticles as an important parameter in toxicity evaluation, “EFCA International Symposium”, May 19 and 20, 2009, Brussels

Danke...

...Prof. Dr. Claus-Michael Lehr, für das in mich gesetzte Vertrauen, die Geduld und das stete Bemühen, immer das Beste aus mir herauszuholen.

... Prof. Dr. Ingolf Bernhardt, für die prompte Übernahme der Zweitkorrektur.

...Dr. Ulrich Schäfer, Uli, für die stete und rückhaltlose Unterstützung sowohl in fachlicher als auch in menschlicher Hinsicht. Du warst immer für mich da und hast Dir Zeit für mich genommen, auch wenn es manchmal nicht leicht war. Einen besseren Betreuer kann man sich kaum wünschen.

...den Post-Docs der Abteilung, die stets bei Problemen hilfsbereit und offen waren.

...dem Techniker-Team, das immer alle Anfragen und Wünsche schnellst- und bestmöglich erledigt hat. Besonders Petra König ein Dankeschön für das gute Auge auf meine Zellkultur.

...meinen Mit-Doktoranden, allen voran Birgit, Claudia, Andrea und Fransisca, für das unkomplizierte und freundschaftliche Arbeitsklima.

...Dr. Wendel Wohlleben, für die angenehme Kooperation und stete Hilfsbereitschaft sowie die Quantifizierung der CeO₂-Partikel.

...den Industriepartnern des Projekts NanoCare, BASF SE, Evonik Degussa GmbH, Bayer Material Science AG, ItN Nanovation AG und Solvay Infra Bad Hönningen GmbH, für die Bereitstellung der Partikel sowie deren physikalisch-chemische Charakterisierung. Ein Dankeschön auch an Herrn Voetz und Herrn Venzago, für die Quantifizierung der Metalloxidpartikel.

...Dr. Alexandra Kroll, für das freundschaftliche Verhältnis und die gute Zusammenarbeit im Projekt.

...dem Projekt des Bundesministeriums für Bildung und Forschung NanoCare (Förderkennzeichen 03X0021C), für die finanzielle Unterstützung.

...meinem Freundeskreis, der des Öfteren zugunsten der Promotion auf mich verzichten musste, für das entgegengebrachte Verständnis.

...meinen Eltern, die mir immer die Freiheit gelassen haben, mich zu verwirklichen und geholfen haben, den Grundstein für meinen akademischen Werdegang zu legen.

...meinen Schwiegereltern, für die immense Unterstützung im privaten Bereich. Ihr habt immer ohne große Worte geholfen, wo es nötig war. Auch und vor allem in schwierigen Zeiten gab mir das die Möglichkeit, mich auf mich selbst zu konzentrieren. Ihr habt mir damit mein Leben sehr viel einfacher gemacht.

...meinem Mann Sascha, ohne Dich wäre es nicht gegangen. Du hast Dich mit mir gefreut wenn es gut lief und an schlechten Tagen meine Laune ertragen. In stürmischen Zeiten warst Du der Kapitän, der mich über Wasser gehalten hat. Als moralische Unterstützung warst Du unersetzbar.

Ganz ehrlich: Auch wenn ich manchmal gemeckert habe, wütend oder traurig war, ist es doch insgesamt eine schöne Zeit gewesen. Alle, die ich eben erwähnt habe, haben zum guten Gelingen dieser Arbeit beigetragen. Ich werde diese Jahre in schöner Erinnerung behalten. Nochmal: Danke.

Curriculum Vitae

Christine Schulze

maiden name: Lang

*18.07.1977 in Kusel

Marital Status

married,

no children

academic studies and work experience

since 08/10 Scientific Co-worker at Saarland University, Department of Biopharmaceutics and Pharmaceutical Technology

07/06-07/09 PhD candidate and scientific co-worker at Saarland University, Department of Biopharmaceutics and Pharmaceutical Technology

04/18/2006 diploma biology
Concentrations: Human Biology
Zoology
Biochemistry

05/2006 interdisciplinary diploma dissertation at the faculties of Human Biology and of Physics (department Lasers in Medicine) at Technische Universität Kaiserslautern, Germany
Subject: Investigations of the accumulation of protoporphyrin IX in different cell lines in monolayer and

spheroid culture after treatment with different derivatives of ALA

11/97-04/01 vocational training (midwife) at the Hebammenlehranstalt der Universitätskliniken Homburg/Saar, Germany

school education

07/94-06/97 Staatliches Gymnasium Landstuhl, Sekundarabschluss II

07/88-06/94 Konrad-Adenauer-Realschule Landstuhl, Sekundarabschluss I

07/84-06/88 Grundschule Steinwenden